https://doi.org/10.5194/egusphere-2026-3595
Preprint. Discussion started: 3 August 2026

MioMIP2: Experimental design for Phase 1 & 2 of the Miocene component of the CMIP7/PMIP7 Deep-time Model Intercomparison Project (DeepMIP-Miocene)

Natalie J. Burls[1†], Nicky M. Wright[2†], R. Paul Acosta[1], Catherine D. Bradshaw[3,4], Edward Gasson[5], Lennert B. Stap[6,7], Gilles Ramstein[8,9], Anna Ruth Halberstadt[10], Agatha M. de Boer[11], Funda Akgün[12], David J. Cantrill[13,14], Manuel Casas-Gallego[15], Nela Doláková[16], Boglarka Erdei[17], Alex Farnsworth[18], Sarah Feakins[19], Ran Feng[20], Tamara Fletcher[21], Frédéric Fluteau[22], J. A. Mattias Green[23], Anna S. von der Heydt[24], Matthew Huber[25], David K. Hutchinson[26], Dimiter Ivanov[27], Mine Sezgül Kayseri-Özer[28], Gregor Knorr[29], Marianna Kováčová[30], Caroline H. Lear[31], Allegra N. LeGrande[32], Shufeng Li[33], Xiaoqing Liu[25], Daniel J. Lunt[18], Katrin Meissner[26], Yunfa Miao[34], Trusha J. Naik[11], Javier B. Navarro[35], Joseph B. Novak[36], Diana Ochoa[37], Guy J. G. Paxman[38], Matthew J. Pound[39], James W. B. Rae[40], Tammo Reichgelt[20], Martin Renoult[11], Francesca Sangiorgi[41], Anta-Clarisse Sarr[42], Diane Segalla[8], Pierre Sepulchre[8], Amelia Shevenell[43], Sebastian Steinig[18], Eivind Straume[44], Caroline A. E. Strömberg[45], Clay Tabor[20], Torsten Utescher[46,47], Julia E. Weiffenbach[24], Elżbieta Worobiec[48], Yurui Zhang[49], Feng Zhu[50], Jiang Zhu[50], Alexandra Auderset[51], Florence Colleoni[52], Aisling Dolan[53], Rachel Havranek[54], Ann Holbourn[55‡], Nicholas Herold[56], Daeun Lee[57], James W. Marschalek[58], Bryce Mitsunaga[59], Sevi Modestou[60], Lina Perez-Angel[61], Mae Saslaw[62], Sinda Sosdian[63], Elena Stiles[64], Yong Sun[65], Ning Tan[66], Zhongshi Zhang[67], Yan Zhao[65]

1. Department of Atmospheric, Oceanic and Earth Sciences & the Center for Ocean-Land-Atmosphere Studies, George Mason University, Fairfax, VA, United States
2. EarthByte Group, School of Geosciences, The University of Sydney, NSW, Australia
3. The Global Systems Institute, University of Exeter, Exeter, United Kingdom
4. Met Office Hadley Centre, Exeter, United Kingdom
5. University of Exeter, Exeter, EX4, United Kingdom
6. Institute for Marine and Atmospheric Research Utrecht, Utrecht University, Utrecht, Netherlands
7. Statistics Netherlands, The Hague, Netherlands
8. Laboratoire des Sciences du Climat et de l'Environnement (LSCE), CEA, CNRS, UVSQ, Université Paris-Saclay, Gif-sur-Yvette, France
9. Institut Pierre-Simon Laplace (IPSL), Université Versailles Saint-Quentin, Guyancourt, France
10. The University of Texas at Austin, Austin, United States
11. Department of Geological Sciences, Bolin Center for Climate Research, Stockholm University, Stockholm, Sweden
12. Dokuz Eylül University, Department of Geology Engineering, Tınaztepe Campus, Buca-İzmir, Türkiye
13. Royal Botanic Gardens Victoria, Victoria, Australia
14. School of BioSciences, The University of Melbourne, Victoria, Australia
15. Department of Geodynamics, Stratigraphy and Paleontology, Complutense University of Madrid, Spain
16. Department of Geological Sciences, Masaryk University, Czech Republic

† Joint first authors

‡ deceased

https://doi.org/10.5194/egusphere-2026-3595
Preprint. Discussion started: 3 August 2026

17. Botanical Department, Hungarian Natural History Museum, Budapest, Hungary
18. School of Geographical Sciences, University of Bristol, Bristol, United Kingdom
19. Department of Earth Sciences, University of Southern California, Los Angeles, CA, United States
20. Department of Earth Sciences, University of Connecticut, Storrs, CT, United States
21. School of Physics, Chemistry and Earth Sciences, The University of Adelaide, Adelaide, SA, Australia
22. Université Paris Cité, Institut de physique du globe de Paris, CNRS, F-75005 Paris, France
23. School of Ocean Sciences, Bangor University, Menai Bridge, United Kingdom
24. Institute for Marine and Atmospheric Research Utrecht, Department of Physics, Utrecht University, Utrecht, The Netherlands
25. Department of Earth, Atmospheric, and Planetary Sciences, Purdue University, West Lafayette, IN, United States
26. Climate Change Research Centre, University of New South Wales, Sydney, Australia
27. Institute of Biodiversity and Ecosystem Research, Bulgarian Academy of Sciences, Sofia, Bulgaria
28. Dokuz Eylül University, Institute of Marine Science and Technology, İzmir, Türkiye
29. Alfred Wegener Institute Helmholtz Centre for Polar and Marine Research, Bremerhaven, Germany
30. Department of Geology and Paleontology, Faculty of Natural Sciences, Comenius University Bratislava, Mlynská dolina, Ilkovičova 6, 842 15 Bratislava, Slovak Republic
31. School of Earth and Environmental Sciences, Cardiff University, Cardiff, United Kingdom
32. NASA Goddard Institute for Space Studies, New York, NY, United States
33. State Key Laboratory of Plant Diversity and Specialty Crops, Xishuangbanna Tropical Botanical Garden, Chinese Academy of Sciences
34. Key Laboratory of Ecological Safety and Sustainable Development in Arid Lands, Northwest Institute of Eco-Environment and Resources, Chinese Academy of Sciences, China
35. Alfred Wegener Institute, Helmholtz Centre for Polar and Marine Research, Potsdam, Germany
36. Ocean Sciences Department, University of California, Santa Cruz, CA, United States
37. Geology Department, Salamanca University, Salamanca, Spain
38. Department of Geography, Durham University, Durham, United Kingdom
39. School of Geography and Natural Sciences, Northumbria University, Newcastle upon Tyne, United Kingdom
40. School of Earth and Environmental Sciences, University of St Andrews, St Andrews, United Kingdom
41. Department of Earth Sciences, Utrecht University, Utrecht, The Netherlands
42. Department of Earth Sciences, University of Oregon, Eugene, USA; Now at: Aix Marseille Univ, CNRS, IRD, INRAE, CEREGE, Aix-en-Provence, France
43. University of South Florida, College of Marine Science, Saint Petersburg, FL, United States
44. Department of Geosciences, University of Oslo, Oslo, Norway
45. Department of Biology & Burke Museum of Natural History and Culture, University of Washington, Seattle, WA, United States
46. Senckenberg Research Institute and Natural History Museum Frankfurt/M., Senckenberg Research Station of Quaternary Palaeontology, Weimar, Germany
47. Research Station of Quaternary Palaeontology, Weimar; Institute for Geosciences, Geological Department, Bonn University, Germany
48. W. Szafer Institute of Botany, Polish Academy of Sciences, Kraków, Poland
49. State Key Laboratory of Marine Environmental Science, College of Ocean & Earth Sciences, Xiamen University, Xiamen, China
50. NSF National Center for Atmospheric Research, United States
51. University of Southampton, School of Ocean and Earth Science, Southampton, United Kingdom
52. National Institute of Oceanography and Applied Geophysics, OGS, Trieste, Italy
53. School of Earth and Environment, University of Leeds, Leeds, United Kingdom
54. Science Research Initiative, University of Utah, Salt Lake City, Utah, United States

https://doi.org/10.5194/egusphere-2026-3595
Preprint. Discussion started: 3 August 2026

55. Institute of Geosciences, Christian-Albrechts-University, Germany
56. Applied Climate Science Pty Ltd., Adelaide, SA, Australia
57. Department of Earth and Environmental Sciences, University of Michigan, Ann Arbor, MI, United States
58. Department of Earth Science and Engineering, Imperial College London, United Kingdom
59. Departments of Earth and Planetary Sciences and Human Evolutionary Biology, Harvard University, Cambridge, MA, United States
60. Geography and Environmental Sciences, Northumbria University, Newcastle, United Kingdom
61. Department of Earth, Environmental, and Planetary Sciences, Brown University, Providence, RI, United States
62. The Earth Commons, Georgetown University, Washington, DC, United States
63. School of Earth & Environmental Sciences, Cardiff University, Cardiff, UK
64. Department of Geological and Planetary Sciences, California Institute of Technology, Pasadena CA, United States
65. State Key Laboratory of Tibetan Plateau Earth System, Resources and Environment (TPESRE), Institute of Tibetan Plateau Research, Chinese Academy of Sciences, Beijing, China
66. State Key Laboratory Lithospheric and Environmental Coevolution, Institute of Geology and Geophysics, Chinese Academy of Sciences, Beijing, China
67. Department of Atmospheric and Oceanic Sciences, School of Physics, School of Earth and Space Science, Peking University, Beijing, China

Correspondence to: Natalie J. Burls (nburls@gmu.edu)

Abstract. The Miocene Epoch has emerged as an important paleoclimate model intercomparison target due to its dynamic nature, global warmth, and reconstructed atmospheric CO_2 concentrations. Miocene CO_2 estimates range from as low as 300–600 ppmv to as high as 800–1100 ppmv. The formalized Miocene Model Intercomparison Project (MioMIP2) aims to address questions about the mechanisms driving the climatic changes and tipping points seen in the geological record and improve confidence in the ability of climate models to predict future climates and constrain climate sensitivity. Through alignment with PlioMIP and DeepMIP-Eocene efforts, a coordinated MioMIP (DeepMIP-Miocene) effort will allow for cross-time-period studies that sample the full range of Shared Socioeconomic Pathway paleo analogues. Building on the MioMIP1 "MIP of opportunity", the Miocene community has been developing the experimental design for MioMIP2. The MioMIP1 effort was an ensemble of opportunity that leveraged existing Miocene simulations run with different models, boundary conditions, and reference datasets. MioMIP2 will be the first formal Miocene MIP with common boundary conditions and will target the Miocene Climatic Optimum (MCO; 16.75–14.5 Ma). We present the experimental design for coordinated "CORE" MCO simulations and sensitivity studies. This community effort synthesizes paleogeography, ice sheet, CO_2, and vegetation boundary conditions based on the latest available literature and will use geological data from companion proxy synthesis efforts to evaluate the simulations.

1 Introduction

There is a long history of using climate models to simulate Earth's paleoclimates (Kutzbach, 1985). These scientific studies have been motivated by questions on the drivers of deep-time climate, as well as a desire to assess our confidence in the ability of climate models to predict future climates (Braconnot et

https://doi.org/10.5194/egusphere-2026-3595
Preprint. Discussion started: 3 August 2026

al., 2012; Tierney et al., 2020; Burls and Sagoo, 2022; Zhu et al., 2024), and constrain climate sensitivity (Hoffert and Covey, 1992; Rohling et al., 2012; Sherwood et al., 2020). With the realization that climate models can differ significantly in their response to climate forcings, model intercomparison efforts (MIPs) arose (Gates, 1992; Meehl et al., 1997). Early Paleoclimate Modelling Intercomparison Project (PMIP) efforts focused on the Holocene and the Last Glacial Maximum (Braconnot et al., 2007), which are relatively recent with low atmospheric CO_2 levels. At the same time an effort developed for investigation of the 'modern analog' for CO_2 levels with close examination of the Pliocene e.g., Chandler et al., (1994).

If climate models are to be applied to climates for comparison to future elevated atmospheric CO_2 scenarios (Riahi et al., 2017), paleoclimate MIPs need to target intervals with high atmospheric CO_2 levels and global mean temperatures. To date, coordinated MIPs have been performed for two such deep-time paleoclimate periods: the Pliocene (PRISM then PlioMIP) (Chandler et al., 2008; Haywood et al., 2009, 2011, 2013, 2016, 2020) and the Eocene (DeepMIP-Eocene) (Lunt et al., 2012, 2017, 2020). Both efforts have supported a broad range of studies investigating both the response of climate models to changes in paleoclimate forcings and the comparison of the climate simulations to available proxy evidence. The Miocene Epoch (23.03–5.33 Ma) falls between the Eocene and Pliocene epochs, in terms of both age and reconstructed global warmth. Miocene temperatures are estimated to have been 8 to 10°C warmer than pre-industrial (PI) during the peak warmth of the Miocene Climatic Optimum (MCO; 16.75–14.5 Ma), cooling to an estimated 4–6°C warmer than pre-industrial during the Late Miocene (11.63–5.33 Ma) (Burls et al., 2021). This long-term Miocene cooling (order of millions of years) is thought to have been primarily driven by declining atmospheric CO_2 concentrations (Foster et al., 2012a), with other factors such as changes in orbital forcing and slow-climate feedbacks (e.g., ice sheets and vegetation) acting in concert with changes in CO_2 and other radiative forcings to drive substantial climate variability on shorter orbital to millennial timescales (Herbert et al., 2022; Steinthorsdottir et al., 2021b).

https://doi.org/10.5194/egusphere-2026-3595
Preprint. Discussion started: 3 August 2026

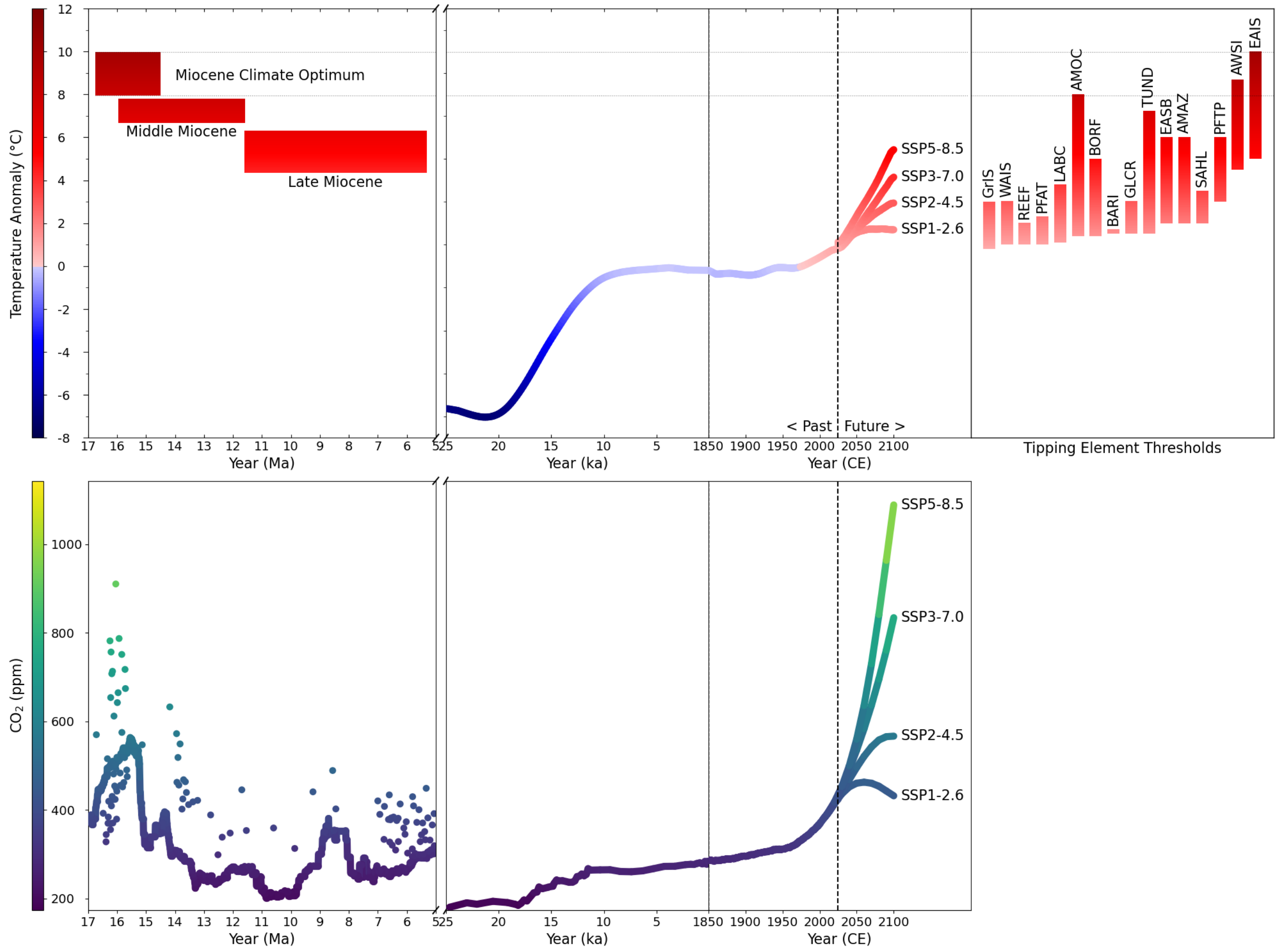

Figure 1: Global mean annual temperature and CO_2 ranges for the Late Miocene, Middle Miocene and Miocene Climate Optimum in relation to the global mean annual temperature and CO_2 timeseries from the Holocene to the end of the century and calculated temperature thresholds for tipping elements. The Miocene global annual mean temperature estimates are taken from Burls et al., (2021). The Last Glacial Maximum to Holocene data are taken from (Osman et al., 2021); the current climate data are taken from HadCRUT5 (Morice et al., 2021), and the future climate projection data are taken from (Nicholls et al., 2021). All temperature timeseries data are the anomaly relative to 1961-1990 and have been smoothed using a rolling mean window of size 20. The Miocene CO2 estimates are taken from (THE CENOZOIC CO2 PROXY INTEGRATION PROJECT (CENCO2PIP) CONSORTIUM, 2023) and plotted are the means of the 10,000 year intervals smoothed using a rolling mean window of size 100 (line) and the individual datapoints for the boron proxy data (circles). The Last Glacial Maximum to Holocene CO_2 data are taken from the Antarctic Ice Core 800,000 year record (Bereiter et al., 2015); the current climate CO_2 data are taken from the Law Dome ice core record and the NOAA Global Monitoring Laboratory records from Mauna Loa (Dlugokencky and Tans, n.d.; Etheridge, D.M., et al., 2010; Keeling et al., 1976; MacFarling Meure et al., 2006) and the future climate projection CO2 data are taken from (Riahi et al. 2017). Literature-based temperature threshold estimates for the tipping elements are taken from (Armstrong McKay et al., 2022) and the Global Tipping Points Report (2025): GRIS=Greenland Ice Sheet (collapse), WAIS=West Antarctic Ice Sheet (collapse), LABC=Labrador-Irminger Seas/Sub-polar Gyre Convection (collapse), EASB=East Antarctic Subglacial Basins (collapse), AWSI=Arctic Winter Sea Ice (collapse), AMOC=Atlantic Meridional Overturning Circulation (collapse), AMAZ=Amazon Rainforest (dieback), PFTP=Boreal Permafrost (collapse), EAIS=East Antarctic Ice Sheet (collapse), REEF=Low-latitude Coral Reefs (die-off), PFAT=Boreal Permafrost (abrupt thaw), BARI=Barents Sea Ice (abrupt loss), GLCR=Mountain Glaciers (loss), SAHL=Sahel and West African Monsoon (greening), BORF=Boreal Forest (southern dieback), TUND=Boreal Forest (northern expansion).

https://doi.org/10.5194/egusphere-2026-3595
Preprint. Discussion started: 3 August 2026

The Miocene has emerged as an important target for a paleoclimate MIP due to its similarity to near-future projections in terms of global warmth and reconstructed atmospheric CO_2 concentrations. Atmospheric CO_2 estimates for the Miocene range between 300 and 1100 ppmv (Foster et al., 2012b, 2017; Rae et al., 2021a; Sosdian et al., 2018; Steinthorsdottir et al., 2021b; Stoll et al., 2019; Tanner et al., 2025; THE CENOZOIC CO2 PROXY INTEGRATION PROJECT (CENCO2PIP) CONSORTIUM, 2023), covering the full range from the 20th century to the worst case future scenario projected under Shared Socioeconomic Pathways (SSP) 5 (Riahi et al., 2017). Miocene climate modelling studies paired with proxy reconstructions of Miocene climate can provide insights on the sensitivity and tipping points of various elements of Earth's climate system to elevated CO_2 concentrations and global warmth, as illustrated in Fig. 1. Furthermore, through alignment with PlioMIP and DeepMIP Eocene efforts, a coordinated MIP targeted at the Miocene will allow for cross-time-period studies that sample the full range of paleo analogues to future scenarios in a consistent manner.

The Burls et al. (2021) MioMIP1 study provided a comprehensive quantitative assessment of published Miocene climate simulations and the range of model-data agreement, highlighting mechanisms common to all Miocene simulations and regions where differences across experiments result in a large spread in warming responses. The MIP of opportunity approach offers certain advantages in that it samples the full range of sensitivity, not only across different climate models but to differing boundary conditions chosen to be representative of the Miocene. Yet this approach comes with its limitations, specifically when the question at hand requires an assessment of the robustness of a result across climate models. Burls et al. (2021) recommends a formalized Miocene MIP (MioMIP2), bringing the community together under the auspices of DeepMIP-Miocene to write this experimental design paper.

This paper is the result of a coordinated community effort in which both experts from the Miocene paleoclimate modelling and data communities have worked to design the outlined boundary conditions and experimental setups. DeepMIP-Miocene's "MioMIP2" effort will target the MCO and consist of 2 phases. Phase 1 uses the Middle Miocene paleogeography, vegetation, and land-ice boundary conditions published and described in Burls et al. (2021), hereafter referred to as "updated Herold". Phase 2,

https://doi.org/10.5194/egusphere-2026-3595
Preprint. Discussion started: 3 August 2026

described herein, uses the state-of-the-art paleogeography, vegetation, and land-ice boundary compiled by consulting experts, and the literature, to incorporate the latest advances in our understanding of conditions during the MCO. In accordance with the previous deep-time PlioMIP and DeepMIP-Eocene efforts, we outline "CORE" experiments that each modelling group participating in MioMIP2 should complete, as well as suggested sensitivity experiments that will benefit from a multi-model approach to testing process uncertainty. Additionally, we hope that the boundary conditions published with this paper will also support a broader range of Miocene sensitivity experiments with individual models that target scientific questions suited to a single model approach. The Miocene community envisions that the simulations conducted as part of the MioMIP2 effort outlined in this paper (as well as future MioMIP efforts targeting other Miocene time intervals) will help address a range of scientific questions.

2 The Chosen Interval

Comprehensive investigations of all recognized climatic events throughout the Miocene are envisaged. In the present study, as an initial step, the focus is placed on one of the major climatic events of the Miocene, namely the Miocene Climatic Optimum (MCO; 16.75–14.5 Ma).

3 Experimental Design

The DeepMIP-Miocene, "MioMIP2" experimental protocol has 4 CORE experiments and several optional sensitivity experiments (Table 1). The CORE experiments consist of a pre-industrial control simulation (Section 3.1), an abrupt 4xCO_2 simulation (Section 3.1), a Phase 1 MCO simulation (Section 3.2), and a Phase 2 MCO simulation (Section 3.3). Some modeling groups may choose not to do Phase 1 experiments, in which case they can omit the Phase 1 CORE MCO simulation. Optional sensitivity experiments are described in Section 3.4 and summarized in Table 1. Of the possible sensitivity experiments proposed, modelling groups are asked to prioritize the CO_2 sensitivity experiments, specifically the 1xCO_2 experiment, because this sensitivity study allows the non-CO_2 forcings to be distinguished from the CO_2 forcing.

https://doi.org/10.5194/egusphere-2026-3595
Preprint. Discussion started: 3 August 2026

3.1 Pre-industrial Control and Abrupt 4xCO_2 Simulations

As in DeepMIP-Eocene (Lunt et al., 2017, 2026), the pre-industrial simulation should be as close as possible to the piControl run with 1850 forcings that is associated with the Coupled Model Intercomparison Project (CMIP) version of the model being used to conduct the MioMIP experiments e.g., Eyring et al., (2015) if a CMIP6 model is being used and Dunne et al., (2025) if a CMIP7 model. As far as is possible, model physics and parameterization schemes should be consistent between the pre-industrial simulation and Miocene experiments unless the Miocene experiment is a sensitivity experiment designed to test the implications of changing a parameterized process such as tidal mixing (see Section 3.3.5).

The piControl simulation should be initialized from observations or a similar control simulation. The length of simulation and output saved should be the same as the Miocene control simulation, as outlined in Sections 3.3.7 and 3.3.8.

To evaluate each model's equilibrium climate sensitivity under modern boundary conditions, each modelling group is asked to perform the standard CMIP abrupt 4xCO_2 simulation run for at least 150 years, ideally 300 years as this is now part of the new CMIP7 protocol (Dunne et al., 2025).

3.2 Phase 1 Middle Miocene Climate Optimum Simulation

MioMIP2 Phase 1 uses the "updated Herold" Middle Miocene paleogeography (Figure 2b), vegetation, and land-ice boundary conditions described in Burls et al. (2021). The starting point for this paleogeography is the Miocene dataset described in Herold et al. (2008) with the minor modifications of Herold et al. (2011). For a full description of the "updated Herold" dataset see the supporting information of Burls et al. (2021). The "updated Herold" boundary condition files published in Burls et al. (2021) are available on Zenodo, as outlined in Table 2. Modelling groups participating in MioMIP2 should download these files for their CORE Phase 1 experiment (deepmip-mio-mco-p2-3xCO2), and any of the three Phase 1 sensitivity experiments (deepmip-mio-mco-p1-XxCO2) they choose to do (Table 1). For guidance on how to address the applicable experimental setup choices when running their

https://doi.org/10.5194/egusphere-2026-3595
Preprint. Discussion started: 3 August 2026

Phase 1 experiments, modeling groups should follow the Phase 2 instructions outlined in Sections 3.3.3 to 3.3.8. Any required deviations from these guidelines will not necessarily preclude contribution to MioMIP2 but should be documented in the metadata and associated publications.

Table 1: DeepMIP-Miocene MioMIP2 Phase 1 & 2 CORE simulations as well as optional sensitivity experiments

Experiment Name	Experiment Description	CO_2 (ppmv)*	Paleogeography
	CORE Experiments		
piControl	Pre-industrial control	280	Modern
abrupt-4xCO2	Abrupt 4×CO_2	1120	Modern
deepmip-mio-mco-p1-3xCO2	MCO best guess	840	“updated Herold” Burls et al. (2021)
deepmip-mio-mco-p2-3xCO2	MCO best guess	840	This paper
	Phase 1 & 2 CO_2 Sensitivity Experiments		
deepmip-mio-mco-p1-1xCO2	Phase 1 PI CO_2	280	“updated Herold” Burls et al. (2021)
deepmip-mio-mco-p1-2xCO2	Phase 1 low CO_2	560	“updated Herold” Burls et al. (2021)
deepmip-mio-mco-p1-4xCO2	Phase 1 high CO_2	1120	“updated Herold” Burls et al. (2021)
deepmip-mio-mco-p2-1xCO2	Phase 2 PI CO_2	280	“MioMIP2” This paper
deepmip-mio-mco-p2-2xCO2	Phase 2 low CO_2	560	“MioMIP2” This paper
deepmip-mio-mco-p2-4xCO2	Phase 2 high CO_2	1120	“MioMIP2” This paper
	Other Phase 2 Sensitivity Experiments		
deepmip-mio-mco-p2-ICE-small	Small MCO ice sheet	840	“MioMIP2” This paper
deepmip-mio-mco-p2-ICE-large	Large MCO ice sheet	560	“MioMIP2” This paper
deepmip-mio-mco-p2-ICE-none	No MCO ice sheet	840	“MioMIP2” This paper
deepmip-mio-mco-p2-deepFramStrait	Deeper Fram Strait	840	“MioMIP2” This paper
deepmip-mio-mco-p2-deepCAS	Deeper Central American Seaway	840	“MioMIP2” This paper
deepmip-mio-mco-p2-OpenTethys	Open Tethys	840	“MioMIP2” This paper
deepmip-mio-mco-p2-HotSpot	Hotspot reference frame	840	“MioMIP2” This paper
deepmip-mio-mco-p2-solar	0.14% decrease in solar constant	840	“MioMIP2” This paper
deepmip-mio-mco-p2-ISlo	Minimum Northern Hemisphere summer insolation	840	“MioMIP2” This paper
deepmip-mio-mco-p2-IShi	Maximum Northern Hemisphere summer insolation	840	“MioMIP2” This paper

* If a value other than 280 ppmv is used for piControl, then all other CO_2 values in the table should be changed accordingly. For example, CESM uses 284.7 ppmv

https://doi.org/10.5194/egusphere-2026-3595
Preprint. Discussion started: 3 August 2026

Table 2: DeepMIP-Miocene MioMIP2 boundary conditions

Experiment Name	Boundary Condition	Location	Filename	Variable Name
CORE Experiments and CO_2 Sensitivity Experiments				
MioMIP2 Phase 1 Boundary Conditions ("Updated Herold")				
deepmip-mio-mco-p1-**X**xCO2	Topography/Bathymetry	"Updated Herold" in Burls et al. (2021) Supplement https://zenodo.org/records/4568897 & https://zenodo.org/records/8179390	miocene_topo_pollard_antscape_dolan0.5x0.5.nc	topo
	Ice sheets		miocene_veg_2x2.nc	pft - land ice
	Sea level (Land/Sea Mask)		miocene_veg_2x2.nc	landmask
	Vegetation[$]		miocene_veg_2x2.nc	pft
	Soils		modern	
	Lakes		No lakes	NA
MioMIP2 Phase 2 Boundary Conditions (MioMIP2)				
deepmip-mio-mco-p2-**X**xCO2	Topography/Bathymetry	https://zenodo.org/records/20646213	MioMIP2-Phase2-CORE-paleogeography.nc	topo
	Ice sheets		MioMIP2_Phase2_CORE_biome.nc	mco_biome - land ice
	Ice sheet thickness		MioMIP2_Phase2_CORE_paleogeography.nc	icesheet_thickness
	Sea level (Land/Sea Mask)		MioMIP2_Phase2_CORE_paleogeography.nc	landmask
	Runoff[#]		MioMIP2_Phase2_CORE _rivers.nc	route
	Vegetation[$]		MioMIP2_Phase2_CORE_biome.nc	mco_biome
	Soil order		MioMIP2_Phase2_CORE_soil	mco_soil
	Soil water holding capacity		MioMIP2_Phase2_CORE_soil.nc	mco_whc_mm
	Soil hydraulic conductivity		MioMIP2-Phase2-CORE-soil.nc	mco_ksat_mmhr-1
	Lakes		No lakes	NA
Other Phase 2 Sensitivity Experiments				
deepmip-mio-mco-p2-ICE-small	Topography/Bathymetry, Ice sheets, Ice sheet thickness, Sea level, Runoff[#], Vegetation, Soil order, Soil water holding capacity, Soil hydraulic conductivity	https://zenodo.org/records/20646213	MioMIP2_Phase2_ICE_small_*.nc	Topo, mco_biome – land ice, icesheet_thickness, landmask, route, mco_biome, mco_soil, mco_whc_mm, mco_ksat_mmhr-1
deepmip-mio-mco-p2-ICE-large			MioMIP2_Phase2_ICE_large_*.nc	
deepmip-mio-mco-p2-ICE-none			MioMIP2_Phase2_ICE_none_*.nc	
deepmip-mio-mco-p2-deepFramStrait			MioMIP2_Phase2_FramStrait_*.nc	
deepmip-mio-mco-p2-deepCAS			MioMIP2_Phase2_CentralAmericanSeaway_*.nc	

https://doi.org/10.5194/egusphere-2026-3595
Preprint. Discussion started: 3 August 2026

deepmip-mio-mco-p2-OpenTethys	MioMIP2_Phase2_TethysSeaway_*.nc
deepmip-mio-mco-p2-HotSpot	MioMIP2_Phase2_HotSpot_*.nc

Corresponding 2-degree version of Phase 2 boundary condition file is available with filename ending in "_2deg.nc"
[$] Simulations run with dynamical vegetation should initialize from specified vegetation file
[#] It is recommended that modelling groups use the 2-degree version (filename ending in "_2deg.nc") to help ensure consistency in river routes across different model resolutions

3.3 Phase 2 Middle Miocene Climate Optimum Simulation

Several studies advancing our understanding of the MCO have been published since the "updated Herold" Middle Miocene boundary conditions were created (Burls et al., 2021). We therefore review the latest literature and compile state-of-the-art paleogeography, vegetation, and land-ice boundary conditions as described in the following two subsections (Sections 3.3.1 & 3.3.2). We refer to these boundary conditions as the "MioMIP2" Phase 2 paleogeography, vegetation, and land-ice boundary conditions (Table 2) which are used to carry out the Phase 2 experiments as summarized in Table 1.

3.3.1 Paleogeography and land–sea mask

Since the "updated Herold" paleogeography in Burls et al. (2021) was compiled, new paleogeographic information and reconstructions for several important regions have been published. Using the "updated Herold" paleogeography (Figure 2b) as our starting point, topographic/bathymetric updates were applied to produce the MioMIP2 Phase 2 boundary conditions (Table 2 & Figure 2c) as described below. Note, we do not make any modifications to large parts of eastern North America, Siberia, Northern Asia, Australia, and New Zealand, and so these regions retain the "updated Herold" reconstruction; see Figure S1 for a comparison of the Phase 1 "updated Herold" and Phase 2 paleogeography. We create our final MioMIP2 Phase 2 paleogeography at a 0.25° x 0.25° resolution and additionally make a 2° x 2° version available using conversative regridding (Figure S2).

We update the plate tectonic reconstruction using Zahirovic et al. (2022), but notably depart from the default mantle-based reference frame of this model and use the paleomagnetic reference frame available as part of this model (from Merdith et al. (2021); anchored plate '701701') as the basis for our new paleogeography. This change reflects both an update in the overall plate kinematic reconstruction

https://doi.org/10.5194/egusphere-2026-3595
Preprint. Discussion started: 3 August 2026

(Müller et al., 2008a) and its mantle-based (hot spot) reference frame that was used as the basis within Herold et al. (2008) and its derivations, including Burls et al. (2021), and is consistent with the plate tectonic model and reference frame used in DeepMIP-Eocene-Phase 2 (Lunt et al., 2026). We note that many of the following paleogeography advancements described below and subsequently incorporated into our paleogeography reconstruction were originally published in alternative plate tectonic models; as such, we ensure prior to any paleogeography modifications and incorporations that all reconstructions are rotated into the same absolute reference frame and/or plate tectonic reconstruction model, using software such as pyGPlates (Mather et al., 2024) and Generic Mapping Tools (GMT) (Wessel et al., 2019a) or GPlately (Mather et al., 2024).

Paleobathymetry

Global paleobathymetry has traditionally been reconstructed based on the oceanic crustal age ('age grids') generated using the underlying plate tectonic model, applying an oceanic thermal subsidence relationship to determine basement depths, e.g., Stein and Stein, (1992) ['GDH1']; Crosby and McKenzie, (2009); Richards et al. (2018), with the addition of a model of predicted sediment thickness, e.g., Müller et al., (2008b); Dutkiewicz et al., (2017); Straume et al., (2020), its isostatic correction (Sykes, 1996), and a model of oceanic plateau and/or large igneous province emplacement, see Müller et al. (2008b) and Wright et al. (2020). This approach was used in the paleobathymetry of Müller et al. (2008b), which forms the paleobathymetry in Herold et al. (2008) and its iterations, though refinements to this approach and its components have since been explored in Wright et al. (2020).

While there will always be some difficulties in reconstructing paleobathymetry, especially for regions where oceanic crust has been lost due to subduction and therefore requires synthetic reconstruction, there have been several recent advancements in the reconstruction of regional paleobathymetry in the Cenozoic. In particular, Hochmuth et al. (2020b) provide a detailed reconstruction of Southern Ocean paleobathymetry at key time intervals since 34 Ma (including the Middle Miocene; 14 Ma), determined using backstripping combined with drill core data and seismic stratigraphy. This reconstruction incorporates the Southern Ocean gateways, i.e., the Drake Passage and Tasman Gateway, which are

https://doi.org/10.5194/egusphere-2026-3595
Preprint. Discussion started: 3 August 2026

thought to have allowed for deep-water exchange during this time (2020b). Hochmuth et al. (2020a) merge their reconstructed paleobathymetry with the recent Antarctic bedrock by Paxman et al. (2019).

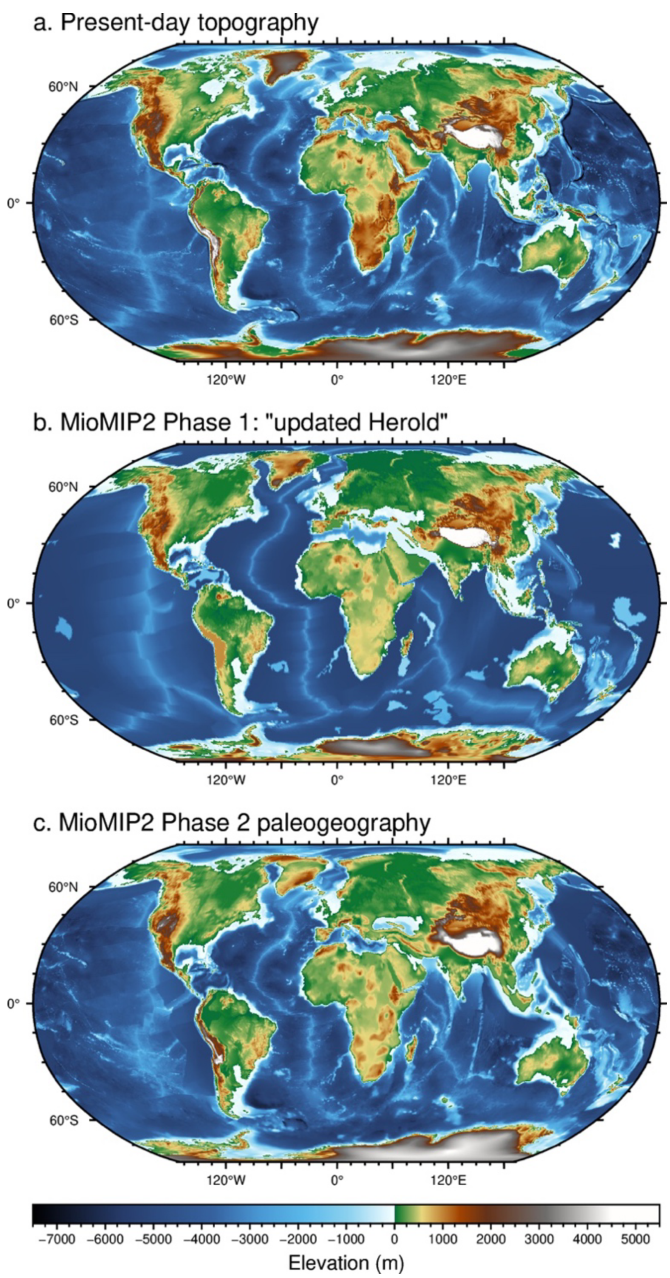

Figure 2: MioMIP2 Paleogeography. a. modern topography; b. MioMIP2 Phase 1 paleogeography ("updated Herold" at 0.5° x 0.5°; c. MioMIP2 Phase 2 paleogeography (this study), at 0.25° x 0.25°. See Supplementary Figure S1 for a comparison of MioMIP2 Phase 2 in its high (0.25°x0.25°) and low (2°x2°) resolution.

https://doi.org/10.5194/egusphere-2026-3595
Preprint. Discussion started: 3 August 2026

In addition, Straume et al. (2020) reconstruct global paleogeography for the Cenozoic, with a specific focus on the evolution of oceanic gateways. While Straume et al. (2020) use a similar method to Herold et al. (2008) globally, they reconstruct and modify key regions using additional geological and geophysical data. Key regions and oceanic gateways include the Fram Strait, Greenland-Scotland Ridge, the Central American Seaway and the Tethys Seaway, with further refinements to the Tethys Seaway, Arabia, and Eurasia made in Straume et al. (2024, 2025). Furthermore, a new method to reconstruct paleobathymetry has been made available using 'pybacktrack v1.4' software (Müller et al., 2018) which allows for both the reconstruction of presently preserved oceanic crust and continental crust, where the former is based on an oceanic subsidence relationship, while the latter is based on its rifting and deformation history, and both methods incorporate the progressive decompaction of sediments (and other user-optional parameters). As this method can only reconstruct presently preserved regions, to derive a global paleobathymetry it still requires the integration of paleobathymetry reconstructed in the more traditional manner for synthetically reconstructed oceanic crust.

There are physiographic uncertainties for several oceanic gateways during the Middle Miocene, including the Fram Strait, Tethys Seaway Central American Seaway, and Indonesian Seaway. We review these below and conclude this section with a summary of how we combine these recent advances to construct the paleobathymetry and oceanic gateways in MioMIP2 Phase 2 (Figure 2c).

The Fram Strait is a key gateway allowing for exchange between the northern Atlantic and Arctic Oceans and is thought to have had an influence on North Atlantic Deep Water (NADW) and Atlantic Meridional Overturning Circulation (AMOC). In the present climate, it is the only deep-water connection between the Arctic and Atlantic, impacting overturning in the Nordic Seas (Årthun et al., 2023). While there is some uncertainty in the specific timing and the depth evolution of the Fram Strait, it is thought to have transitioned from a shallow connection to a deep connection around 17.5 Ma (Jakobsson et al., 2007). Within the "updated Herold" paleogeography, this gateway was a narrow deepwater (~3500 m) connection. Straume et al. (2020, 2024) however, reconstruct the Fram Strait as

https://doi.org/10.5194/egusphere-2026-3595
Preprint. Discussion started: 3 August 2026

somewhat shallower (~2500 m) but a wider connection, encompassing more of the surrounding submerged continental shelves. Additionally, the Faroe-Shetland Channel is much less deep in Straume et al. (2024) (~500 m), whereas it is ~4500 m in “updated Herold” (Figure S3).

Long standing debates have persisted around the configuration of the Central American Seaway during the Middle Miocene (Bacon et al., 2015; Jaramillo et al., 2017, 2018; Molnar, 2017; Montes et al., 2012, 2015; O’Dea et al., 2016; Sepulchre et al., 2014). Herold et al. (2008) and “updated Herold” depict the Central American Seaway as a wide and deep (~4500 m) seaway (Figure S4). However, most recent studies suggest that intermediate to deep (~> 2000 m) water connections persisted through the Middle Miocene in some part of the seaway (O’Dea et al., 2016; Vallejo-Hincapié et al., 2024), but that its width might have been restricted by the presence of volcanic arcs (Vallejo-Hincapié et al., 2024) explaining diverging local paleobathymetry evidence (Montes et al., 2012, 2015; Vallejo-Hincapié et al., 2024). Shoaling is suggested to have occurred during the Late Miocene, around 11–9 Ma (Kirillova et al., 2019; Osborne et al., 2014).

The Tethys Seaway was shown as a deep connection (~4200 m) in Herold et al. (2008) and modified to be a shallow seaway (~200 m) in the “updated Herold” (Figure S5). Since then, Straume et al. (2024) has explored the detailed evolution of the Tethys Seaway based on reconstructions from the Darius Programme (Barrier et al., 2018), various geologic and biogeographic indicators for seaway morphology (Bialik et al., 2019; Okay et al., 2010; Segev et al., 2017), and a modified version of the regional kinematic model of van Hinsbergen et al. (2020). In their reconstruction, the Tethys Seaway closed by ~19–20 Ma with the drying of the Mesopotamian Trough and emergence of the *Gophotherium* Landbridge (Bialik et al., 2019; Harzhauser et al., 2007; Segev et al., 2017; Straume et al., 2024). Recent studies on faunal assemblages suggest that any substantial oceanic exchange between the Indian Ocean and Atlantic Ocean ceased by the Early Miocene. At 15 Ma, the Tethys Seaway was in a transitional stage, likely shallow and narrow or completely closed, where evidence suggests there may have been a temporary reflooding of the seaway in the Early and Middle Miocene before its final closure at ~14 Ma (Bialik et al., 2019; Straume et al., 2025). Consequently, a shallower connection

https://doi.org/10.5194/egusphere-2026-3595
Preprint. Discussion started: 3 August 2026

between the proto-Mediterranean and Indo-Pacific may have been operational at 15 Ma, however, no deep connections (> 300 m) were likely at this time (Straume et al., 2024, 2025).

The Indonesian Seaway allows water masses from the tropical Pacific Ocean to be transferred into the tropical Indian Ocean (Gordon, 2005) and is thought to have had major impact on Neogene climate evolution (Gallagher et al., 2024; Kuhnt et al., 2004). Paleogeographic evolution of the region during the Miocene is essentially forced by the northward migration of the Australian continent and its collision with Papua New Guinea and South-East Asia (Hall et al., 2012). A recent synthesis by Gallagher et al. (2024) suggests that the seaway was only partially restricted during the Middle Miocene, with constriction occurring later. We note that reconstructing the paleogeography of such a complex seaway is far from straightforward, high uncertainty persists due to active tectonic deformation, the presence of many small islands and narrow straits and a lack of direct quantitative paleobathymetric evidence. Frigola et al (2018) made some modifications to the Herold et al. (2008) Middle Miocene reconstruction, including an alternative reconstruction for this region, based on the more recent work from Hall (2012). However, as Hall (2012) does not provide any absolute elevation values, Frigola et al. (2018) assigned average elevation and bathymetry values to Hall's (2012) geographic feature categories and modified the depth of the gateway so that intermediate depth passages exist at depths between 600 and 1000 m.

Here, we combine many of these recent advances in paleobathymetry and oceanic gateways configurations. We create our paleobathymetry using the plate tectonic model (Zahirovic et al., 2022) based on the combination of pybacktrack 1.4, for presently preserved regions and submerged continental crust, and we use the workflow described in Wright et al. (2020) for regions requiring synthetically reconstructed oceanic crust. We use the Stein and Stein oceanic subsidence relationship within both these workflows. We incorporate the Hochmuth et al. (2020a) reconstruction for the Southern Ocean, and Straume et al. (2020) for the Fram Strait (Figure S3), Central American Seaway (Figure S4), and Tethys Seaway and surrounds (including the Paratethys; Figure S5). We additionally adopt the reconstruction from Frigola et al. (2018) for the Maritime Continent region and Indonesian

https://doi.org/10.5194/egusphere-2026-3595
Preprint. Discussion started: 3 August 2026

Seaway (Figure S6). Herold et al. (2008) (and consequently "updated Herold") incorporate a sea-level adjustment based on Müller et al. (consistent with their paleobathymetry) and their ice sheet scenario. Here we adjust sea level in our starting paleogeography ("updated Herold") for the effects of tectonics (20 m) based on Wright et al. , as well as the effect of the CORE ice sheet and small ice sheet scenarios respectively (see Sections 3.3.2, 3.4.3 and Table 6 for further details).

Antarctica and Greenland

The paleotopography of the Antarctic bedrock since 34 Ma was reconstructed in high resolution by Paxman et al. (2019), including at (~14 Ma). This reconstruction has been combined with the Hochmuth et al. (2020b) Southern Ocean paleobathymetry reconstruction. Here, we leverage this reconstruction in our global paleobathymetry, and bedrock topography of Antarctica is isostatically adjusted to account for the loading effect of the Antarctic Ice Sheet (see Section 3.3.2 for further discussion on the configuration of the ice sheet). Straume et al. (2020) also provides a new paleogeography reconstruction for Greenland, where they modify its paleotopography to account for the Eurekan orogeny (Medvedev et al., 2018). We incorporate this reconstruction for Greenland into our Phase 2 paleogeography, with a slight adjustment to the paleoelevations of the eastern Greenland margin to better match its conjugate margin, as well as modifying the Canadian archipelago to ensure no oceanic throughflow (similar to "updated Herold").

North America

The western North American cordillera has immense impact on the regional climate, behaving like water towers interacting with atmospheric rivers and the North American monsoon, while redirecting atmospheric flow influencing westerly storms in North America (Feng et al., 2013; Spaur et al., 2025; Wheeler et al., 2016). The western mountain ranges began their development during the Early Cretaceous as part of the subduction of the Farallon Plate into North America (Bahadori et al., 2022; Cassel et al., 2018; Licht et al., 2017). Using geodynamic models and terrestrial climate-derived proxies (water isotopes and paleobotany), the maximum orogenic elevation was estimated to have occurred during the early Cenozoic where a Nevadaplano and Mogollon highland was present (Bahadori et al.,

https://doi.org/10.5194/egusphere-2026-3595
Preprint. Discussion started: 3 August 2026

2022; Chamberlain et al., 2012; Liu, 2015). Progressive collapse of the highlands occurred during the Oligocene-Miocene transition as part of the Basin and Range expansion. Middle-to-Late Miocene evidence alludes to the subsequent uplift of the Colorado Plateau while the Great Basin and Sierra Nevada formed further west. We therefore implement the Early-to-Middle Miocene western North American cordillera generated by Bahadori et al., (2022), with an elevated Nevadaplano, but a lower Colorado Plateau (Figure S7).

Central America

The Mexican Plateau is bordered by two meridionally oriented cordilleras, an eastern feature the Sierra Madre Occidental, and a western feature, the Sierra Madre Oriental (Fan et al., 2022). Elevated terrain primarily resides over the Sierra Madre Occidental and its orogeny have been shown to strongly influence the Intertropical Convergence Zone (ITCZ) and guide the northward progress of the North American Monsoon (Adams and Comrie, 1997; Boos and Pascale, 2021). Like the western North American cordilleras, the uplift of the Mexican Plateau began its development during the Early Cretaceous as part of the subduction of the Farallon Plate under North America. The majority of the volcanic activity and uplift of the Sierra Madre Occidental occurred between the Early Oligocene and Early Miocene, forming prior to the opening of the Gulf of California (Ferrari et al., 2007). For our work, we implement a modified version of the modern-day Sierra Madre Occidental since much of its elevation gain occurred prior to the Middle Miocene (Figure S7). However, further work like Bahadori et al. (2022) should be done to fully ascertain the Mexican Plateau orogeny.

South America

Today, the Andean Mountain range is longest mountain chain in the world, spanning the entire western border of South America. The orogenic history of the Andes has implications for the development of the South American Monsoon (Acosta et al., 2022; Jeffery et al., 2012), orientation of the Amazon rivers (Hoorn et al., 2022; Jaramillo et al., 2017) and ocean circulation in the East Equatorial Pacific (Feng and Poulsen, 2014; Takahashi and Battisti, 2007). The uplift sequence of the Andes was diachronous beginning during the Late Cretaceous-Paleocene as part of the Farallon Plate subducted under South

https://doi.org/10.5194/egusphere-2026-3595
Preprint. Discussion started: 3 August 2026

America (Boschman, 2021). The uplift history of the Andes during the Miocene is still debated. In the central Andes, the elevation of the eastern cordillera in Boschman (2021) is substantially lower than the western cordillera (~2 km difference), where paleoaltimetry evidence suggests rapid uplift occurring between 15 and 5 Ma (Garzione et al., 2017). Using water isotopes, paleobotany, and stratigraphic data the western cordillera is estimated to have been uplifted above 4 km between the Eocene-Oligocene, and the eastern cordillera uplifted to 2–3 km elevation between the Late Oligocene and Middle Miocene (Martínez et al., 2020; Sundell et al., 2025).

A long-lived mega-wetland in western Amazonia known as the Pebas System existed during the Middle Miocene with a significant influence on biodiversity. However, the spatial extent and its paleoenvironmental evolution (e.g., lacustrine vs marine influence, as well as extent and timing of possible marine incursions) have been debated (Bernal et al., 2019; Bicudo et al., 2020; Gross et al., 2016; Hoorn et al., 2010, 2022; Jaramillo et al., 2017).

Here, we rely on the 15 Ma paleotopography of Boschman (2021), with the following modifications to account for the Pebas System and the Paranaense Sea. We account for the Pebas System by following its spatial extent as suggested in Hoorn et al. (2022), adjusting its elevation from 35 m in its center, gradating to sea level at its mouth where it drains towards the Caribbean. To account for grid resolution changes (i.e., 0.25° to 2°), we slightly widened the outlet so that it is preserved at the lower 2° resolution. The Pebas region should be designated by modelling groups as wetland in the land surface model (see Figure S8 for its incorporated extent). The extent of the marine incursion, known as the Paranaense Sea, is much less certain. Here, we incorporate the values and extent of the Paranaense Sea from the "updated Herold" paleogeography, which in turn derives from Markwick, (2007) (Figure S8).

Africa

The East African Rift System extends from the Afar region towards southeastern Africa. The uplift of these reliefs results from mantle dynamics (plume activity and convective cell processes), which drive basement uplift, magmatic activity leading to volcanic flow accumulation, and rifting responsible for

https://doi.org/10.5194/egusphere-2026-3595
Preprint. Discussion started: 3 August 2026

the formation of rift shoulders (Cai et al., 2023; McGregor et al., 2015; Michon et al., 2022; Morley, 2020; Vetel and Le Gall, 2006). The Ethiopian Plateau may have reached an altitude of 2500 m as early as the Oligocene (Pik et al., 2008; Sembroni et al., 2016). Located south of the Ethiopian Plateau, previous paleobiology evidence found at 17 Ma (Wichura et al., 2015) estimated the altitude of the East African Plateau (Kenya Dome) was low enough to have fluvial systems that connected the Indian Ocean during the Middle Miocene, and only has exceeded 1400 m after 13.5 Ma (Wichura et al., 2010).

In north Africa, large sedimentary basins were marine and connected to the Tethys Ocean during the Paleocene, persisting until the Middle Eocene for the Taoudenni Basin (Guiraud et al., 2005; Swezey, 2009). Long-wavelength deformation (100–1000 km) induced by mantle upwellings drove the uplift of the Tibesti, Darfur, and Hoggar-Air massifs from the Middle Eocene onwards (LeMasurier, 2022). The rise of these landforms was large enough to reshape the drainage patterns from the Early Oligocene onwards (Chardon et al., 2016).

The Jos Plateau (Nigeria), Cameroon Highlands, and Ubangian Rise (located between the Congo Basin and the Chad Basin) experienced uplift between the Middle Eocene and the Oligocene (45–23 Ma), although the elevation did not exceed a few hundred meters (Guillocheau et al., 2015). To the west of the Congo Basin, the Central African Atlantic Swell began rising during the Middle Miocene (Guillocheau et al., 2015).

Today, southern Africa is characterized by a high plateau bordered by a prominent escarpment. Estimates of sediment volumes and accumulation rates in marginal basins off southern Africa (ranging from the Walvis Basin in the Atlantic Ocean to the Durban Basin in the Indian Ocean) indicate a sharp increase in sediment accumulation rates during the Late Cretaceous, driven by a peak in erosion (Baby et al., 2020). This event suggests that the uplift of the South African plateau occurred between 93 and 70 Ma, likely induced by dynamic topography associated with the motion of Africa over the superplume (Braun et al., 2014). A second uplift, primarily affecting the eastern part of the South African plateau,

https://doi.org/10.5194/egusphere-2026-3595
Preprint. Discussion started: 3 August 2026

took place during the Neogene between 25 and 15 Ma (Baby et al., 2020). Therefore, by the Middle Miocene, the South African plateau had likely reached an elevation close to its present height.

In the north-west of the African continent, the uplift of the High Atlas began at the end of the Eocene in Morocco and progressed eastwards, reaching Tunisia only during the Late Miocene (Missenard et al., 2007). This orogeny is not directly linked to the Europe-Africa collision but instead results from the Cenozoic inversion of a rift system that was active during the Triassic and Jurassic (Frizon de Lamotte et al., 2000). During the Middle Miocene, the Atlas Mountains in Morocco likely exhibited lower relief than today, as an episode of crustal deformation and exhumation occurred during the Middle to Late Miocene, driven by dynamic mantle upwelling (Lanari et al., 2023).

Poblete et al. (2021) produced a paleogeographic reconstruction at 20 Ma, in which the topography of Africa aligns with the main features described above for the Middle Miocene. However, the absence of any slope in low-lying areas prevents the accurate representation of watersheds. The current bimodal hypsometry of Africa was likely established around 30 Ma, coinciding with the development of the modern drainage network. Therefore, we reconstruct the paleogeography of the African and Arabian plates by integrating the aforementioned features in the paleogeographic reconstruction of Poblete et al. (2020) combined with the adjusted present day topographic features (rotation and elevation) into the well-established version in the "updated Herold" (Figure S9).

Europe

Tectonic activity, including throughout the Miocene, has resulted in significant orogenies and played a large role in influencing the paleogeography of the European region. Key regions include the European Alps and Anatolia, where their respective elevations may act as water towers capturing a substantial amount of rain and moisture from atmospheric rivers, and holds significant importance to the regional land-surface hydrological cycle. The European Alps evolved from the continental collision as the African plate moved northwards toward Eurasia beginning in the Late Cretaceous, with much of its heterogenous uplift occurring during the Miocene (Kissling and Schlunegger, 2018). Late Oligocene to

https://doi.org/10.5194/egusphere-2026-3595
Preprint. Discussion started: 3 August 2026

Early Miocene records suggest elevations of ~2 km and subsequent rapid uplift during Early to Middle Miocene, when the European Alps reached an elevation of ~4 km (Krsnik et al., 2021). In the "updated Herold" paleogeography, the European Alps are ~2 km in elevation, thus we raise its elevation to ~4 km. However, since its surrounding mountain range such as the Dinaric Alps are contingent on the extent of the Tethys Sea (based on the Straume et al., (2024) reconstruction that is adopted in our Phase 2 paleogeography), here we primarily implement changes on the central European Alps and maintain the continental configuration implemented in the "updated Herold" (Figure S5).

During the Early to Middle Miocene, the Anatolian region experienced intense tectonic activity, which played a primary role in shaping its topography. The ongoing extensional and strike-slip tectonics in Western, Central, and Eastern Anatolia led to the formation of grabens, horsts, and elevated plateaus, generating a highly heterogeneous relief. Geochemical data indicates widespread volcanism occurred across the Anatolian region, with magmatic intrusions and eruptive centers developing along fault zones and extensional basins (Ersoy and Helvacı, 2016; Kurum et al., 2008; Özkul et al., 2022), which likely played a role in shaping both the morphology and sedimentary environments of Miocene Anatolia. For Anatolia, we rely on the paleogeography reconstruction from Straume et al. (2024) in our Phase 2 paleogeography. For all other regions of Europe (except as outlined elsewhere, i.e., the Tethys and surrounds), we rely on the paleogeography reconstruction from "updated Herold".

Asia

One of the most studied topographic features, the Tibetan-Himalayan complex imposes substantial forcing on Asia's climate and is associated with atmospheric teleconnection patterns both in present day (Molnar et al., 2010) as well as past climates (Farnsworth et al., 2019b; Huber and Goldner, 2012; Sarr et al., 2022). Its elevation and horizontal extent influences both the Indo-Asian and East Asian Monsoons and regions of high biodiversity, while far field effects impact the high latitude jet stream (Acosta and Huber, 2020; Geen et al., 2020). Much of the elevation gain of the Tibetan Plateau and Himalayan Mountains was due to the northward movement of the Indian subcontinent and single stage collision into Eurasia which began ~60 Mya (Ding et al., 2022). While Arabia–Eurasia collision

https://doi.org/10.5194/egusphere-2026-3595
Preprint. Discussion started: 3 August 2026

initiated ~35 Mya (Wang et al., 2025) may have indirectly impacted the western regions west of the Tibetan-Himalayan orogen, such as the Pamir. During the Miocene, most of the plateau was near its present-day elevation above 4 km. However, the presence of a substantially higher Himalayan front (>5 km) during the Middle Miocene remains debated (Botsyun et al., 2019; Spicer et al., 2021b, a), while its elevation and ability to redirect moisture (Acosta and Huber, 2017; White et al., 2017) will impact how climate models simulate Indo-Asian climate. Although its full impact is resolution dependent, coarse grid paleo-models still capture first order effects on water vapor transport, wind speed, and precipitation (Johnson et al., 2016). Water isotope and paleobotanical evidence suggest the Himalayas exceeded 5 km elevation during the Early–Middle Miocene (18–15 Ma). For MioMIP2 Phase 2, we maintain the 4 km elevation of Herold et al. (2008) for the Tibetan Plateau but modify the Himalayan front to be uniformly at 5 km (Figure S6) in general agreement with Wang et al. (2022). Northern Tibet plays a crucial role in strengthening the East Asian summer monsoon and biodiversity in the region (Li et al., 2021), as well aridification of central Asia. The timing of the uplift of northern Tibet is poorly constrained due to the scarcity of paleo-altimetric data from the region. By the Middle Miocene conflicting estimates suggest a height of anywhere between 1.4 km to near-present elevations (Wang et al., 2025). A recent study by Miao et al. (2022) has suggested a later uplift, with elevations at ~ 2–3 km in the Middle Miocene and only achieving a near-present elevation by the Late Miocene (8–6 Mya).

The major topographic features found in Mongolia are the Tian Shan and Altai mountains. These mountain ranges act as barriers to moisture from westerly mid-latitude flow, preventing rainfall from entering the Gobi Desert. By ~ 15 Mya, across inland eastern Asia (e.g., Chinese Loess Plateau, central China, and the northeastern Tibetan Plateau) climate proxy-evidence indicate progressive aridification, marked by a stepwise shift from sub-humid to arid conditions (Barbolini et al., 2020). The orogenic sequence of the Tian Shan and Altai mountains are controversial, with much of the evidence suggesting major uplift toward its present-day elevation during the Late Miocene (Caves, 2017; Rugenstein et al., 2022). To revise the “updated Herold” paleogeography, we lower both Tian Shan and Altai mountains to be half of the present-day elevation (Figure S6). However, much work is still needed to determine the

https://doi.org/10.5194/egusphere-2026-3595
Preprint. Discussion started: 3 August 2026

extent of uplift between the Early to Late Miocene, so further revision of the Mongolian mountains should be done as new evidence becomes available.

The western Eurasian mountains consist of the southwestern Zagros belt and the greater Iranian Plateau. As part of the northward movement of the Arabian plate toward Eurasia, the western Eurasian mountains orogeny began during the Late Oligocene to Early Miocene and continued throughout the Miocene (Mouthereau, 2011). This sequence is inherently tied to the closure of Tethys Seaway (Straume et al., 2024). The greater Iranian Plateau has immense impact on the Indo-Asian monsoon as it acts a barrier for northwesterly dry air from entering the Indo-Gangetic plains and disrupting the monsoon environment as suggest by modeling work (Acosta and Huber, 2020; Farnsworth et al., 2019b; Sarr et al., 2022; Zuo et al., 2024). Stratigraphic evidence from the Early Miocene suggests the region was still below sea level, with subsequent rapid uplift of ~2 km occurring between the Early to Middle Miocene and reaching near present-day elevation during the Late Miocene (Mouthereau, 2011). However, constrained age and paleo-altimetric elevation estimates are still lacking, however the main uplift, deformation, and exhumation across the Zagros and the wider Arabia–Eurasia collision zone likely began later, at ~15–12 Ma (Mouthereau, 2011). Here, we modify the "updated Herold" paleogeography by implementing the reconstruction of Straume et al. (2024) for the Zagros and Iranian Plateau (Figure S5). However, uplift rates across the region are complex and most likely require further refinement as more data becomes available.

3.3.2 Land surface

Ice sheets

A key constraint for the ice sheet boundary conditions to be prescribed in MioMIP2 Phase 2 is that they should be physically realistic, and so we have therefore considered output from state-of-the-art 3D thermodynamical ice sheet models. An inventory of recent studies simulating the Antarctic Ice Sheet during the Miocene is given in Table 3. These studies comprise only of equilibrium simulations, because transient behavior of the Antarctic Ice Sheet is currently still understudied and under constrained (Stap et al., 2022). The Antarctic Ice Sheet was dynamic throughout the Middle Miocene and even during the MCO (Gasson et al., 2016; Levy et al., 2016), so defining one ice sheet extent as

https://doi.org/10.5194/egusphere-2026-3595
Preprint. Discussion started: 3 August 2026

representative of the MCO is challenging. For the CORE experiment, the ice sheet configuration chosen attempts to reflect this as we have purposely not selected the minimum ice sheet extent during peak warmth (McKay et al., 2025). Sensitivity experiments with larger and smaller Antarctic Ice Sheets are discussed in Section 3.4.3.

Table 3: Inventory of recent studies, using 3D thermodynamical ice sheet modelling studies used to address the Antarctic Ice sheet during the Miocene

Study	Ice sheet model + forcing climate model	Setup climate forcing	Research goal
Gasson et al. (2016)	PSU-ISM + GENESIS	Climate downscaled through regional climate model, asynchronous coupling	Sensitivity to bedrock topography, climate and ocean forcing, comparison to data (AND-2A)
Paxman et al. (2020)	PSU-ISM + GENESIS	Climate downscaled through regional climate model, asynchronous coupling, offline forcing	Sensitivity to bedrock topography
Halberstadt et al. (2021)	PSU-ISM + GENESIS	Climate downscaled through regional climate model, asynchronous coupling	Sensitivity to bedrock topography, climate and ocean forcing, comparison to data (AND-2A)
Stap et al. (2022)	IMAU-ICE + GENESIS	Transient interpolation between warm (high CO_2, no ice cover) and cold (low CO_2, large EAIS) climate simulations	Sensitivity to ice sheet - atmosphere interactions
Segalla et al. (unpublished)	Yelmo + IPSLCM5A2	Forcing YELMO with climate outputs	Sensitivity to CO_2 (420 ppm & 700 ppm), insolation (min max at 75°S) and ice sheet

For the CORE experiment, the setup used by Halberstadt et al. (2021) has the advantage that, a) compared to Paxman et al. (2020) and Stap et al. (2022), it consists of a coupled climate-ice sheet model rather than a stand-alone ice sheet model, and b) compared to Gasson et al., (2016), it uses the Paxman et al. (2019) reconstruction pertaining to 14 Ma for the bedrock and bathymetry boundary conditions, which, as described in Section 3.3.1, is used as topography in the MioMIP2 Phase 2 paleogeography. We consider the Halberstadt et al. (2021) simulation with atmospheric CO_2 set at 930 ppm and an “interglacial” astronomical configuration (eccentricity=0.05, obliquity=24.5, precession=270) as best suited for the CORE experiment (Figure 3). The results of this simulation are broadly in-line with data

https://doi.org/10.5194/egusphere-2026-3595
Preprint. Discussion started: 3 August 2026

studies suggesting at least a part of the East Antarctic Ice Sheet remained during the MCO (Miller et al., 2024). It is also consistent with evidence for open marine deposits in the Ross Sea from ANDRILL-2A and IODP Site U1521 between 16.5 and 15.9 Ma (McKay et al., 2019; Pérez et al., 2021), and ice-free conditions in the Transantarctic Dry Valleys (Chorley et al., 2022; Lewis and Ashworth, 2016; Sugden, 1996). However, the presence of ice-rafted debris (IRD) at ANDRILL-2A throughout the Miocene suggest that Transantarctic glaciers were present and reached the coast even during the warmest interglacials (Levy et al., 2016). The CORE ice sheet is consistent with extensive ice-free conditions in the Wilkes Subglacial Basin (Sangiorgi et al., 2018) and periodic ice-free conditions in the Sabrina Coast (Gulick et al., 2017; Montelli et al., 2020). We note that the CORE ice sheet is larger (21.2 million km^3) than that used in the "updated Herold" paleogeography (6 million km^3) (Burls et al., 2021). The small ice sheet sensitivity experiment recommended in Section 3.4.3 is an ice sheet comparable to the “updated Herold”.

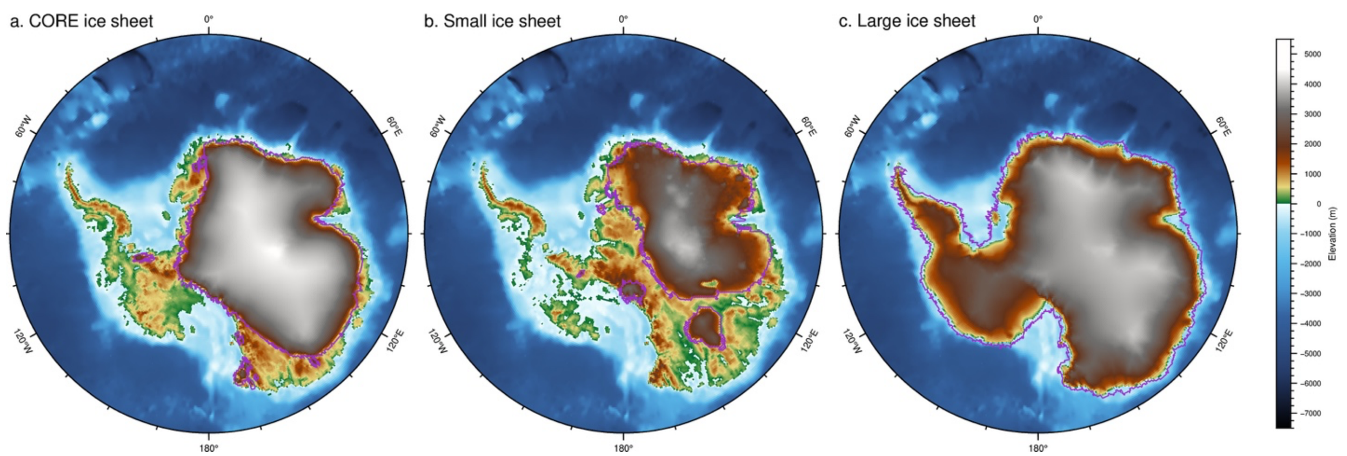

Figure 3: Ice sheet boundary conditions for MioMIP2 Phase 2. a. CORE experiment; b. the large; and c. small ice sheet sensitivity experiments described in Section 3.4.3. The purple line indicates the edge of the ice sheet.

Constraining the extent of glaciation (if any) on Greenland during the Middle Miocene is equally challenging. There is evidence for IRD in cores proximal to Greenland since ~18 Ma (Thiede et al., 2011); however, the temporal resolution of these records is low and individual glacial-interglacial cycles are not resolved. The extent of glaciation is difficult to determine from these records and transportation by sea ice cannot be ruled out. For the PlioMIP PRISM4 reconstruction, the Greenland

https://doi.org/10.5194/egusphere-2026-3595
Preprint. Discussion started: 3 August 2026

Ice Sheet extent is 25% of the present-day area (Dowsett et al., 2016). Given that the Middle Miocene was warmer than the middle Pliocene, the Greenland Ice Sheet likely had an even smaller extent. Global cooling and uplift of the Greenland continent since ~10 Ma also means that glaciation was more favorable during the Late Miocene (Herbert et al., 2016; Jakobsen et al., 2025; Japsen et al., 2014). Given that any ice sheet would likely have been small in extent and would have limited impact on the climate system, especially given the resolution of the models typically used to simulate the Miocene, ice-free conditions on Greenland are used for the CORE experiment.

Vegetation

Whilst some climate models now allow for dynamical vegetation modelling, there is a need for MioMIP2 to generate a baseline vegetation distribution that can be used by modelling centers without a dynamical vegetation component, to initialize the models with dynamical vegetation, and to allow for comparison of simulated vegetation with the data reconstructions. The MioVeg1 group has updated previous Middle Miocene vegetation syntheses (Herbert et al., 2016; Jakobsen et al., 2025; Japsen et al., 2014; Pound et al., 2012) and filled in the gaps regionally using modeled vegetation fields selected based on paleobotanical expert-opinion (Bradshaw et al., 2025). The modeled vegetation fields were derived from MioMIP1 climate simulation using the BIOME4 (Kaplan, 2001) vegetation model. The resulting Middle Miocene vegetation reconstruction (Bradshaw et al., 2025) has been updated to the MioMIP2 Phase 2 paleogeography as shown in Figure 4 to provide the vegetation boundary conditions for MioMIP2 (Table 2). A key constraint of the approach taken in MioVeg1 was that it was more important for the simulated vegetation to best match proxy-based vegetation reconstructions from the paleorecord than it was for the same model or the same model boundary conditions to be used in the model-data synthesis. This means that the vegetation reconstructions are a blend of different models and CO_2 concentrations but the overall vegetation distribution reconstructed is as close to the available paleobotanical data as possible.

While no vegetation-specific sensitivity studies are proposed for MioMIP2 (Table 1), the MioVeg1 reconstruction effort highlighted novel uncertainties that could be the target of individual modelling sensitivity studies and proxy studies. The paleobotanical data that was used to match the modelled

https://doi.org/10.5194/egusphere-2026-3595
Preprint. Discussion started: 3 August 2026

vegetation may partly have a wet bias as a result of more favorable preservation conditions in wetter environments, at least for plant macrofossils (Xing et al., 2016). In contrast, pollen records tend to reflect regional vegetation, thereby also capturing plant communities farther away from lakes and wetlands (Traverse, 2007). In addition, evidence of plants that preserve in drier facies such as paleosols, such as phytoliths and *n*-alkanes (Strömberg et al., 2018; Tweedy et al., 2025), may represent an opportunity to fill gaps in the paleobotanical record. Fire-vegetation feedbacks may have been a significant limiting factor to forest expansion in the Middle Miocene. In contemporary ecosystems, pyrophylic and pyrophobic vegetation can grow in climatically identical conditions and simply be maintained by promotion or suppression of fire by plant species within those vegetation types, e.g., Staver et al., (2011). As BIOME4 is an equilibrium global vegetation model, it does not incorporate a disturbance regime such as fire and therefore MioVeg1 may be overrepresenting vegetation types such as dense forest, and high fire recurrence vegetation types such as grasslands may be underrepresented in some regions. In addition to differences in primary productivity and carbon storage between grasslands and forests, underrepresenting grasslands may affect hydrological fluxes, aerosol production and albedo. In certain areas grassland is expected, but not produced in MioVeg1, such as the continental interior of North America. Likewise, MioVeg1 features extensive Arctic and sub-Arctic grasslands, but there is no Middle Miocene paleobotanical data that indicates grasslands in these regions. Sensitivity tests by individual modelling groups may be desirable to determine the effect of grassland underrepresentation (or overrepresentation). Future Miocene paleo-data compilations could focus on amplifying evidence for fire-controlled ecosystems, such as tropical (C_4) savannas, by including fire markers (e.g., charcoal, microfossils PAHs) (Karp et al., 2020; Vachula et al., 2021) and stable carbon isotopic evidence for C_4 biomass (Cerling et al., 1997).

Modelling groups should use lookup Table 4 for prescribing the phenology variables associated with each biome: leaf area index, stem area index, top and bottom tree heights.

https://doi.org/10.5194/egusphere-2026-3595
Preprint. Discussion started: 3 August 2026

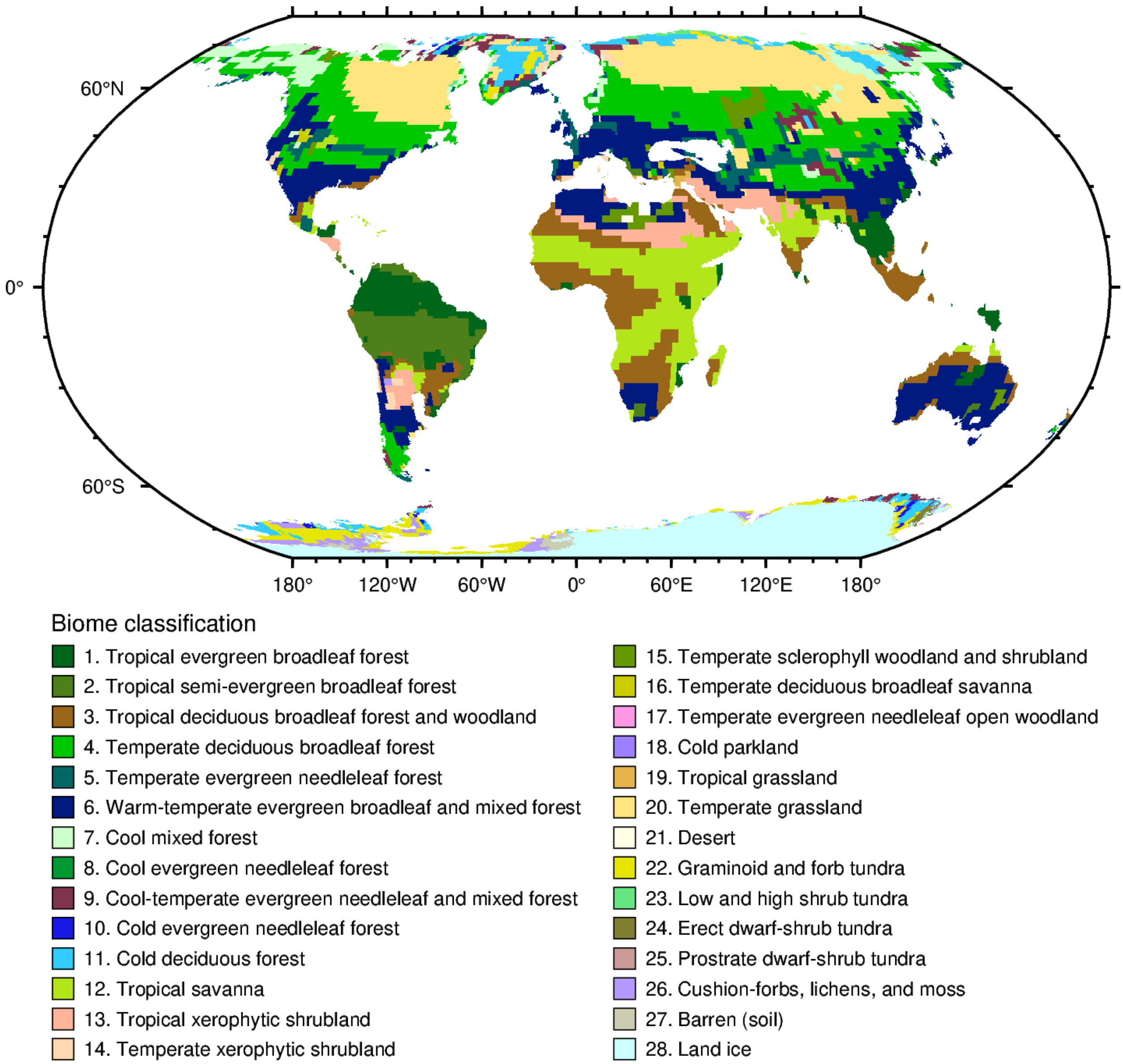

Figure 4: MioMIP2 Phase 2 CORE experiment biome orders. Biome reconstruction is based on Bradshaw et al. 2025 and updated to the MioMIP2 Phase 2 paleogeography, including minor updates to proxy locations in Central Asia (due to differences in the plate tectonic reconstruction) and the addition of land ice as described in the Section 3.3.2.

https://doi.org/10.5194/egusphere-2026-3595
Preprint. Discussion started: 3 August 2026

Table 4. Vegetation model parameters. Values taken from Haywood et al. (2010)

Key	Biome	Root depth (m)	Snow free albedo	Cold deep snow albedo	Surface resistance to evaporation (sm-1)	Surface roughness length (m)	Canopy water (surface) capcity (mm)	Vegetation infiltration enhancement	Leaf area index of vegetated fraction	Canopy height of vegetated fraction (m)	Vegetation fraction
1	Tropical evergreen forest	1.430	0.121	0.230	129	1.140	0.690	5.730	8.58	29.400	0.95
2	Tropical semi-deciduous forest	1.430	0.121	0.230	129	1.140	0.690	5.730	8.58	29.400	0.95
3	Tropical deciduous forest/woodland	0.696	0.137	0.436	98	0.685	0.592	3.060	4.85	12.800	0.80
4	Temperate deciduous forest	1.080	0.136	0.355	96	0.851	0.585	5.280	4.68	13.400	0.95
5	Temperate conifer forest	0.840	0.136	0.255	85	0.901	1.130	5.500	5.79	18.100	0.95
6	Warm-temperate mixed forest	0.975	0.131	0.300	91	0.900	0.860	5.500	5.32	16.100	0.95
7	Cool mixed forest	0.975	0.131	0.300	91	0.900	0.860	5.500	5.32	16.100	0.95
8	Cool conifer forest	0.840	0.136	0.255	85	0.901	1.130	5.500	5.79	18.100	0.95
9	Cold mixed forest	0.975	0.131	0.300	91	0.900	0.860	5.500	5.32	16.100	0.95
10	Evergreen taiga/montane forest	0.840	0.136	0.255	85	0.901	1.130	5.500	5.79	18.100	0.95
11	Deciduous taiga/montane forest	0.840	0.127	0.345	85	0.901	0.950	5.500	3.89	9.490	0.95
12	Tropical savanna	0.830	0.176	0.530	91	0.270	0.690	2.730	5.05	6.820	0.95
13	Tropical xerophytic shrubland	0.690	0.186	0.590	86	0.164	0.730	2.180	4.06	2.690	0.85
14	Temperate xerophytic shrubland	0.680	0.176	0.595	78	0.243	0.800	2.250	2.71	1.320	0.90
15	Temperate sclerophyll woodland	0.910	0.148	0.460	89	0.602	0.675	4.030	3.94	8.820	0.90
16	Temperate broadleaved savanna	0.920	0.151	0.455	87	0.623	0.585	4.230	3.95	9.630	0.95
17	Open conifer woodland	0.700	0.157	0.410	79	0.603	0.920	4.100	4.67	12.900	0.90

18	Boreal parkland	0.700	0.157	0.410	79	0.603	0.920	4.100	4.67	12.900	0.90
19	Tropical grassland	0.690	0.179	0.590	86	0.164	0.730	2.180	4.06	2.690	0.85
20	Temperate grassland	0.478	0.189	0.699	66	0.029	0.531	1.470	2.13	0.488	0.88
21	Desert	0.160	0.250	0.773	98	0.031	0.543	0.725	2.75	1.330	0.10
22	Steppe tundra	0.160	0.150	0.800	76	0.004	0.580	0.700	1.00	1.000	0.40
23	Shrub tundra	0.560	0.159	0.650	66	0.204	0.830	1.950	2.11	1.390	0.90
24	Dwarf-shrub tundra	0.160	0.150	0.800	76	0.004	0.580	0.700	1.00	1.000	0.40
25	Prostrate shrub tundra	0.160	0.150	0.800	76	0.004	0.580	0.700	1.00	1.000	0.40
26	Cushion-forb, lichen, moss tundra	0.160	0.150	0.800	76	0.004	0.580	0.700	1.00	1.000	0.40
27	Barren (soil)	0.100	n/a	0.800	100	0.000	0.500	0.500	0.00	0.000	0.00
28	Land ice	0.000	0.750	0.800	0	0.000	0.000	0.000	0.00	0.000	0.00

Soils

As part of the MioVeg1 effort (Bradshaw et al., 2025), a new soil reconstruction for the MCO was constructed using the available paleosol data for the Middle Miocene (Retallack, 2022). Soil order transformations were applied to MCO biome reconstructions where available, or simulated biomes where proxy reconstructions were not available, and these were used to fill the gaps in the paleosol record (Figure 5).

Lakes

There are no prescribed lakes in the MioMIP2 boundary conditions (Table 2). As described in Section 3.3.1, the Pebas System in South America should be prescribed as wetland. The Paratethys should be treated as a marginal sea.

https://doi.org/10.5194/egusphere-2026-3595
Preprint. Discussion started: 3 August 2026

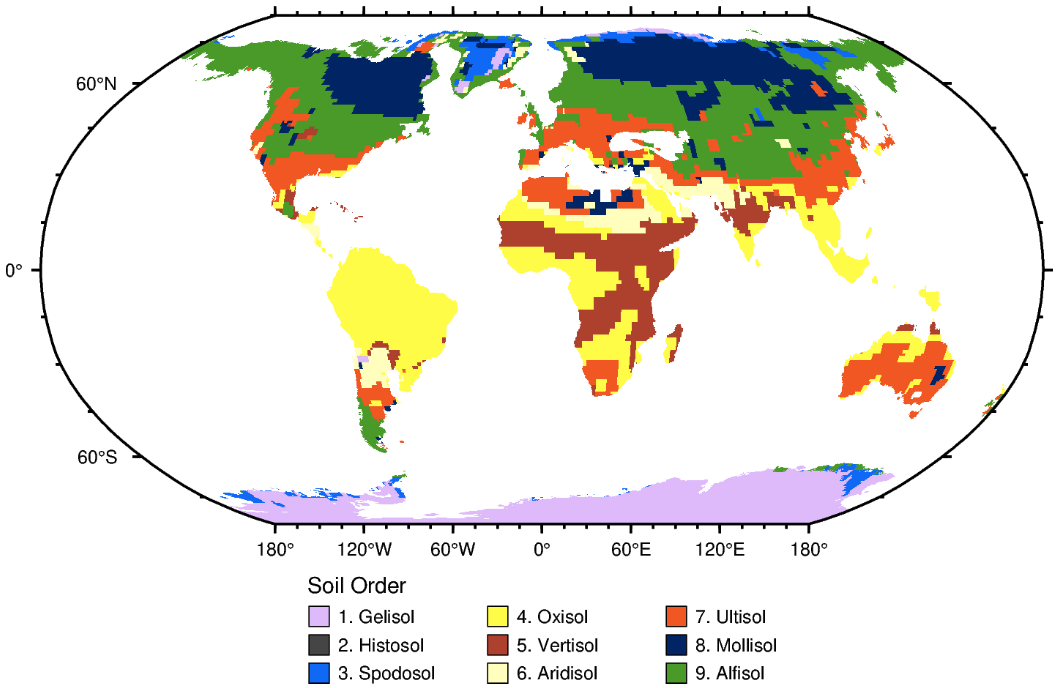

Figure 5: MioMIP2 Phase 2 CORE experiment soil orders. Soil reconstruction is based on Bradshaw et al. (2025), and updated to the MioMIP2 Phase 2 paleogeography, including minor updates to proxy locations in Central Asia (due to differences in the plate tectonic reconstruction) and the addition of land ice.

River runoff

The routing of riverine freshwater fluxes can influence ocean salinity and overturning circulation. This is particularly important in high CO_2 climates as the freshwater balance of the Arctic Basin and other high latitude areas can shift towards too much runoff for deep convection. River routing files are provided as boundary conditions (Table 2), derived from both the low (2° x 2°; Figure 6) and high (0.25° x 0.25°; Figure S10) resolution paleogeography files. It is recommended that modelling groups use the version based on the low (2° x 2°) resolution to help ensure consistency in river routes across different model resolutions. The river routing model uses the elevation gradient to calculate flow direction. For runoff purposes, the paleotopography is first adjusted to remove any land-based sink points (i.e., lakes), using the "FillDepressions" algorithm from the "RichDEM" software package (Barnes, 2016). This algorithm automatically raises the level of any local minima of topography to the lowest adjacent saddle point, i.e., it finds an optimal pathway through low-lying topography so that

https://doi.org/10.5194/egusphere-2026-3595
Preprint. Discussion started: 3 August 2026

rivers drain into the ocean in all cases. The adjusted paleotopographies are then converted into flow directions using a downslope relocation algorithm. The flow directions are provided as a common river routing scheme to ensure consistency across the MioMIP2 Phase 2 simulations (Figure 6). Modelling groups are encouraged to use this common river runoff scheme (low 2° x 2° resolution, so that the simulated differences in ocean salinity across models are primarily the result of simulated differences in precipitation minus evaporation fields and the associated runoff rather than differences in the configuration of drainage basins. If modelling groups implement a different runoff scheme, this should be clearly explained and documented.

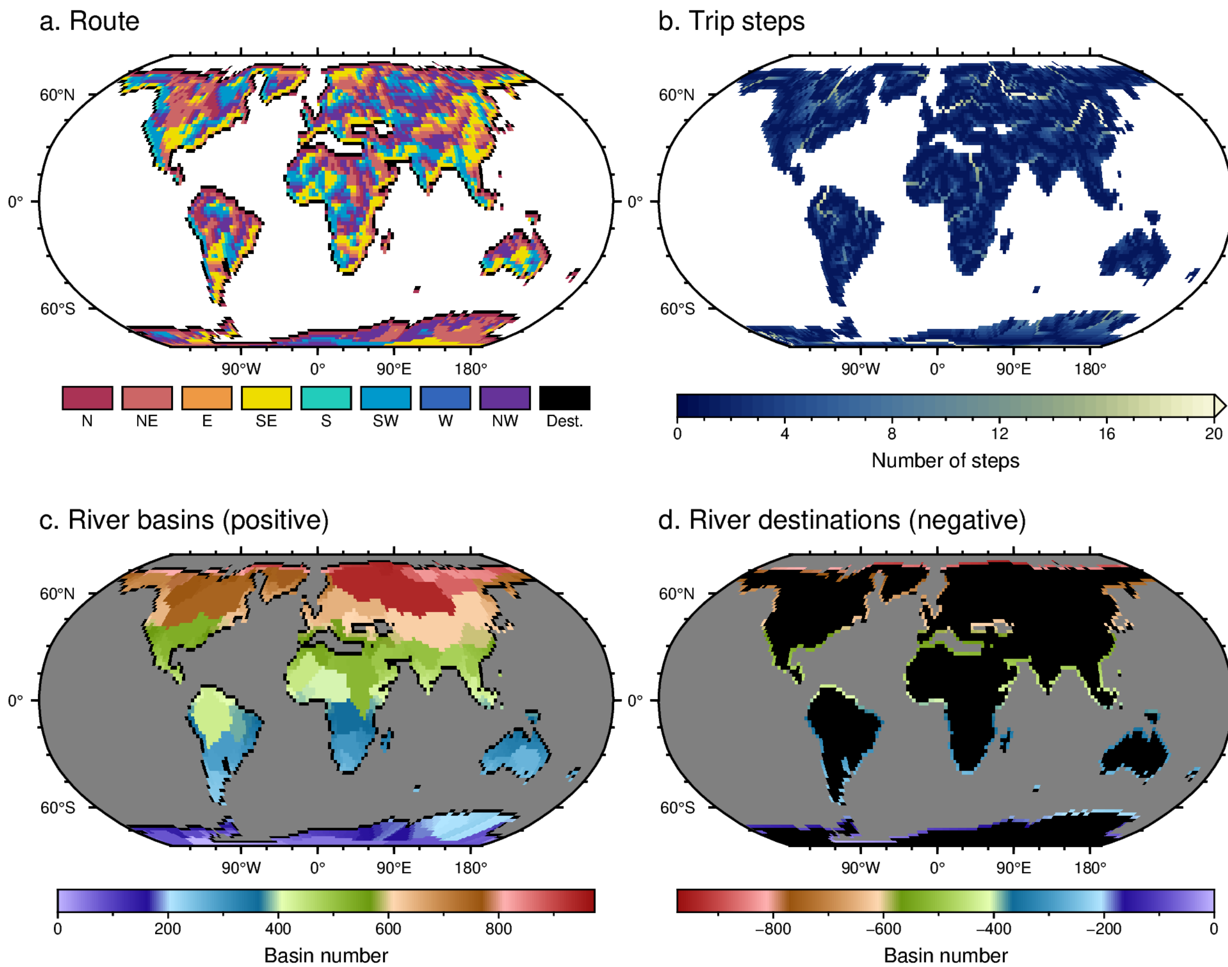

Figure 6: MioMIP2 Phase 2 CORE experiment river routing scheme at 2° x 2° resolution. a. river routes, direction of runoff in each grid cell where 'Dest' refers to the ocean destination; b. river trip steps, demonstrating the number of steps for a river to get to an ocean (i.e., major drainage pathways are indicated by a higher number of steps); c. river basins and d. river destinations, showing the source and destination of unique drainage points based on their unique positive value (panel c) and corresponding negative value (panel d), respectively.

https://doi.org/10.5194/egusphere-2026-3595
Preprint. Discussion started: 3 August 2026

3.3.3 Greenhouse gas concentrations

Reconstructing the concentration of atmospheric CO_2 during the Miocene has been the subject of considerable and ongoing research, using a wide range of proxy types. Pioneering early CO_2 reconstructions based on boron isotope and alkenone data (Pagani et al., 1999; Pearson and Palmer, 2000) yielded relatively low and invariant values of ~200–300 ppm, which are now considered unreliable (Rae et al., 2021b; THE CENOZOIC CO2 PROXY INTEGRATION PROJECT (CENCO2PIP) CONSORTIUM, 2023). Next generation reconstructions using these approaches (Bolton et al., 2016; Foster et al., 2012b; Greenop et al., 2014; Mejía et al., 2017; Rae et al., 2021b; Sosdian et al., 2018; Stoll et al., 2019; Super et al., 2018; Witkowski et al., 2024; Zhang et al., 2013), along with reconstructions from plant leaf stomatal proxies (Beerling et al., 2009; Franks et al., 2014; Grein et al., 2013; Kürschner et al., 2008; Londoño et al., 2018; Royer et al., 2001; Steinthorsdottir et al., 2021a; Wang et al., 2015), plant carbon isotopes (Cui et al., 2020; Steinthorsdottir et al., 2021a), and paleosol data (Breecker and Retallack, 2014; Ji et al., 2018), have tended to yield higher and more variable CO_2 concentrations (~400–1000 ppm), coupled to changes in Miocene climate; see Steinthorsdottir et al. (2021b) for a detailed review of Miocene proxy data. Such CO_2-climate coupling is well demonstrated in the recent CO_2 proxy compilations (Rae et al., 2021b; THE CENOZOIC CO2 PROXY INTEGRATION PROJECT (CENCO2PIP) CONSORTIUM, 2023), which have revised earlier studies.

While the structure of relative changes in CO_2 reconstructions are often relatively robust, significant uncertainty remains in determining absolute CO_2 values due to structural uncertainties in calibrations or other secondary assumptions, including for the boron isotope and phytoplankton $\delta^{13}C$ data which make up the majority of Miocene CO_2 estimates (Rae et al., 2021b; THE CENOZOIC CO2 PROXY INTEGRATION PROJECT (CENCO2PIP) CONSORTIUM, 2023).

For boron isotopes, a key uncertainty is the boron isotopic composition of seawater ($\delta^{11}B_{sw}$), required to convert a foraminiferal $\delta^{11}B$ measurement into a reconstruction of paleo pH, from which CO_2 can be estimated. As $\delta^{11}B_{sw}$ varies with a ~10 Myr residence time (Lemarchand et al., 2000), it is likely to have

https://doi.org/10.5194/egusphere-2026-3595
Preprint. Discussion started: 3 August 2026

been different in the Miocene compared to the present day. Current estimates of Miocene $\delta^{11}B_{sw}$ are provided by Greenop et al., (2017), but the data have substantial uncertainties. Using the original fit to these data, Sosdian et al., (2018) obtain CO_2 values of ~300–800 ppm for the MCO, and these values are adopted in the Cenozoic CO_2 Proxy Integration Project (CENCO2PIP) Consortium (2023) compilation. However, recent studies have noted that the original fit of Greenop et al. (2017)'s has a rate of change faster than that permitted by the long residence time of boron in seawater, which dictates a more gradual $\delta^{11}B_{sw}$ evolution. Using a very simple fit to the $\delta^{11}B_{sw}$ data consistent with this slow rate of change, Rae et al. (2021b) obtain lower pH and thus higher CO_2 values, spanning ~600–1400 ppm in the MCO. Whiteford et al. (2024) use a more statistically sophisticated and robust Gaussian process method to fit the $\delta^{11}B_{sw}$ data and find still lower pH suggesting central CO_2 values in the MCO of ~860 ppm.

For phytoplankton proxies, where $\delta^{13}C$ is measured, the main uncertainties are the assumptions in $\varepsilon_{p,}$ the carbon isotope fractionation between dissolved CO_2 in seawater and phytoplankton organic matter (often alkenones), needed to convert measurements into a reconstruction of atmospheric CO_2 (Badger et al., 2019; Stoll et al., 2019; Zhang et al., 2020). Diffusion model calibrations have typically yielded MCO values of ~400–600 ppmv (Super et al., 2018; Zhang et al., 2013). Iterations of this approach have used cell size and productivity data to better constrain secondary calibration parameters (Bolton et al., (Bolton et al., 2016; Zhang et al., 2020), but such data are sparse in the MCO. An alternative approach is to use empirical relationships between ε_p and ice core CO_2 data from the Quaternary, which yields MCO CO_2 values of ~300–1100 ppm (Rae et al., 2021b). This range of approaches inform the values in the Cenozoic CO2 Proxy Integration Project (CENCO2PIP) Consortium (2023) reconstruction. Calibration models have also recently been re-evaluated using an extensive compilation of laboratory culture data (Stoll et al., 2019), highlighting an important role for active carbon concentration, and suggesting revision is required to diffusion centric models. Application to published ε_p data (Bolton et al., 2016; Zhang et al., 2013) yields much higher MCO CO_2 estimates, ranging from ~600 to over 2000 ppm (Steinthorsdottir et al., 2021c; Stoll et al., 2019). Estimates from tectonic degassing and carbon budget modelling leads to values of 500–1100 ppm for the MCO (Herbert et al., 2022). Finally, recent

https://doi.org/10.5194/egusphere-2026-3595
Preprint. Discussion started: 3 August 2026

$\delta^{13}C$ data in sterane and phytane compounds (Witkowski et al., 2024) suggest MCO CO_2 concentrations around ~1100 ppm from ~18–16 Ma, and ~640 ppm at 15 Ma.

Leaf gas-exchange based proxies (Franks et al., 2014; Konrad et al., 2017) use a mechanistic approach to fossil leaf-based CO_2 reconstructions. Gas-exchange proxies are increasingly used over the empirically calibrated stomatal index proxy. This is because stomatal index reconstructions require a nearest living relative for calibration of SI to CO_2 (e.g., Kürschner et al., 2008), but stomatal and other cell densities are more responsive to light regime than they are to CO_2 (Poorter et al., 2025) and related species are less consistent in their carbon assimilation rates, than phylogenetically disparate but ecologically similar species (Reichgelt and D'Andrea, 2019). Moreover, gas-exchange models allow the user to apply an inclusive error range (based for example on the uncertainty inherent in plant metabolic processes) whereas stomatal index error is entirely based on residuals in calibration. Taken together, the potential for systemic bias in stomatal index is too great and we therefore recommend that stomatal index-based reconstructions are omitted when incorporating plant-based CO_2 proxies for choosing simulations.

The upshot is that the choice of a single CO_2 concentration for the MioMIP2 simulations remains challenging. The original approaches to conversion of boron isotope and phytoplankton data to CO_2, along with some plant-based proxies, fall around the 2x pre-industrial CO_2 value of 560 ppmv, close to the central estimate of ~500 ppm for the MCO reported by the (The Cenozoic CO2 Proxy Integration Project (CENCO2PIP) Consortium, 2023) compilation. However, application of more recent estimates of $\delta^{11}B_{sw}$ and updated alkenone calibrations discussed above tends to yield higher values, closer to the 840 ppm (3x pre-industrial). We thus encourage modelling groups to run simulations at both 2x and $3xCO_2$ where possible, with $3xCO_2$ chosen for the CORE experiments. Given that the concentration of other greenhouse gases, such as methane, are large unknown for the MCO simulations spanning the 2x to 3x CO_2 range help to address this uncertainty. Additionally, Burls et al., (2021) found that only MioMIP1 simulations forced with $3xCO_2$ overlapped with proxy-based MCO global mean surface

https://doi.org/10.5194/egusphere-2026-3595
Preprint. Discussion started: 3 August 2026

temperature estimates, while still underestimating the degree of polar amplified warmth compared to the surface temperature reconstructions.

3.3.4 Aerosols

Atmospheric aerosol burdens in deep-time paleoclimates such as the Miocene are highly uncertain, and the representation of aerosols in Earth system models is continuously evolving. As such, we follow the approach taken for DeepMIP-Eocene Phase 1 and 2 (Lunt et al., 2017) and leave the implementation of aerosol fields or emissions to the discretion of each modelling group while asking them to document how they have implemented aerosols. Options include leaving aerosol distributions or emissions identical to pre-industrial while taking account of the changed land–sea mask, or for models that treat aerosols prognostically simulating the impact of Miocene boundary on emissions (e.g., dust in CESM). Modeling groups can also consider the Heavens et al. (2012) method, which computes the zonal mean aerosols distribution based on the paleogeography. This step is optional since many modeling groups compute aerosol parameterization differently.

3.3.5 Tidal Dissipation

Tidal energy dissipated in the ocean drives vertical mixing, which in turn sustains primary production (Tuerena et al., 2019) and can influence the meridional overturning circulation and thus meridional heat fluxes (Munk, 1966; Wunsch and Ferrari, 2004). Green et al., (2017, 2023), Ladant et al. (2024), Wilmes et al. (2021) and Huang et al. (2025) show that the representation of physics-based vertical mixing in Earth system model simulations could materially affected simulated ocean states in deep-time. Where feasible, modelling groups are therefore encouraged to explore sensitivity experiments incorporating Miocene tidal effects to account for tidally driven mixing. This can be done in two ways. First, existing tidal dissipation fields can be used to compute vertical diffusivities following, e.g., Schmittner and Egbert (2014). Alternatively, in a manner consistent with pre-industrial simulations, the approach of Simmons et al. (2004) can be used, where tidal currents are used to drive mixing associated with energy dissipation from breaking internal gravity waves. Explicit inclusion of tidal processes in the

https://doi.org/10.5194/egusphere-2026-3595
Preprint. Discussion started: 3 August 2026

CORE MioMIP2 simulations is not required but coordinated sensitivity studies may help to quantify the role of tidal mixing as a source of structural uncertainty in Miocene climate simulations.

3.3.6 Solar constant and astronomical parameters

The solar constant and orbital forcing parameters (eccentricity, obliquity, and precession) should be the same as used for the pre-industrial control experiment, except for in the solar constant and orbital forcing sensitivity experiments described in Table 1, Section 3.4.4 and Table 7.

3.3.7 Initial conditions

We do not make any recommendation on how each modelling group should initialize their atmosphere, land, and sea ice models given the relatively quick equilibration time of these components. The longer equilibration time of the ocean, as well as the warmth of the Miocene ocean relative to pre-industrial, leads us to recommend that modelling groups do not initialize their Miocene simulations from pre-industrial ocean conditions. Starting from relatively cold pre-industrial oceanic conditions results in a strong initial stratification of the Ocean due to both greenhouse gas and non-greenhouse gas (e.g., paleogeography, ice sheets, vegetation) induced warmth. This tends to slow, or shut off, deep ocean overturning resulting in simulations taking thousands of years to equilibrate the deep ocean via diffusive rather than advective processes, e.g., Figure S2 from Zhu et al., (2019). To mitigate this and speed up equilibration, we build on the knowledge gained by modelling groups during DeepMIP-Eocene Phase 1 (Lunt et al., 2017) and recommend that each modelling group either initialize from a previous Miocene simulation or apply a warming correction. Each group should use an approach most suitable for their model. Here we list a few possible approaches.

1) Adding a warming correction to an equilibrated pre-industrial run. Here modelling groups could apply a global mean (or ideally a zonal mean) temperature anomaly profile at the surface (above 500 m) and a uniform temperature anomaly everywhere below 500 m. Starting from pre-industrial conditions this warming correction would need to account for the anticipated equilibrium warmth induced by both the prescribed atmospheric CO_2 concentrations and the Miocene boundary conditions (see Table 5 for typical values from select MioMIP1 simulations).

https://doi.org/10.5194/egusphere-2026-3595
Preprint. Discussion started: 3 August 2026

For the CO_2 induced warming correction, modelling groups should start from initial temperature conditions as close to their model's equilibration state for a given CO_2 concentration if the climate sensitivity of the model is known from previous experiments e.g., an abrupt CO_2 experiment. For the paleogeography correction, the MioMIP1 ensemble mean warming for 1xCO_2 was estimated by Burls et al. (2021) to be ~2°C, but modelers should keep in mind that this will be model and boundary condition dependent. If available, modelling groups should use their model's previously equilibrated 1xCO_2 Miocene experiment to derive this correction. For example, for CESM 1.2 which has a climate sensitivity of 4.1°C , for a Miocene experiment with a prescribed CO_2 concentration of 560 ppmv, the temperature anomaly applied to a pre-industrial ocean state would be ~6.1°C (4.1°C + 2°C) in the top 500 m and 5.9°C below this (Table 5). Alternatively, see Steinig et al. (2026) for a formulation of the initial profile derived as a function of the estimated equilibrium global mean surface temperature for a given simulation. After the first few decades of a given simulation, we recommend checking to see if the global mean temperature (or deep ocean temperature below ~3000 m) is cooling or warming. If it is warming, check if deep water formation has shut off and consider adding an additional temperature anomaly. This initialization approach should help reach equilibrium for the deep ocean faster.

2) Initialize with a previous Miocene simulation that has been performed with the same model (or a similar version of the model). One caveat with this approach is if the previous model version had a lower climate sensitivity, or the Miocene boundary conditions supported less warming, then it might be necessary to check if deep water formation has shut off and consider adding an additional temperature anomaly as suggested above.
3) Initialize with proxy-data informed MCO fields by using the ocean temperature, salinity, and water isotope fields from Zhu et al. (2025). Zhu et al. (2025) performed water isotope-enabled, long-run simulations of the MCO using iCESM1.3 with the "updated Herold" boundary conditions. Unlike many existing simulations, these iCESM1.3 simulations have been run sufficiently long for the deep ocean to reach equilibrium. They were initialized from MCO simulations conducted with an earlier model version (Acosta et al., 2022) and have an

https://doi.org/10.5194/egusphere-2026-3595
Preprint. Discussion started: 3 August 2026

integration length of 9000 and 5000 years for the 3× and 1.5×CO_2 simulations, respectively. We suggest using the maximum likelihood estimation (MLE) of ocean temperature and salinity that produces the best agreement with both benthic foraminifera records and surface temperature reconstructions. The MLE fields, iCESM1.3_MLE_SALT_clim_eq.nc and iCESM1.3_MLE_TEMP_clim_eq.nc are available at https://doi.org/10.5281/zenodo.15883769 under the data folder.

Following the same rational as Lunt et al. (2017) that long-term geological sources and sinks of NaCl associated with crustal recycling make whole ocean salinity values for the MCO uncertain we recommend the modelling groups use the modern mean value of 34.7 psu.

If possible, water-isotope-enabled CORE simulations should be initialized using the MLE $\delta^{18}O_{seawater}$ field of Zhu et al. (2025), iCESM1.3_MLE_d18Osw_clim_eq.nc, available at https://doi.org/10.5281/zenodo.15883769 under the data folder. The MLE $\delta^{18}O_{seawater}$ field has a global mean of -0.55‰ based on the mean value of existing proxy-based estimates (Cramer et al., 2011; Lear et al., 2015; Rohling et al., 2022). This global mean value of -0.55‰ for the CORE experiment is more-or-less consistent with the $\delta^{18}O_{ice}$ based estimate of Gasson et al., (2016) for the corresponding CORE ice sheet volume (Section 3.3.2 and Table 6).

For the ice sheet sensitivity experiments described in Section 3.4.3 (Table 6), global mean $\delta^{18}O_{seawater}$ values are estimated to be -0.25‰ for the large ice sheet experiment and -0.94‰ for the small ice sheet experiment based on the $\delta^{18}O_{ice}$ estimates of Gasson et al., (2016) for the closest corresponding ice volumes and -1.11‰ for the no icesheet experiment based on the ice-free $\delta^{18}O_{seawater}$ estimate of Lhomme et al., (2005). Therefore, to achieve consistency with the ice sheet conditions, a global, spatially-uniform mean offset should be applied to the MLE $\delta^{18}O_{seawater}$ values at every grid point such that the global mean $\delta^{18}O_{seawater}$ value corresponds to the values mentioned above when initializing the respective sensitivity experiments.

For modelling groups running with ocean biogeochemistry, initialization should be based on pre-industrial global budgets of nutrients. Global mean alkalinity can be either kept at pre-industrial levels or slightly enhanced (Meissner et al., 2014).

Table 5: Miocene deep ocean (> 500 m) temperature (°C) increase relative to the pre-industrial simulation from MioMIP1 simulations (Burls et al., 2021). The range of temperatures for a single CO_2 level indicates the influence of different prescribed paleogeography, ice sheet sizes, model climate sensitivities and equilibration. These MioMIP1 simulation targeted ages ranging between ~ 20 and 12 Ma.

Model	1xCO_2	2xCO_2	3xCO_2	400 ppm	Other CO_2 levels (CO_2 : temp)	Reference
CCSM3-H	-	0.89	-	-	355 – 0.45	(Herold et al., 2011)
CCSM3-F	-	-	-	2.58	200 – 1.18	(Frigola et al., 2018)
CCSM4	-	-	-	2.99	-	(Burls et al., 2021)
CESM1	-	-	-	3.81	-	(Burls et al., 2021)
CESM1.2	3.02	5.9	6.62	4.60	-	(Acosta et al., 2022)
COSMOS	1.13	-	-	-	450 – 4.07	(Stärz et al., 2017a)
GISS-E2.1	-	-	-	-	456 – 2.33	(Naik et al., 2025)
HadCM3L-B	0.42–1.26	2.24–2.34	2.83–3.80	1.65–2.61	-	(Bradshaw et al., 2021)
HadCM3L-F	1.43	3.53	-	2.17	494 – 1.32 760 – 5.35	(Farnsworth et al., 2019a)
IPSLCM5	-	2.42–2.55	4.27	-	420 – 1.7	(Pillot et al., 2022)

3.3.8 Length of simulation

We suggest two categories of equilibrium criteria. Category 1 is stricter and for simulations to be used in model intercomparison studies targeting questions where deep ocean and dynamic ocean (ocean circulation) equilibration is necessary for drawing robust conclusions. At a minimum, the modelling groups should aim for their MioMIP2 Phase 2 CORE simulation and pre-industrial control simulation to fall in this category, and ideally also their MioMIP2 Phase 1 CORE simulation and any CO_2 sensitivity experiments. Category 1 is also appropriate for paleogeography sensitivity experiments, as these tend to focus on changes in ocean circulation. Category 2 is more relaxed and for simulations where thousands of years of integration are not computationally feasible, and the main purpose of the experiment is a topic where one might expect that a relatively robust conclusion can be reached even if the ocean circulation has not reached its final mean ocean circulation state (e.g., the first order effects of Miocene

https://doi.org/10.5194/egusphere-2026-3595
Preprint. Discussion started: 3 August 2026

boundary conditions on atmospheric circulation, the hydrological cycle, and global mean surface temperature change).

For Category 1, we suggest applying the criteria recently put forward by de Boer et al. (2025). These comprise tests for both thermal equilibrium and equilibration of ocean circulation:

- the mean top of atmosphere (TOA) imbalance should be < 0.1 Wm^{-2} for last 1000 years
- global mean ocean temperature trend at ~3500 m should be <1 °C/1000 years
- trends in the AMOC, PMOC and SOMOC should be < 1 Sv for the last 1000 years of the simulation

The longer-term trends are to avoid peaks due to multi-decadal and longer internal variability. The stability in the ocean circulation is evaluated through trends in the basin specific peaks of the Eulerian Meridional Overturning Circulation Streamfunction (MOC), calculated in the usual way of integrating the meridional velocities zonally and then from the surface to a variable depth e.g., Naik et al. (2025). There are various options for reducing this two-dimensional streamfunction field to a single value for each basin, and to ensure a consistent choice between modelling groups, we suggested that the Atlantic MOC (AMOC) and the Pacific MOC (PMOC) are defined by the maximum streamfunction values in their respective basins between 30°N and 60°N and below 500 m, and the Southern Ocean MOC (SOMOC) is defined as the minimum south of 60°S. The threshold criteria are then to have trends in the AMOC, PMOC and SOMOC that are < 1 Sv for the last 1000 years of the simulation.

Category 2 aligns with the recommendation for the 2nd phase of DeepMIP-Eocene (Lunt et al., 2026).

- the final 100 years of the simulations has a mean absolute TOA imbalance of less than 0.1 Wm^{-2} (or, for those models for which the TOA energy budget is not closed a similar imbalance to that of an equilibrated pre-industrial control simulation)
- global mean sea-surface temperatures that are not strongly trending (< 0.1°C per century).

https://doi.org/10.5194/egusphere-2026-3595
Preprint. Discussion started: 3 August 2026

3.3.9 Output format

To facilitate the planned products described in Section 5, the output and boundary conditions from each simulation completed should be uploaded to the DeepMIP database (Steinig et al., 2024). Instructions for uploading data are provided at https://www.deepmip.org/data/ and are similar to those described in Lunt et al (2026) for DeepMIP-Eocene-Phase2. As with other DeepMIP projects, we encourage groups to provide means and standard deviations of the last 100 years of their simulations for multiple variables, and monthly-mean timeseries of the last 100 years of their simulations for selected variables. Additionally, we ask that modelling groups upload full simulation-length annual time series of the following oceanic variables to diagnose the degree of equilibration: mean temperature at 3500 m, mean ocean ideal age tracer at 3500 m (if available), Atlantic MOC: maximum between 45°N and 68°N; Pacific MOC: maximum between 25°N and 58°N; Global GMOC: maximum global MOC north of 40°S; Southern Ocean MOC: absolute of minimum of the GMOC south of 60°S; Bottom MOC; absolute of minimum of the GMOC north of 60°S. All metrics should be calculated below 500 m depth to exclude the wind driven gyres (de Boer et al., 2025). Finally, if possible, modeling groups are asked to upload daily timeseries of surface temperature and precipitation fields from the last 100 years of their simulations.

Each output variable is stored in a separate file according to the following structure: directory = deepmip-miomip2-p1/<Family>/<Model>/<Experiment>/<Version>/<Averaging> for MioMIP2 Phase 1 and directory = deepmip-miomip2-p2/<Family>/<Model>/<Experiment>/<Version>/<Averaging> for MioMIP2 Phase 2. filename = <Variable>_<Model>_<Experiment>_<Version>.<Statistic>.nc
where: <Family> and <Model> describe the model used to carry out the simulations (see Table 1 in Steinig et al., 2024, for examples from DeepMIP-Eocene Phase 1). The <Experiment> options are listed in Table 1 of this paper. <Variable> represents the variable name. The variable names that should be used are listed on https://www.deepmip.org/data/ <Statistic> is either 'mean' (1 or 12 timesteps for annual or monthly means), 'std' (1 or 12 timesteps for annual or monthly means), 'time_series' (100, 1200 or 36500 timesteps) or omitted for the time-independent boundary conditions. The 'mean'

https://doi.org/10.5194/egusphere-2026-3595
Preprint. Discussion started: 3 August 2026

and 'std' files are stored in the <Averaging>=climatology directory and the larger 'time_series' files in the <Averaging>=time_series directory to facilitate efficient download options. Output on an irregular grid (oceanic or atmospheric) should be conservatively interpolated to a regular lat-lon grid prior to depositing it in the database, it is important that the global mean of relevant variables is conserved after interpolation to the regular grid.

3.4 Sensitivity studies

In addition to the CORE experiments, interested modelling groups are asked to perform several sensitivity experiments that will benefit from a multi-model assessment as documented below. Beyond the sensitivity experiments outlined here, individual modelling groups are encouraged to use the boundary conditions provided to perform single model studies that address additional questions of scientific interest within the modelling and proxy communities.

3.4.1 Sensitivity to CO_2

As described in Section 3.3.3, the choice of a single CO_2 concentration for the CORE experiments is challenging due to uncertainties in the available reconstructions. Alongside the CORE experiment at 3xCO_2 (840 ppm), which characterizes some recent data treatments (Rae et al., 2021b; Steinthorsdottir et al., 2021c; Stoll et al., 2019; Whiteford et al., 2024) groups are encouraged to run 2xCO_2 (560 ppm), as such levels are also commonly reconstructed for the MCO (Steinthorsdottir et al., 2021c; THE CENOZOIC CO2 PROXY INTEGRATION PROJECT (CENCO2PIP) CONSORTIUM, 2023). Additional sensitivity experiments include 1xCO_2 (280 ppm), to allow for the characterization of the climatic influence of non-CO_2 boundary conditions at the MCO, and 4xCO_2 (1120 ppm), bracketing the upper end of proxy reconstructions. Together, these simulations with multiple levels of atmospheric CO_2 levels can be used to evaluate the state dependence of climate and hydroclimate sensitivity (Caballero and Huber, 2013; Cramwinckel et al., 2023; Farnsworth et al., 2019a; Zhu et al., 2019).

https://doi.org/10.5194/egusphere-2026-3595
Preprint. Discussion started: 3 August 2026

3.4.2 Sensitivity to paleogeography

During the Miocene, tropical gateways were narrowing, whilst the polar gateways were broadening. Our current understanding of the impact of these gateway changes on ocean circulation and climate is dependent on the climate model and the specific background paleogeography in which they are investigated (Naik et al., 2025). While several single model studies have been performed, our understanding of the impact of gateways would benefit from more multi-model assessments in which a standard background paleogeography is used across models. The closure of the Central American Seaway has been associated with a strengthening of the AMOC (Brierley and Fedorov, 2016; Butzin et al., 2011; Lunt et al., 2008) but it is not a necessary condition (Krapp and Jungclaus, 2011). Likewise, the closure of the Tethys has been linked to an AMOC start up (Zhang et al., 2011), but again, other studies have found the gateway to have a negligible impact on the AMOC (Pillot et al., 2022). Focus has recently shifted to the Arctic gateways of Fram Strait, the Greenland Scotland Ridge and the Canadian Arctic Archipelago and their effects on the AMOC, with the results that are similarly conflicted. In general, the complete closing of the Arctic from the Atlantic is associated with salinification of the North Atlantic and a start-up of the AMOC (Hossain et al., 2021; Hutchinson et al., 2019; Roberts et al., 2009; Straume et al., 2022), but the impact of the depth of the Greenland Scotland Ridge (Stärz et al., 2017b) and the interplay of both gateways are more complex (Hossain et al., 2020). Some models find that the AMOC convection region shift from the Labrador Seas to the Nordic Seas as the ridge deepens (Hutchinson et al., 2019), whilst others suggest the deepening of the strait leads alternatively to a stronger or weaker AMOC (Straume et al. 2022). Lui et al., (2024) find that opening the Canadian Arctic Archipelago gateway in a sensitivity simulation leads to a strengthened AMOC. All these gateways would therefore justify a sensitivity experiment in the context of MioMIP2, but given limited modelling group resources, choices must be made.

Here, we suggest three gateway-related sensitivity studies: the Fram Strait, Central American Seaway, and the Tethys Seaway (Figure 7, Table 2). Paleogeography and associated files for all these proposed sensitivity studies are provided (see Table 2). The Fram Strait is depicted as a wider gateway with a broader shallow shelf and reaching depths of ~2500 m in the Phase 2 paleogeography, however, there

https://doi.org/10.5194/egusphere-2026-3595
Preprint. Discussion started: 3 August 2026

are uncertainties in the depths and widths of this gateway, and any changes may have happened in a relatively short time, leading to an impact on ocean circulation. To test the sensitivity of the model circulation to the deepening and constriction of the Fram Strait, we propose a sensitivity study that incorporates a relatively narrow and deep (~3000 m) Fram Strait configuration (Figure 7b), similar to the Phase 1 “updated Herold” Burls et al (2021) paleogeography.

The Central American Seaway forms a crucial tropical connection between the Pacific and Atlantic Oceans, and there is still uncertainty around the physiography and timing of its closure. The Phase 2 paleogeography implements a shallower (~900 m) and narrow seaway (Figure 7c), and so here we suggest a sensitivity experiment that incorporates a wide and deep (~4500 m) seaway (Figure 7d), similar to the Phase 1 “updated Herold” paleogeography.

For the Tethys Seaway, we wish to isolate the impact of the shallow (~200 m) open Tethys Seaway used in the Phase 1 “updated Herold” Burls et al (2021) paleogeography and therefore suggest a sensitivity study where the Tethys Seaway has a similar shallow (~200 m) and open configuration as the Phase 1 “updated Herold” Burls et al. (2021) paleogeography (Figure 7f), compared to the constricted and ultimately closed seaway in the Phase 2 paleogeography (Figure 7e).

A further paleogeography-based recommended sensitivity study is to test the impact of the hot spot reference frame as compared to the paleomagnetic reference frame of the MioMIP2 Phase 2 CORE simulation (Figure S11). The hot spot reference frame used in this sensitivity study (2008; O’Neill et al., 2005) is the same as the absolute reference frame used in the Phase 1 paleogeography (i.e., “updated Herold”).

https://doi.org/10.5194/egusphere-2026-3595
Preprint. Discussion started: 3 August 2026

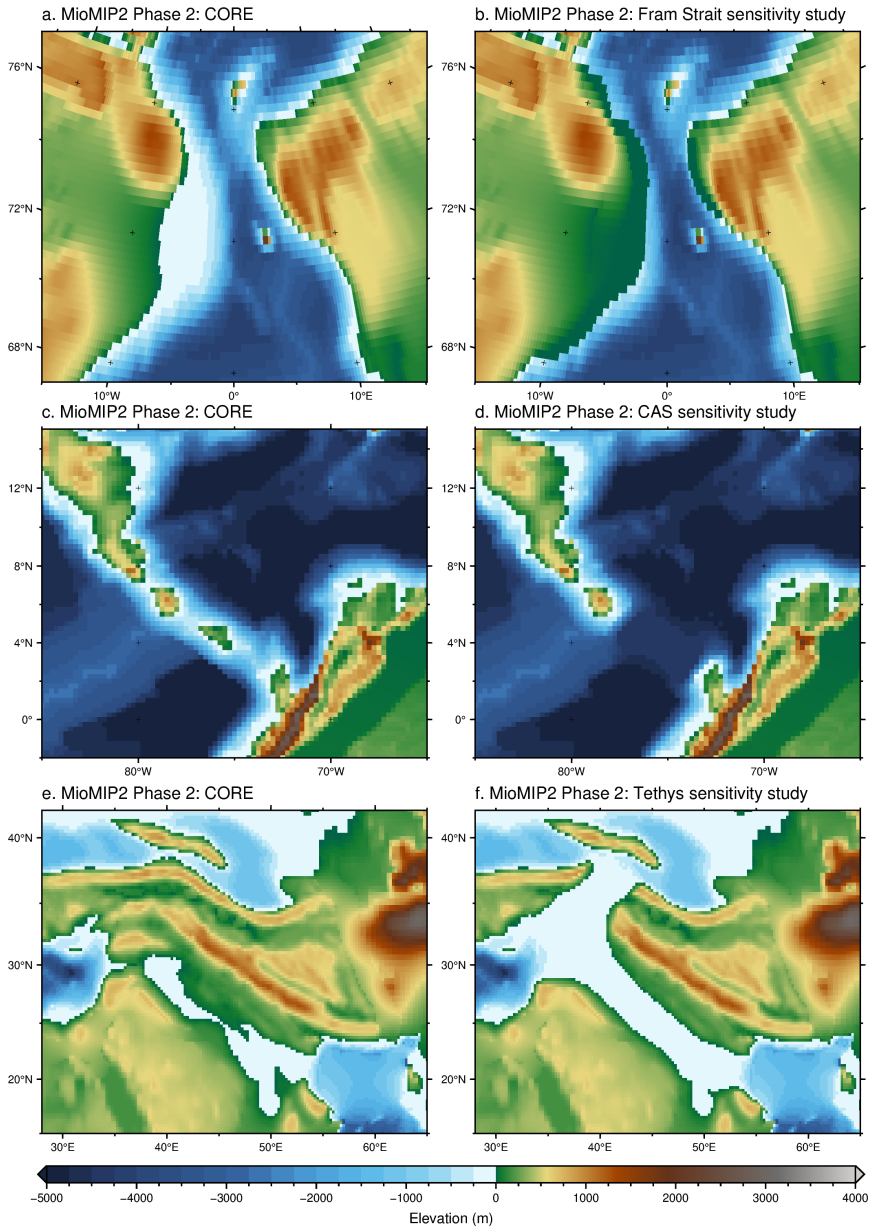

Figure 7: Comparison of paleogeography for oceanic gateway sensitivity experiments for MioMIP2 Phase 2. a, c, e. MioMIP2 Phase 2 CORE experiment; b. Fram Strait sensitivity experiment; d. Central American Seaway (CAS) sensitivity experiment; f. Tethys Seaway sensitivity experiment.

3.4.3 Sensitivity to ice sheets

The Antarctic Ice Sheet was likely different in configuration than the CORE ice sheet during some intervals of the Middle Miocene and effects of ice sheet variations have been shown to produce

https://doi.org/10.5194/egusphere-2026-3595
Preprint. Discussion started: 3 August 2026

feedbacks in the coupled atmosphere-ocean system (Bradshaw et al., 2021; Frigola et al., 2018; Hamon et al., 2012; Knorr and Lohmann, 2014). To further our understanding of how a larger or smaller ice sheet may have impacted the climate system, we recommend MioMIP2 Phase 2 ice sheet sensitivity experiments (Figure 3, Tables 1 & 6).

For the smaller end-member, one possibility would be ice-free conditions in Antarctica; however, we do not consider this to be a plausible configuration. Although sea-level reconstructions based on $\delta^{18}O_{seawater}$ (Miller et al., 2020) and sequence stratigraphy (Kominz et al., 2008) are high enough to suggest ice-free conditions, more recent sea-level reconstructions suggest a core ice sheet of 10–20 m sea-level equivalent persisted throughout the peak warmth of the MCO (Miller et al., 2024). This is supported by evidence for an ice sheet in West Antarctica during the Early Miocene and evidence that ice extended to at least the mid-shelf in the Ross Sea during the late MCO (Marschalek et al., 2021; McKay et al., 2025; Pérez et al., 2021). We therefore provide an ice sheet minimum scenario (Figure 3b) with an ice volume of 6.5 million km^3 (+42 m ESL, Table 6) that is comparable to that used in the "updated Herold" paleogeography but based on the Paxman et al. (2019) Antarctic paleotopography. This ice sheet was produced following the same climate forcing and methodology as Halberstadt et al. (2021) with an added surface temperature anomaly of +3.0˚C. Given the large change in ESL, the paleoshorelines have been adjusted in deepmip-mio-mco-p2-ICE-small (Figure S12).

There is also evidence for periodic ice advance during the Middle Miocene; an Antarctic Ice Sheet greater in extent than the CORE experiment is therefore plausible. In the Ross Sea, the ANDRILL-2A record and mid-shelf record from IODP Site U1521 reveal episodes of large-scale marine ice sheet advance to at least the mid shelf after 15.8 Ma (McKay et al., 2025; Passchier et al., 2011; Pérez et al., 2021). On the Sabrina Coast there is evidence for East Antarctic Ice Sheet (EAIS) continental shelf progradation and erosion happening during the MCO (Gulick et al., 2017; Montelli et al., 2020). Based on this geophysical evidence, the results of the 460 ppmv glacial simulation by Halberstadt et al. (2021) is used as a 'maximum-ice' configuration for the large ice sheet scenario (Figure 3c). This simulation yields a large Antarctic ice sheet with an ice volume of 28.6 million km^3 (-2.6 m ESL, Table 6), it

https://doi.org/10.5194/egusphere-2026-3595
Preprint. Discussion started: 3 August 2026

covers almost the entire continent but is not grounded in the Ross and Filchner-Ronne marine embayments. This larger-than-present ice volume is supported by enhanced precipitation under warmer air temperatures, leading to a thickening of the ice sheet interior as suggested by Shevenell et al., (2004, 2008), and maintains consistency with geologic records of Miocene ice-free conditions in Antarctic marine basins (McKay et al., 2025; Sangiorgi et al., 2018). Although this large ice sheet is geologically and glaciologically feasible, we note that the ice sheet modeling equilibrium technique used by Halberstadt et al. (2021) could have artificially inflated the simulated ice volumes compared to the transient evolution of the ice sheet (Stap et al., 2019). Given the small change in ESL, the paleoshorelines have not been adjusted in deepmip-mio-mco-p2-ICE-large (Figure S12c).

The synthesis of Antarctic continental and shelf geologic data indicates episodes of ice advance and retreat through the Middle Miocene; while we do not attempt to align geologic records to target specific time periods that correspond to our minimum and maximum configurations, we consider 16.5 Ma as an interval when the Antarctic Ice Sheet were generally smaller and 14.7 Ma as an interval where there is dynamic ice advance resembling the large extent sensitivity study chosen. In both sets of ice sheet sensitivity experiments, Greenland remains as it is in the CORE experiment, ice free.

Finally, while ice-free conditions on Antarctica are not regarded as a plausible MOC configuration, to allow for an assessment of the impact of the ice sheet on Earth System Sensitivity we include a sensitivity experiment without an Antarctic Ice Sheet (Tables 1 & 6), while preserving the paleoshorelines of the CORE (Figure S12d).

Table 6: Antarctic ice volume, the change in Eustatic Sea Level (ESL) relative to modern, and the orbital parameters used in the ice-sheet model.

Experiment	Antarctic Ice volume	Antarctic Ice Area	ESL	Eccentricity	Obliquity	Precession*
CORE	21.2 million km^3	7.67 million km^2	+5.6 m	0.05	24.5°	90°
Large	28.6 million km^3	13.87 million km^2	-2.6 m	0.05	22.0°	270°
Small	6.5 million km^3	4.9 million km^2	+42.0 m	0.05	24.5°	90°
None	0 km^3	0 km2	+56.96 m	NA	NA	NA

*Precession is defined as degrees prograde from perihelion at Northern Hemisphere Vernal Equinox.

https://doi.org/10.5194/egusphere-2026-3595
Preprint. Discussion started: 3 August 2026

3.4.4 Sensitivity to solar constant and astronomical parameters

Compared to most boundary conditions in deep-time climates, the solar constant is well-constrained and can be approximated by a standard luminosity model which is described by Gough (1981). The effectiveness of solar insolation changes in producing a global mean surface temperature change differs from that of CO_2 differs (Modak et al., 2016). We therefore suggest conducting a Phase 2 sensitivity experiment with a solar constant value estimated for the MCO (Table 1). Since climate models might have different pre-industrial solar constants, we suggest a decrease of 0.14% from the pre-industrial value, following Gough (1981). Such a decrease should not have a significant impact on global temperature but has led to polar cooling of around 1°C in recent Miocene simulations (Renoult et al., 2025).

Astronomical parameters—eccentricity, obliquity, and precession—control the seasonal and spatial distribution of incoming radiation, pacing periodic climate evolutions throughout Earth history (Berger, 1978; Laskar et al., 2011). These insolation changes trigger feedbacks within the climate system that yield large variations, including Pleistocene glacial and interglacial cycles. Orbital sensitivity experiments are therefore fundamental for interpreting proxy signals with limited chronological precision and for constraining end-member climatic states, ice sheet, biogeochemical responses. Critically, the magnitude and structure of these feedbacks depend strongly on the background climate state (Bloch-Johnson et al., 2021), implying that orbital forcing may generate different regional and global responses under warmer climate conditions.

Recent modelling studies demonstrate that orbital forcing alone can generate summer temperature anomalies approaching ~8°C over mid- and high-latitude Eurasia (Battisti et al., 2014; Zhang et al., 2025). Compared to the pre-industrial period, the warm Miocene climate exhibits reduced high-latitude temperature sensitivity but amplified hydrological response over tropical North Africa (Zhang et al., 2025). Collectively, these findings highlight the need to quantify how orbital forcing interacts with warm boundary conditions during the Miocene.

https://doi.org/10.5194/egusphere-2026-3595
Preprint. Discussion started: 3 August 2026

To address this, we propose orbital sensitivity experiments consisting of two Northern Hemisphere summer insolation end-members that occurred during the MCO (DeepMIP-MCO-Phase2-IShi & DeepMIP-MCO-Phase2-IShi in Table 1). We focus on a representative time slice at 15.603 Ma and 14.724 Ma, which capture the largest June-insolation variability at ~65°N near the peak of MCO. The high- and low insolation end-members (DeepMIP-MCO-Phase2-IShi and DeepMIP-MCO-Phase2-ISlo at 15.603 Ma and 14.724 Ma, respectively) differ by +87 Wm^{-2} and -53 Wm^{-2} at 65°N relative to the present-day, corresponding to opposite precession phases (longitudes of perihelion at 287° vs. 66°), respectively. All orbital parameters are summarized in Table 7.

In addition to these MioMIP2 sensitivity experiments (Table 1), for modelling groups that have the capacity to run additional experiments we proposed optional complementary experiments under pre-industrial boundary conditions with identical insolation forcing, enabling a clean assessment of Miocene versus pre-industrial differences in orbital sensitivity (Table 7). A reduced eccentricity experiment (at 15.751 Ma) with all other orbital parameters identical to DeepMIP-MCO-Phase2-IShi, is an additional optional experiment to further isolate the role of precessional amplitude (Table 7).

Table 7: Orbital parameters setup for orbital sensitivity experiments

Simulation	**Orbital forcing**		
	Eccentricity	**Obliquity** (rad)	**Long. Perihelion**
DeepMIP-MCO-Phase2-IShi, PI_IShi	0.0553	24.08° (0.4202)	287.294° (-0.0528)
DeepMIP-MCO-Phase2-ISlo, PI_ISlo	0.0490	22.37° (0.3904)	66.105° (0.0448)
MCO_ECCm	0.0019	24.08° (0.4202)	287.294° (-0.0528)

4. Summary of proxy compilation efforts complementing MioMIP2

4.1 Miocene ocean data compilation (MioOcean)

The MioOcean project is compiling Miocene global ocean records from five available temperature proxies: $U^{k'}_{37}$, TEX_{86}, Mg/Ca, Δ_{47}, and oxygen isotope compositions of excellently preserved or 'glassy' planktic foraminifera (GF) (Auderset et al., 2024). The resulting database product to date includes nearly 100 unique sites, with over 24,500 data points from 97 publications. The MioOcean effort is distinct in that state-of-the-art temperature estimates are made by recalculating ocean temperatures

https://doi.org/10.5194/egusphere-2026-3595
Preprint. Discussion started: 3 August 2026

using the most up-to-date methods and calibrations. Proxy systematics are revised with consistent methods, the plate tectonic model is updated to be consistent with the Phase 2 paleogeography i.e., Zahirovic et al. (2022), and the age models for a subset of key sites have also been updated.

This standardized, multi-proxy MioOcean database will provide an internally consistent Miocene ocean temperature dataset and will result in several key additional outcomes. One such outcome includes determination of spatial and temporal data knowledge gaps, allowing identification of regions and intervals that could be priorities for additional sampling or improved records if the sediments are available. To facilitate this, an interactive MioOcean website (https://research.soton.ac.uk/mioocean/), using the online Streamlit app allows for the visualization and comparison of records. This tool promotes accessibility without coding steps for specialists and non-specialists to work with the data. Additionally, the updated age information produced within the MioOcean initiative provides a framework for age model generation applicable to the wider paleoceanography community. Companion publications released alongside the database will reflect these key advances in geochronology. The MioOcean database enables convenient access to the data, facilitating ease of cross-proxy comparisons, model validation, and analysis of global climate patterns, such as latitudinal temperature gradients and major climate transitions.

4.2 Miocene terrestrial data compilations

Terrestrial climate records have been compiled by two working groups focused on land temperature and terrestrial hydroclimate reconstructions, respectively. Major differences between marine and terrestrial records are the generally greater uncertainties in age control on land, and that terrestrial records more commonly comprise a single observation (one data point) or a short floating series, rather than multi-millennial records. For this reason, land data has been grouped into broad time bins: Early Miocene (23.03–15.97 Ma), Middle Miocene (15.97–11.63 Ma), Late Miocene (11.63–5.33 Ma), as well as a time bin specifically targeting the MCO (16.75–14.5 Ma). Dates with uncertainties will also be provided. These datasets will be deposited in NOAA WDS-Paleo, associated with the Neogene Terrestrial Climate Synthesis (Fletcher, 2024).

https://doi.org/10.5194/egusphere-2026-3595
Preprint. Discussion started: 3 August 2026

One working group collated Miocene land temperature records (Pérez-Angel et al., 2024). This compilation focused on a thorough assessment of five major proxies: pollen assemblages, leaf physiognomy, Δ_{47} of pedogenic carbonate and speleothem, brGDGTs, and other macrofossils. Previous compilation efforts (Burls et al., 2021; Pound et al., 2012) were updated with standard criteria for each proxy to assess their temperature estimate reliability, updating age constraints for a subset of the data, updating uncertainty for each proxy, and recalculating temperature estimates to reflect the state of the art for each method. When original publications were accessible, temperature uncertainties, age control method, type of sedimentary environment and specific method for each proxy used to estimate the temperature were included in the compilation.

The land temperature compilation includes a complete compilation of all data and a subset filtered for accuracy criteria. For the five major proxies additional relevant metadata is provided. Overall, over 560 data points have been compiled from Miocene terrestrial proxies. The filtered database contains nearly 385 unique sites, of which ~300 come from the Northern Hemisphere and ~80 from the Southern Hemisphere. Exclusion criteria include data not reported in peer-reviewed articles; inconsistent location coordinates; unverifiable temperature estimates; superseded or invalidated temperature estimate methods, or, in some cases, absence of open data required for reproducibility. This dataset reports temperature estimates that are accurate reconstructions of temperature (i.e., mean annual, months above freezing, seasonal, etc.) for each proxy and contextualizes them with model outputs (i.e., mean annual and seasonal surface temperature, monthly minima surface temperature, etc.). This compilation allows for assessment of proxy-proxy and proxy-model mismatch by proxy experts.

Another working group collated evidence for terrestrial hydroclimate reconstructions for the MCO (Stiles et al., 2024). This hydroclimate compilation includes geochemical, sedimentological, paleobotanical, and vertebrate-based proxies. These provide qualitative and quantitative measures that reflect different aspects of the hydroclimate system, such as mean annual precipitation and lake extent. To synthesize these proxy records into a coherent dataset for data-model comparison, these data were

https://doi.org/10.5194/egusphere-2026-3595
Preprint. Discussion started: 3 August 2026

compared to the matching Preindustrial or Holocene variables in that location and scored as wetter, the same, or drier. Confidence levels have been assigned to the data for age and geographic location.

The hydroclimate compilation includes a compilation of the original publication data, and comparison of the synthesized dataset relative to modern climate. Currently, the compilation comprises 93 records, from 93 unique sites, and has been used to define target areas for further research based on the largest data-model discrepancies. The dataset has been used to test hydroclimate change between the MCO, the Late Miocene and present, finding the MCO was generally wetter compared with both the Late Miocene and current climate, but the extent and seasonality of change is regionally variable (Stiles et al., 2024).

Additionally, a recent data compilation of globally distributed leaf fossil sites targeted broad biome reconstructions in addition to terrestrial primary productivity (Reichgelt and West, 2025). Both the leaf physiognomy as well as reconstructed BIOCLIM variables were made available, using a single paleobotanical proxy and a rigorous filtering process. This resulted in 108 unique sites, higher-than-modern precipitation for >90% of localities and globally enhanced net primary productivity of at least ~250 gC m^{-2} yr^{-1}.

5. Products

Once the model simulations and proxy data synthesis effort are completed, we anticipate a few overview papers that summarize the large-scale features of the simulations, and the skill of the models when compared with proxy records. These large-scale features may include, but are not limited to, global surface temperature and precipitation patterns, sea ice conditions, and ocean circulation. Several spin-off papers focusing on understanding inter-model differences, regional climate features, and climate variability will likely follow this. We especially encourage studies that explore the application of MioMIP2 simulations and data synthesis products to study warming trajectories, tipping points, and physical processes that are relevant to future climate. Additionally, we expect that participating

https://doi.org/10.5194/egusphere-2026-3595
Preprint. Discussion started: 3 August 2026

modelling groups will publish individual studies that document their model configuration, parameter choice, implementation of boundary conditions, and diagnostics of their participating experiments.

Code, data, or code and data availability

The paleogeography reconstruction was facilitated by tools from Python 3, pyGPlates, GPlately (Mather et al., 2024), Generic Mapping Tools (GMT) (Wessel et al., 2019b) and pyGMT (Tian et al., 2025). The runoff calculation was facilitated by the "FillDepressions" algorithm from the "RichDEM" software package (Barnes, 2016). The MioMIP2 boundary condition files listed in Table 2, as well as the Python notebooks used to created them, have been archived in a Zenodo dataset repository (Burls et al., 2026). Additionally, this Zenodo dataset repository contains the code used to make the figures and a notebook for calculating the paleo-coordinates of modern sites using the plate tectonic models associated with the phase 1 and phase 2 paleogeography respectively.

Supplement link

The link to the supplement will be included by Copernicus, if applicable.

Author contributions

Tier 1: N.J.B. Conceptualization, Methodology & Writing; N.M.W. Paleogeography Data Curation, Formal Analysis, Investigation, Software, Visualization & Writing; R.P.A. Paleogeography Data Curation, Formal Analysis, Investigation, & Writing; C.D.B. Vegetation & Soil Data Curation, Formal Analysis, Investigation, & Writing; E.G. Ice sheets Data Curation, Formal Analysis, Investigation & Writing; L.B.S. Ice Sheets Data Curation, Formal Analysis, Investigation & Writing; G.R. Ice Sheets Investigation & Writing; A.R.H. Ice Sheets Data Curation, Formal Analysis, Investigation & Writing; A.M.D.B. Methodology & Writing. **Tier 2**: F.A. Vegetation Data Curation; D.J.C. Vegetation Data Curation; M.C.G. Vegetation Data Curation; N.D. Vegetation Data Curation; B.E. Vegetation Data Curation; A.F. Paleogeography Data Curation, Methodology &Writing; S.F. Vegetation Data Curation, Geological Datasets & Writing; R.F. Writing; T.F. Vegetation Data Curation, Geological Datasets & Writing; FF. Paleogeography Data Curation & Writing; M.G. Tidal Mixing & Writing; A.S.v.d.H. Paleogeography Investigation & Writing; M.H. Paleogeography Investigation, Tidal Mixing & Writing; D.K.H. Paleogeography Investigation & Methodology; D.I. Vegetation Data Curation; M.S.K.O Vegetation Data Curation; G.K. Paleogeography Investigation; M.K. Vegetation Data Curation; C.H.L

https://doi.org/10.5194/egusphere-2026-3595
Preprint. Discussion started: 3 August 2026

Ice sheets Investigation & Writing; A.N.L.G. Paleogeography Investigation; S.L. Vegetation Data Curation; X.L. Carbon Dioxide Investigation; D.J.L Methodology & Writing; K.M. Methodology & Writing; Y.M. Vegetation Data Curation; T.J.N. Ocean Temperature Data Curation & Writing; J.B.N. Ice sheets Investigation; J.B.N. Vegetation Data Curation & Geological Datasets; D.O. Vegetation Data Curation; G.J.G.P. Ice Sheet Data Curation & Writing; M.J.P Vegetation & Soil Data Curation; J.W.B.R Carbon Dioxide Investigation & Writing; T.R. Vegetation Data Curation; M.R. Methodology & Writing; F.S. Ice Sheet Investigation; A.C.S. Paleogeography Investigation; D.S. Ice Sheet Investigation; P.S. Vegetation Data Curation & Paleogeography Investigation; A.E.S. Ice Sheet Investigation, Ocean Temperature Data Curation & Writing; S.S. Data Curation & Writing; E.S. Paleogeography Investigation & Writing; C.A.E.S, Vegetation Data Curation; C.T. Orbit and Solar Constant Methodology & Writing; T.U. Vegetation Data Curation; J.E.W. Paleogeography Investigation & Writing; E.W. Vegetation Data Curation; Y.Z. Orbit and Solar Constant Methodology & Writing; F.Z Methodology & Writing; J.Z. Methodology & Writing; **Tier 3**: A.A. Geological Datasets & Writing; F.C. Ice Sheet Investigation; A.D Ice Sheet Investigation; R.H. Geological Datasets & Writing; A.H. Geological Datasets & Writing; N.H. Paleogeography Investigation; D.L. Geological Datasets & Writing; J.W.M. Ice sheet Investigation & Writing; B.M. Geological Datasets & Writing; S.M. Geological Datasets & Writing; L.P.A. Geological Datasets & Writing; M.S. Geological Datasets & Writing; S.S. Geological Datasets & Writing; E.S. Geological Datasets & Writing; Y.S. Writing; N.T. Ice Sheet Investigation; Z.Z. Paleogeography Investigation; Y.Z Carbon Dioxide Investigation & Writing

Competing interests

The authors declare that they have no conflict of interest.

Disclaimer

Copernicus Publications remains neutral with regard to jurisdictional claims made in the text, published maps, institutional affiliations, or any other geographical representation in this paper. While Copernicus Publications makes every effort to include appropriate place names, the final responsibility lies with the authors. Views expressed in the text are those of the authors and do not necessarily reflect the views of the publisher.

https://doi.org/10.5194/egusphere-2026-3595
Preprint. Discussion started: 3 August 2026

Acknowledgements

We thank Alireza Bahadori, Jeremy Caves Rugenstein, Frank Pazzaglia, Lydian Boschman, and Paul Markwick for their thoughtful contribution in creating various aspects of the paleogeography. We also acknowledge previous DeepMIP-Eocene and PlioMIP experimental design papers that have provided example frameworks for the design of a deep-time model intercomparison project. The CESM project is supported primarily by the National Science Foundation (NSF). This material is based upon work supported by the National Center for Atmospheric Research (NCAR), which is a major facility sponsored by the NSF under Cooperative Agreement No. 1852977. The tidal dissipations fields were done on Supercomputing Wales, which is part-funded by the European Regional Development Fund (ERDF) via the Welsh Government.

Financial support

NJB acknowledges NSF Grants AGS-1844380 and NSF EAR-2303417. RF acknowledges NSF Grants AGS-2238875 and AGS-2303566. CRT acknowledges NSF Grant EAR-2002440. RPA acknowledges NSF Grants EAR-2303417 and EAR-2316735. MCG acknowledges grant SBPLY/25/180801/000028 from the Government of Castilla-La Mancha. ARH and RPA acknowledge NSF OPP-2503812. AvdH acknowledges support from the EMBRACER program, the Earth System Feedback Research Centre, financially supported by the SUMMIT program of the Dutch Research Council (NWO). NMW was supported by Australian Research Council (ARC) grant IE230100098. JZ acknowledges the support of NSF grants P4CLIMATE 2303567 and P2C2 2202777, as well as the Heising-Simons Foundation grant #2023-4716. CHL acknowledges European Union's Horizon 2020 research and innovation programme under grant agreement No. 101184070 (P2F). FS was financially supported by NWO (Dutch Research Council) Grant NWO OCENW M.21.200 and acknowledges support from the EMBRACER program, the Earth System Feedback Research Centre, financially supported by the SUMMIT program of the Dutch Research Council (NWO). MP was financially supported by NERC grant NE/V01501X/1 and Royal Society IECR2202086. DJL acknowledges EU grant Past2Future (Grant Agreement: 101184070). AES acknowledges NSF OPP-1947646. JAMG acknowledges support from The Natural Environment Research Council, grant NE/S009566/1. SS, SM, AA, and AH acknowledge financial support from PAGES and UKIODP for the MioOcean effort. EOS acknowledges the Research Council of Norway grant number 314371 (DOTpaleo) and its Centers of Excellence Scheme, project number 332523 (PHAB). CUB was supported by SRDA-23-0227 and VEGA 1/0336/25 projects. EW was supported by the W. Szafer Institute of Botany, Polish Academy of Sciences, through its statutory funds. MS acknowledges NSF Grant EAR 20-21579. ANL thanks NASA GISS for institutional support and the NCCS for computer time. MH acknowledges support from NSF OCE-2217530 and OCE-243668.

https://doi.org/10.5194/egusphere-2026-3595
Preprint. Discussion started: 3 August 2026

Review statement

The review statement will be added by Copernicus Publications listing the handling editor as well as all contributing referees according to their status anonymous or identified.

References

Acosta, R. P. and Huber, M.: The neglected Indo-Gangetic Plains low-level jet and its importance for moisture transport and precipitation during the peak summer monsoon, Geophysical Research Letters, 44, 8601–8610, https://doi.org/10.1002/2017GL074440, 2017.

Acosta, R. P. and Huber, M.: Competing Topographic Mechanisms for the Summer Indo-Asian Monsoon, Geophysical Research Letters, 47, e2019GL085112, https://doi.org/10.1029/2019GL085112, 2020.

Acosta, R. P., Ladant, J.-B., Zhu, J., and Poulsen, C. J.: Evolution of the Atlantic Intertropical Convergence Zone, and the South American and African Monsoons Over the Past 95-Myr and Their Impact on the Tropical Rainforests, Paleoceanography and Paleoclimatology, 37, e2021PA004383, https://doi.org/10.1029/2021PA004383, 2022.

Adams, D. K. and Comrie, A. C.: The North American Monsoon, Bulletin of the American Meteorological Society, 78(10), 2197–2214, 1997.

Armstrong McKay, D. I., Staal, A., Abrams, J. F., Winkelmann, R., Sakschewski, B., Loriani, S., Fetzer, I., Cornell, S. E., Rockström, J., and Lenton, T. M.: Exceeding 1.5°C global warming could trigger multiple climate tipping points, Science, 377, eabn7950, https://doi.org/10.1126/science.abn7950, 2022.

Årthun, M., Asbjørnsen, H., Chafik, L., Johnson, H. L., and Våge, K.: Future strengthening of the Nordic Seas overturning circulation, Nat Commun, 14, 2065, https://doi.org/10.1038/s41467-023-37846-6, 2023.

Auderset, A., Liu, X., Shah, N. S., Feakins, S. J., Sangiorgi, F., Shevenell, A., Sliwinska, K., Sluijs, A., Wubben, E., Zhang, Y., Modestou, S., Holbourn, A. E., and Sosdian, S. M.: MioTEX - A comprehensive GDGT-based sea surface temperature compilation for the Miocene, in: AGU Fall Meeting Abstracts, PP33F-05, 2024.

Baby, G., Guillocheau, F., Braun, J., Robin, C., and Dall'Asta, M.: Solid sedimentation rates history of the Southern African continental margins: Implications for the uplift history of the South African Plateau, Terra Nova, 32, 53–65, https://doi.org/10.1111/ter.12435, 2020.

https://doi.org/10.5194/egusphere-2026-3595
Preprint. Discussion started: 3 August 2026

Bacon, C. D., Silvestro, D., Jaramillo, C., Smith, B. T., Chakrabarty, P., and Antonelli, A.: Biological evidence supports an early and complex emergence of the Isthmus of Panama, Proceedings of the National Academy of Sciences, 112, 6110–6115, https://doi.org/10.1073/pnas.1423853112, 2015.

Badger, M. P. S., Chalk, T. B., Foster, G. L., Bown, P. R., Gibbs, S. J., Sexton, P. F., Schmidt, D. N., Pälike, H., Mackensen, A., and Pancost, R. D.: Insensitivity of alkenone carbon isotopes to atmospheric CO_2 at low to moderate CO_2 levels, Climate of the Past, 15, 539–554, https://doi.org/10.5194/cp-15-539-2019, 2019.

Bahadori, A., Holt, W. E., Feng, R., Austermann, J., Loughney, K. M., Salles, T., Moresi, L., Beucher, R., Lu, N., Flesch, L. M., Calvelage, C. M., Rasbury, E. T., Davis, D. M., Potochnik, A. R., Ward, W. B., Hatton, K., Haq, S. S. B., Smiley, T. M., Wooton, K. M., and Badgley, C.: Coupled influence of tectonics, climate, and surface processes on landscape evolution in southwestern North America, Nat Commun, 13, 4437, https://doi.org/10.1038/s41467-022-31903-2, 2022.

Barbolini, N., Woutersen, A., Dupont-Nivet, G., Silvestro, D., Tardif, D., Coster, P. M. C., Meijer, N., Chang, C., Zhang, H.-X., Licht, A., Rydin, C., Koutsodendris, A., Han, F., Rohrmann, A., Liu, X.-J., Zhang, Y., Donnadieu, Y., Fluteau, F., Ladant, J.-B., Le Hir, G., and Hoorn, C.: Cenozoic evolution of the steppe-desert biome in Central Asia, Science Advances, 6, eabb8227, https://doi.org/10.1126/sciadv.abb8227, 2020.

Barnes, R.: RichDEM: Terrain Analysis Software, 2016.

Barrier, E., Vrielynck, B., Brouillet, J.-F., and Brunet, M.-F.: Paleotectonic reconstruction of the Central Tethyan Realm. Tectonono-sedimentary-palinspastic maps from Late Permian to Pliocene., 2018.

Battisti, D. S., Ding, Q., and Roe, G. H.: Coherent pan-Asian climatic and isotopic response to orbital forcing of tropical insolation, Journal of Geophysical Research: Atmospheres, 119, 11,997-12,020, https://doi.org/10.1002/2014JD021960, 2014.

Beerling, D. J., Fox, A., and Anderson, C. W.: Quantitative uncertainty analyses of ancient atmospheric CO_2 estimates from fossil leaves, American Journal of Science, 309, 775–787, https://doi.org/10.2475/09.2009.01, 2009.

Bereiter, B., Eggleston, S., Schmitt, J., Nehrbass-Ahles, C., Stocker, T. F., Fischer, H., Kipfstuhl, S., and Chappellaz, J. A.: Antarctic Ice Cores Revised 800KYr CO2 Data, 2015.

Berger, A.: Long-Term Variations of Daily Insolation and Quaternary Climatic Changes, 1978.

Bernal, R., Bacon, C. D., Balslev, H., Hoorn, C., Bourlat, S. J., Tuomisto, H., Salamanca, S., van Manen, M. T., Romero, I., Sepulchre, P., and Antonelli, A.: Could coastal plants in western Amazonia be relicts of past marine incursions?, Journal of Biogeography, 46, 1749–1759, https://doi.org/10.1111/jbi.13560, 2019.

https://doi.org/10.5194/egusphere-2026-3595
Preprint. Discussion started: 3 August 2026

Bialik, O. M., Frank, M., Betzler, C., Zammit, R., and Waldmann, N. D.: Two-step closure of the Miocene Indian Ocean Gateway to the Mediterranean, Sci Rep, 9, 8842, https://doi.org/10.1038/s41598-019-45308-7, 2019.

Bicudo, T. C., Sacek, V., and Paes de Almeida, R.: Reappraisal of the relative importance of dynamic topography and Andean orogeny on Amazon landscape evolution, Earth and Planetary Science Letters, 546, 116423, https://doi.org/10.1016/j.epsl.2020.116423, 2020.

Bloch-Johnson, J., Rugenstein, M., Stolpe, M. B., Rohrschneider, T., Zheng, Y., and Gregory, J. M.: Climate Sensitivity Increases Under Higher CO2 Levels Due to Feedback Temperature Dependence, Geophysical Research Letters, 48, e2020GL089074, https://doi.org/10.1029/2020GL089074, 2021.

de Boer, A. M., Krishnan, S., Burls, N. J., Hutchinson, D. K., and Renoult, M.: Evaluation of Quasi-Equilibrium Criteria for Coupled Climate Model Simulations, Geophysical Research Letters, 52, e2025GL117040, https://doi.org/10.1029/2025GL117040, 2025.

Bolton, C. T., Hernández-Sánchez, M. T., Fuertes, M.-Á., González-Lemos, S., Abrevaya, L., Mendez-Vicente, A., Flores, J.-A., Probert, I., Giosan, L., Johnson, J., and Stoll, H. M.: Decrease in coccolithophore calcification and CO2 since the middle Miocene, Nat Commun, 7, 10284, https://doi.org/10.1038/ncomms10284, 2016.

Boos, W. R. and Pascale, S.: Mechanical forcing of the North American monsoon by orography, Nature, 599, 611–615, https://doi.org/10.1038/s41586-021-03978-2, 2021.

Boschman, L. M.: Andean mountain building since the Late Cretaceous: A paleoelevation reconstruction, Earth-Science Reviews, 220, 103640, https://doi.org/10.1016/j.earscirev.2021.103640, 2021.

Botsyun, S., Sepulchre, P., Donnadieu, Y., Risi, C., Licht, A., and Caves Rugenstein, J. K.: Revised paleoaltimetry data show low Tibetan Plateau elevation during the Eocene, Science, 363, eaaq1436, https://doi.org/10.1126/science.aaq1436, 2019.

Braconnot, P., Otto-Bliesner, B., Harrison, S., Joussaume, S., Peterchmitt, J.-Y., Abe-Ouchi, A., Crucifix, M., Driesschaert, E., Fichefet, T., Hewitt, C. D., Kageyama, M., Kitoh, A., Laîné, A., Loutre, M.-F., Marti, O., Merkel, U., Ramstein, G., Valdes, P., Weber, S. L., Yu, Y., and Zhao, Y.: Results of PMIP2 coupled simulations of the Mid-Holocene and Last Glacial Maximum – Part 1: experiments and large-scale features, Climate of the Past, 3, 261–277, https://doi.org/10.5194/cp-3-261-2007, 2007.

Braconnot, P., HARRISON, S. P., Kageyama, M., Bartlein, P. J., Masson-Delmotte, V., Abe-Ouchi, A., Otto-Bliesner, B., and Zhao, Y.: Evaluation of climate models using palaeoclimatic data, Nature Climate Change, 2, 417–424, https://doi.org/10.1038/nclimate1456, 2012.

https://doi.org/10.5194/egusphere-2026-3595
Preprint. Discussion started: 3 August 2026

Bradshaw, C. D., Langebroek, P. M., Lear, C. H., Lunt, D. J., Coxall, H. K., Sosdian, S. M., and de Boer, A. M.: Hydrological impact of Middle Miocene Antarctic ice-free areas coupled to deep ocean temperatures, Nat. Geosci., 14, 429–436, https://doi.org/10.1038/s41561-021-00745-w, 2021.

Bradshaw, C. D., Fletcher, T., Reichgelt, T., Akgün, F., Cantrill, D. J., Casas-Gallego, M., Doláková, N., Erdei, B., Kayseri-Özer, M. S., Kováčová, M., Ochoa, D., Pound, M., Utescher, T., Zhao, J., Sepulchre, P., Feakins, S. J., Ivanov, D., Li, S., Miao, Y., Worobiec, E., Strömberg, C. A. E., Novak, J., Herold, N., Huber, M., Frigola, A., Prange, M., Knorr, G., Lohmann, G., Farnsworth, A., Li, Y., Lunt, D. J., Pillot, Q., Donnadieu, Y., Acosta, R. P., and Burls, N.: MioVeg1: A Global Middle Miocene Vegetation Reconstruction for Climate Modeling, Paleoceanography and Paleoclimatology, 40, e2025PA005213, https://doi.org/10.1029/2025PA005213, 2025.

Braun, J., Guillocheau, F., Robin, C., Baby, G., and Jelsma, H.: Rapid erosion of the Southern African Plateau as it climbs over a mantle superswell, Journal of Geophysical Research: Solid Earth, 119, 6093–6112, https://doi.org/10.1002/2014JB010998, 2014.

Breecker, D. O. and Retallack, G. J.: Refining the pedogenic carbonate atmospheric CO2 proxy and application to Miocene CO2, Palaeogeography, Palaeoclimatology, Palaeoecology, 406, 1–8, https://doi.org/10.1016/j.palaeo.2014.04.012, 2014.

Brierley, C. M. and Fedorov, A. V.: Comparing the impacts of Miocene–Pliocene changes in inter-ocean gateways on climate: Central American Seaway, Bering Strait, and Indonesia, Earth and Planetary Science Letters, 444, 116–130, 2016.

Burls, N. et al.: Supplementary Data and Code for MioMIP2 Experimental Design Paper, https://doi.org/10.5281/zenodo.20646213, 2026.

Burls, N. J. and Sagoo, N.: Increasingly Sophisticated Climate Models Need the Out-Of-Sample Tests Paleoclimates Provide, Journal of Advances in Modeling Earth Systems, 14, e2022MS003389, https://doi.org/10.1029/2022MS003389, 2022.

Burls, N. J., Bradshaw, C. D., De Boer, A. M., Herold, N., Huber, M., Pound, M., Donnadieu, Y., Farnsworth, A., Frigola, A., Gasson, E., von der Heydt, A. S., Hutchinson, D. K., Knorr, G., Lawrence, K. T., Lear, C. H., Li, X., Lohmann, G., Lunt, D. J., Marzocchi, A., Prange, M., Riihimaki, C. A., Sarr, A.-C., Siler, N., and Zhang, Z.: Simulating Miocene Warmth: Insights From an Opportunistic Multi-Model Ensemble (MioMIP1), Paleoceanography and Paleoclimatology, 36, e2020PA004054, https://doi.org/10.1029/2020PA004054, 2021.

Butzin, M., Lohmann, G., and Bickert, T.: Miocene ocean circulation inferred from marine carbon cycle modeling combined with benthic isotope records, Paleoceanography, 26, https://doi.org/10.1029/2009pa001901, 2011.

https://doi.org/10.5194/egusphere-2026-3595
Preprint. Discussion started: 3 August 2026

Caballero, R. and Huber, M.: State-dependent climate sensitivity in past warm climates and its implications for future climate projections, Proceedings of the National Academy of Sciences, 110, 14162–14167, https://doi.org/10.1073/pnas.1303365110, 2013.

Cai, Y., Mana, S., Cox, S. E., Beck, C. C., Feibel, C., Hanley, J., Liu, T., Bolge, L., Hemming, S., and Goldstein, S. L.: Geodynamic Evolution of the East African Superplume: Insights From Volcanism in the Western Turkana Basin, Journal of Geophysical Research: Solid Earth, 128, e2023JB026755, https://doi.org/10.1029/2023JB026755, 2023.

Cassel, E. J., Smith, M. E., and Jicha, B. R.: The Impact of Slab Rollback on Earth's Surface: Uplift and Extension in the Hinterland of the North American Cordillera, Geophysical Research Letters, 45, 10,996-11,004, https://doi.org/10.1029/2018GL079887, 2018.

Caves, J. K.: Late Miocene Uplift of the Tian Shan and Altai and Reorganization of Central Asia Climate, GSAT, https://doi.org/10.1130/GSATG305A.1, 2017.

Cerling, T. E., Harris, J. M., MacFadden, B. J., Leakey, M. G., Quade, J., Eisenmann, V., and Ehleringer, J. R.: Global vegetation change through the Miocene/Pliocene boundary, Nature, 389, 153–158, https://doi.org/10.1038/38229, 1997.

Chamberlain, C. P., Mix, H. T., Mulch, A., Hren, M. T., Kent-Corson, M. L., Davis, S. J., Horton, T., and Graham, S. A.: The Cenozoic climatic and topographic evolution of the western North American Cordillera, 2012.

Chandler, M., Rind, D., and Thompson, R.: Joint investigations of the middle Pliocene climate II: GISS GCM Northern Hemisphere results, Global and Planetary Change, 9, 197–219, https://doi.org/10.1016/0921-8181(94)90016-7, 1994.

Chandler, M., Dowsett, H., and Haywood, A.: The PRISM Model/Data Cooperative: Mid-Pliocene data-model comparisons, PAGES News, 16, 24–25, 2008.

Chardon, D., Grimaud, J.-L., Rouby, D., Beauvais, A., and Christophoul, F.: Stabilization of large drainage basins over geological time scales: Cenozoic West Africa, hot spot swell growth, and the Niger River, Geochemistry, Geophysics, Geosystems, 17, 1164–1181, https://doi.org/10.1002/2015GC006169, 2016.

Chorley, H., Levy, R., Naish, T., Lewis, A., Cox, S., Hemming, S., Ohneiser, C., Gorman, A., Harper, M., Homes, A., Hopkins, J., Prebble, J., Verret, M., Dickinson, W., Florindo, F., Golledge, N., Halberstadt, A. R., Kowalewski, D., McKay, R., Meyers, S., Anderson, J., Dagg, B., and Lurcock, P.: East Antarctic Ice Sheet variability during the middle Miocene Climate Transition captured in drill cores from the Friis Hills, Transantarctic Mountains, GSA Bulletin, 135, 1503–1529, https://doi.org/10.1130/B36531.1, 2022.

Cramer, B. S., Miller, K. G., Barrett, P. J., and Wright, J. D.: Late Cretaceous–Neogene trends in deep ocean temperature and continental ice volume: Reconciling records of benthic foraminiferal geochemistry (δ18O and Mg/Ca) with sea level history, Journal of Geophysical Research: Oceans, 116, https://doi.org/10.1029/2011JC007255, 2011.

Cramwinckel, M. J., Burls, N. J., Fahad, A. A., Knapp, S., West, C. K., Reichgelt, T., Greenwood, D. R., Chan, W.-L., Donnadieu, Y., Hutchinson, D. K., de Boer, A. M., Ladant, J.-B., Morozova, P. A., Niezgodzki, I., Knorr, G., Steinig, S., Zhang, Z., Zhu, J., Feng, R., Lunt, D. J., Abe-Ouchi, A., and Inglis, G. N.: Global and Zonal-Mean Hydrological Response to Early Eocene Warmth, Paleoceanography and Paleoclimatology, 38, e2022PA004542, https://doi.org/10.1029/2022PA004542, 2023.

Crosby, A. G. and McKenzie, D.: An analysis of young ocean depth, gravity and global residual topography, Geophys J Int, 178, 1198–1219, https://doi.org/10.1111/j.1365-246X.2009.04224.x, 2009.

Cui, Y., Schubert, B. A., and Jahren, A. H.: A 23 m.y. record of low atmospheric CO2, Geology, 48, 888–892, https://doi.org/10.1130/G47681.1, 2020.

Ding, L., Kapp, P., Cai, F., Garzione, C. N., Xiong, Z., Wang, H., and Wang, C.: Timing and mechanisms of Tibetan Plateau uplift, Nat Rev Earth Environ, 3, 652–667, https://doi.org/10.1038/s43017-022-00318-4, 2022.

Dlugokencky, E. and Tans, P.: Trends in Atmospheric Carbon Dioxide, n.d.

Dowsett, H., Dolan, A., Rowley, D., Moucha, R., Forte, A. M., Mitrovica, J. X., Pound, M., Salzmann, U., Robinson, M., Chandler, M., Foley, K., and Haywood, A.: The PRISM4 (mid-Piacenzian) paleoenvironmental reconstruction, Climate of the Past, 12, 1519–1538, https://doi.org/10.5194/cp-12-1519-2016, 2016.

Dunne, J. P., Hewitt, H. T., Arblaster, J. M., Bonou, F., Boucher, O., Cavazos, T., Dingley, B., Durack, P. J., Hassler, B., Juckes, M., Miyakawa, T., Mizielinski, M., Naik, V., Nicholls, Z., O'Rourke, E., Pincus, R., Sanderson, B. M., Simpson, I. R., and Taylor, K. E.: An evolving Coupled Model Intercomparison Project phase 7 (CMIP7) and Fast Track in support of future climate assessment, Geoscientific Model Development, 18, 6671–6700, https://doi.org/10.5194/gmd-18-6671-2025, 2025.

Dutkiewicz, A., Müller, R. D., Wang, X., O'Callaghan, S., Cannon, J., and Wright, N. M.: Predicting Sediment Thickness on Vanished Ocean Crust Since 200 Ma, Geochemistry, Geophysics, Geosystems, 18, 4586–4603, https://doi.org/10.1002/2017GC007258, 2017.

Ersoy, E. Y. and Helvacı, C.: Geochemistry and petrology of the lower Miocene bimodal volcanic units in the Tunçbilek–Domaniç basin, western Anatolia, International Geology Review, 58, 1234–1252, https://doi.org/10.1080/00206814.2016.1147385, 2016.

https://doi.org/10.5194/egusphere-2026-3595
Preprint. Discussion started: 3 August 2026

Etheridge, D.M., et al.: Law Dome Ice Core 2000-Year CO_2, CH_4, and N_2O Data, 2010.

Eyring, V., Bony, S., Meehl, G. A., Senior, C., Stevens, B., Stouffer, R. J., and Taylor, K. E.: Overview of the Coupled Model Intercomparison Project Phase 6 (CMIP6) experimental design and organisation, Geoscientific Model Development Discussions, 8, 10539–10583, https://doi.org/10.5194/gmdd-8-10539-2015, 2015.

Fan, M., Foote, J. M., Martin, A. J., and Zhu, L.: Stable isotope compositions of surface water in Mexico between 22–26 °N, Journal of South American Earth Sciences, 115, 103723, https://doi.org/10.1016/j.jsames.2022.103723, 2022.

Farnsworth, A., Lunt, D. J., O'Brien, C. L., Foster, G. L., Inglis, G. N., Markwick, P., Pancost, R. D., and Robinson, S. A.: Climate Sensitivity on Geological Timescales Controlled by Nonlinear Feedbacks and Ocean Circulation, Geophysical Research Letters, 46, 9880–9889, https://doi.org/10.1029/2019gl083574, 2019a.

Farnsworth, A., Lunt, D. J., Robinson, S. A., Valdes, P. J., Roberts, W. H. G., Clift, P. D., Markwick, P., Su, T., Wrobel, N., Bragg, F., Kelland, S.-J., and Pancost, R. D.: Past East Asian monsoon evolution controlled by paleogeography, not CO2, Science Advances, 5, eaax1697, https://doi.org/10.1126/sciadv.aax1697, 2019b.

Feng, R. and Poulsen, C. J.: Andean elevation control on tropical Pacific climate and ENSO, Paleoceanography, 29, 795–809, https://doi.org/10.1002/2014PA002640, 2014.

Feng, R., Poulsen, C. J., Werner, M., Chamberlain, C. P., Mix, H. T., and Mulch, A.: Early Cenozoic evolution of topography, climate, and stable isotopes in precipitation in the North American Cordillera, American Journal of Science, 313, 613–648, 2013.

Ferrari, L., Valencia-Moreno, M., and Bryan, S.: Magmatism and tectonics of the Sierra Madre Occidental and its relation with the evolution of the western margin of North America, in: Geology of México: Celebrating the Centenary of the Geological Society of México, edited by: Alaniz-Álvarez, S. A. and Nieto-Samaniego, Á. F., Geological Society of America, 0, https://doi.org/10.1130/2007.2422(01), 2007.

Fletcher, T. L.: A global terrestrial climate compilation for the Neogene, PAGES Magazine, 32, 142, https://doi.org/https://doi.org/10.22498/pages.32.2.142, 2024.

Foster, G. L., Lear, C. H., and Rae, J. W. B.: The evolution of pCO2, ice volume and climate during the middle Miocene, Earth and Planetary Science Letters, 341–344, 243–254, https://doi.org/10.1016/j.epsl.2012.06.007, 2012a.

Foster, G. L., Lear, C. H., and Rae, J. W. B.: The evolution of pCO2, ice volume and climate during the middle Miocene, Earth and Planetary Science Letters, 341–344, 243–254, https://doi.org/10.1016/j.epsl.2012.06.007, 2012b.

Foster, G. L., Royer, D. L., and Lunt, D. J.: Future climate forcing potentially without precedent in the last 420 million years, Nature Communications, 8, 14845, https://doi.org/10.1038/ncomms14845, 2017.

Franks, P. J., Royer, D. L., Beerling, D. J., Van de Water, P. K., Cantrill, D. J., Barbour, M. M., and Berry, J. A.: New constraints on atmospheric CO2 concentration for the Phanerozoic, Geophysical Research Letters, 41, 4685–4694, https://doi.org/10.1002/2014GL060457, 2014.

Frigola, A., Prange, M., and Schulz, M.: Boundary conditions for the Middle Miocene Climate Transition (MMCT v1.0), Geoscientific Model Development, 11, 1607–1626, https://doi.org/10.5194/gmd-11-1607-2018, 2018.

Frizon de Lamotte, D., Saint Bezar, B., Bracène, R., and Mercier, E.: The two main steps of the Atlas building and geodynamics of the western Mediterranean, Tectonics, 19, 740–761, https://doi.org/10.1029/2000TC900003, 2000.

Gallagher, S. J., Auer, G., Brierley, C. M., Fulthorpe, C. S., and Hall, R.: Cenozoic History of the Indonesian Gateway, Annual Review of Earth and Planetary Sciences, 52, 581–604, https://doi.org/10.1146/annurev-earth-040722-111322, 2024.

Garzione, C. N., McQuarrie, N., Perez, N. D., Ehlers, T. A., Beck, S. L., Kar, N., Eichelberger, N., Chapman, A. D., Ward, K. M., Ducea, M. N., Lease, R. O., Poulsen, C. J., Wagner, L. S., Saylor, J. E., Zandt, G., and Horton, B. K.: Tectonic Evolution of the Central Andean Plateau and Implications for the Growth of Plateaus, Annual Review of Earth and Planetary Sciences, 45, 529–559, https://doi.org/10.1146/annurev-earth-063016-020612, 2017.

Gasson, E., DeConto, R. M., Pollard, D., and Levy, R. H.: Dynamic Antarctic ice sheet during the early to mid-Miocene, Proceedings of the National Academy of Sciences, 113, 3459–3464, https://doi.org/10.1073/pnas.1516130113, 2016.

Gates, W. L.: AN AMS CONTINUING SERIES: GLOBAL CHANGE--AMIP: The Atmospheric Model Intercomparison Project, Bulletin of the American Meteorological Society, 73, 1962–1970, https://doi.org/10.1175/1520-0477(1992)073%3C1962:ATAMIP%3E2.0.CO;2, 1992.

Geen, R., Bordoni, S., Battisti, D. S., and Hui, K.: Monsoons, ITCZs, and the Concept of the Global Monsoon, Reviews of Geophysics, 58, e2020RG000700, https://doi.org/10.1029/2020RG000700, 2020.

Gordon, A. L.: Oceanography of the Indonesian Seas and Their Throughflow, Oceanography, 18, 14–27, 2005.

Gough, D. O.: Solar interior structure and luminosity variations, Sol Phys, 74, 21–34, https://doi.org/10.1007/BF00151270, 1981.

Green, J. A. M., Huber, M., Waltham, D., Buzan, J., and Wells, M.: Explicitly modelled deep-time tidal dissipation and its implication for Lunar history, Earth and Planetary Science Letters, 461, 46–53, https://doi.org/10.1016/j.epsl.2016.12.038, 2017.

Green, M., Hadley-Pryce, D., and Scotese, C.: Phanerozoic (541 Ma-present day), in: A journey through tides, Elsevier, 157–184, 2023.

Greenop, R., Foster, G. L., Wilson, P. A., and Lear, C. H.: Middle Miocene climate instability associated with high-amplitude CO2 variability, Paleoceanography, 29, 845–853, https://doi.org/10.1002/2014PA002653, 2014.

Greenop, R., Hain, M. P., Sosdian, S. M., Oliver, K. I. C., Goodwin, P., Chalk, T. B., Lear, C. H., Wilson, P. A., and Foster, G. L.: A record of Neogene seawater δ^{11}B reconstructed from paired δ^{11}B analyses on benthic and planktic foraminifera, Climate of the Past, 13, 149–170, https://doi.org/10.5194/cp-13-149-2017, 2017.

Grein, M., Oehm, C., Konrad, W., Utescher, T., Kunzmann, L., and Roth-Nebelsick, A.: Atmospheric CO2 from the late Oligocene to early Miocene based on photosynthesis data and fossil leaf characteristics, Palaeogeography, Palaeoclimatology, Palaeoecology, 374, 41–51, https://doi.org/10.1016/j.palaeo.2012.12.025, 2013.

Gross, M., Ramos, M. I. F., and Piller, W. E.: A minute ostracod (Crustacea: Cytheromatidae) from the Miocene Solimões Formation (western Amazonia, Brazil): evidence for marine incursions?, Journal of Systematic Palaeontology, 14, 581–602, https://doi.org/10.1080/14772019.2015.1078850, 2016.

Guillocheau, F., Chelalou, R., Linol, B., Dauteuil, O., Robin, C., Mvondo, F., Callec, Y., and Colin, J.-P.: Cenozoic Landscape Evolution in and Around the Congo Basin: Constraints from Sediments and Planation Surfaces, in: Geology and Resource Potential of the Congo Basin, edited by: de Wit, M. J., Guillocheau, F., and de Wit, M. C. J., Springer, Berlin, Heidelberg, 271–313, https://doi.org/10.1007/978-3-642-29482-2_14, 2015.

Guiraud, R., Bosworth, W., Thierry, J., and Delplanque, A.: Phanerozoic geological evolution of Northern and Central Africa: An overview, Journal of African Earth Sciences, 43, 83–143, https://doi.org/10.1016/j.jafrearsci.2005.07.017, 2005.

Gulick, S. P. S., Shevenell, A. E., Montelli, A., Fernandez, R., Smith, C., Warny, S., Bohaty, S. M., Sjunneskog, C., Leventer, A., Frederick, B., and Blankenship, D. D.: Initiation and long-term instability of the East Antarctic Ice Sheet, Nature, 552, 225–229, https://doi.org/10.1038/nature25026, 2017.

Halberstadt, A. R. W., Chorley, H., Levy, R. H., Naish, T., DeConto, R. M., Gasson, E., and Kowalewski, D. E.: CO2 and tectonic controls on Antarctic climate and ice-sheet evolution in the mid-Miocene, Earth and Planetary Science Letters, 564, 116908, https://doi.org/10.1016/j.epsl.2021.116908, 2021.

Hall, R., Gower, D., Johnson, K., Richardson, J., Rosen, B., Rüber, L., and Williams, S.: Sundaland and Wallacea: geology, plate tectonics and palaeogeography, Biotic evolution and environmental change in Southeast Asia, 82, 32, 2012.

Hamon, N., Sepulchre, P., Donnadieu, Y., Henrot, A.-J., François, L., Jaeger, J.-J., and Ramstein, G.: Growth of subtropical forests in Miocene Europe: The roles of carbon dioxide and Antarctic ice volume, Geology, 40, 567–570, https://doi.org/10.1130/G32990.1, 2012.

Harzhauser, M., Kroh, A., Mandic, O., Piller, W. E., Göhlich, U., Reuter, M., and Berning, B.: Biogeographic responses to geodynamics: A key study all around the Oligo–Miocene Tethyan Seaway, Zoologischer Anzeiger - A Journal of Comparative Zoology, 246, 241–256, https://doi.org/10.1016/j.jcz.2007.05.001, 2007.

Haywood, A. M., Chandler, M. A., Valdes, P. J., Salzmann, U., Lunt, D. J., and Dowsett, H. J.: Comparison of mid-Pliocene climate predictions produced by the HadAM3 and GCMAM3 General Circulation Models, Global and Planetary Change, 66, 208–224, https://doi.org/10.1016/j.gloplacha.2008.12.014, 2009.

Haywood, A. M., Dowsett, H. J., Otto-Bliesner, B., Chandler, M. A., Dolan, A. M., Hill, D. J., Lunt, D. J., Robinson, M. M., Rosenbloom, N., Salzmann, U., and Sohl, L. E.: Pliocene Model Intercomparison Project (PlioMIP): experimental design and boundary conditions (Experiment 1), Geoscientific Model Development, 3, 227–242, https://doi.org/10.5194/gmd-3-227-2010, 2010.

Haywood, A. M., Dowsett, H. J., Robinson, M. M., Stoll, D. K., Dolan, A. M., Lunt, D. J., Otto-Bliesner, B., and Chandler, M. A.: Pliocene Model Intercomparison Project (PlioMIP): experimental design and boundary conditions (Experiment 2), Geoscientific Model Development, 4, 571–577, https://doi.org/10.5194/gmd-4-571-2011, 2011.

Haywood, A. M., Hill, D. J., Dolan, A. M., Otto-Bliesner, B. L., Bragg, F., Chan, W. L., Chandler, M. A., Contoux, C., Dowsett, H. J., Jost, A., Kamae, Y., Lohmann, G., Lunt, D. J., Abe-Ouchi, A., Pickering, S. J., Ramstein, G., Rosenbloom, N. A., Salzmann, U., Sohl, L., Stepanek, C., Ueda, H., Yan, Q., and Zhang, Z.: Large-scale features of Pliocene climate: results from the Pliocene Model Intercomparison Project, Climate of the Past, 9, 191–209, https://doi.org/10.5194/cp-9-191-2013, 2013.

Haywood, A. M., Dowsett, H. J., Dolan, A. M., Rowley, D., Abe-Ouchi, A., Otto-Bliesner, B., Chandler, M. A., Hunter, S. J., Lunt, D. J., Pound, M., and Salzmann, U.: The Pliocene Model Intercomparison Project (PlioMIP) Phase 2: scientific objectives and experimental design, Climate of the Past, 12, 663–675, https://doi.org/10.5194/cp-12-663-2016, 2016.

Haywood, A. M., Tindall, J. C., Dowsett, H. J., Dolan, A. M., Foley, K. M., Hunter, S. J., Hill, D. J., Chan, W. L., Abe-Ouchi, A., Stepanek, C., Lohmann, G., Chandan, D., Peltier, W. R., Tan, N., Contoux, C., Ramstein, G., Li, X., Zhang, Z., Guo, C., Nisancioglu, K. H., Zhang, Q., Li, Q., Kamae, Y., Chandler, M. A., Sohl, L. E., Otto-Bliesner, B. L., Feng, R., Brady, E. C., Heydt, A. S. von der, Baatsen, M., and Lunt, D. J.: A return to large-scale features of Pliocene climate: the Pliocene Model Intercomparison Project Phase 2, https://doi.org/10.5194/cp-2019-145, 2020.

Herbert, T. D., Lawrence, K. T., Tzanova, A., Peterson, L. C., Caballero-Gill, R., and Kelly, C. S.: Late Miocene global cooling and the rise of modern ecosystems, Nature Geosci, 9, 843–847, https://doi.org/10.1038/ngeo2813, 2016.

Herbert, T. D., Dalton, C. A., Liu, Z., Salazar, A., Si, W., and Wilson, D. S.: Tectonic degassing drove global temperature trends since 20 Ma, Science, https://doi.org/10.1126/science.abl4353, 2022.

Herold, N., Seton, M., Müller, R. D., You, Y., and Huber, M.: Middle Miocene tectonic boundary conditions for use in climate models, Geochemistry, Geophysics, Geosystems, 9, Q10009, https://doi.org/10.1029/2008gc002046, 2008.

Herold, N., Huber, M., and Müller, R. D.: Modeling the Miocene Climatic Optimum. Part I: Land and Atmosphere*, Journal of Climate, 24, 6353–6372, https://doi.org/10.1175/2011jcli4035.1, 2011.

van Hinsbergen, D. J. J., Torsvik, T. H., Schmid, S. M., Maţenco, L. C., Maffione, M., Vissers, R. L. M., Gürer, D., and Spakman, W.: Orogenic architecture of the Mediterranean region and kinematic reconstruction of its tectonic evolution since the Triassic, Gondwana Research, 81, 79–229, https://doi.org/10.1016/j.gr.2019.07.009, 2020.

Hochmuth, K., Paxman, G., Gohl, K., Jamieson, S., Leitchenkov, G., Bentley, M., Ferraccioli, F., Sauermilch, I., Whittaker, J., Uenzelmann-Neben, G., and others: Combined palaeotopography and palaeobathymetry of the Antarctic continent and the Southern Ocean since 34 Ma, 2020a.

Hochmuth, K., Gohl, K., Leitchenkov, G., Sauermilch, I., Whittaker, J. M., Uenzelmann-Neben, G., Davy, B., and De Santis, L.: The Evolving Paleobathymetry of the Circum-Antarctic Southern Ocean Since 34 Ma: A Key to Understanding Past Cryosphere-Ocean Developments, Geochemistry, Geophysics, Geosystems, 21, e2020GC009122, https://doi.org/10.1029/2020GC009122, 2020b.

Hoffert, M. I. and Covey, C.: Deriving global climate sensitivity from palaeoclimate reconstructions, Nature, 360, 573–576, https://doi.org/10.1038/360573a0, 1992.

Hoorn, C., Wesselingh, F. P., Steege, H. T., Bermudez, M. A., Mora, A., Sevink, J., Sanmartín, I., Sanchez-Meseguer, A., Anderson, C. L., Figueiredo, J. P., Jaramillo, C., Riff, D., Negri, F. R., Hooghiemstra, H., Lundberg, J., Stadler, T., Särkinen, T., and Antonelli, A.: Amazonia Through Time: Andean Uplift, Climate Change, Landscape Evolution, and Biodiversity, Science, 330, 927–931, https://doi.org/10.1126/science.1194585, 2010.

https://doi.org/10.5194/egusphere-2026-3595
Preprint. Discussion started: 3 August 2026

Hoorn, C., Boschman, L. M., Kukla, T., Sciumbata, M., and Val, P.: The Miocene wetland of western Amazonia and its role in Neotropical biogeography, Bot J Linn Soc, 199, 25–35, https://doi.org/10.1093/botlinnean/boab098, 2022.

Hossain, A., Knorr, G., Lohmann, G., Stärz, M., and Jokat, W.: Simulated Thermohaline Fingerprints in Response to Different Greenland-Scotland Ridge and Fram Strait Subsidence Histories, Paleoceanography and Paleoclimatology, 35, e2019PA003842, https://doi.org/10.1029/2019PA003842, 2020.

Hossain, A., Knorr, G., Jokat, W., and Lohmann, G.: Opening of the Fram Strait led to the establishment of a modern-like three-layer stratification in the Arctic Ocean during the Miocene, Arktos, 7, 1–12, https://doi.org/10.1007/s41063-020-00079-8, 2021.

Huang, X., Wang, C., Wei, J., Yu, Z., Liu, H., and Lin, P.: Effects of Tide-Induced Mixing on the Equator-to-Pole Surface Temperature Gradient during the Middle Miocene Climate Optimum, https://doi.org/10.1175/JCLI-D-25-0038.1, 2025.

Huber, M. and Goldner, A.: Eocene monsoons, Journal of Asian Earth Sciences, 44, 3–23, https://doi.org/10.1016/j.jseaes.2011.09.014, 2012.

Hutchinson, D. K., Coxall, H. K., O′Regan, M., Nilsson, J., Caballero, R., and Boer, A. M. D.: Arctic closure as a trigger for Atlantic overturning at the Eocene-Oligocene Transition, Nature Communications, 10, 1–9, https://doi.org/10.1038/s41467-019-11828-z, 2019.

Hutchinson, D. K., Meissner, K. J., Menviel, L., Wright, N. M., Berg, J., and Acosta, R. P.: Pacific and Atlantic Modes of Overturning in the Miocene Climatic Optimum, Paleoceanography and Paleoclimatology, 40, e2025PA005220, https://doi.org/10.1029/2025PA005220, 2025.

Jakobsen, F. W., Winsborrow, M., Nielsen, T., Laberg, J. S., Plaza-Faverola, A., Böttner, C., López-Quirós, A., Planke, S., and Bellwald, B.: Continental shelf glaciations off Northeast Greenland since the Late Miocene, Climate of the Past, 21, 2441–2464, https://doi.org/10.5194/cp-21-2441-2025, 2025.

Jakobsson, M., Backman, J., Rudels, B., Nycander, J., Frank, M., Mayer, L., Jokat, W., Sangiorgi, F., O'Regan, M., Brinkhuis, H., King, J., and Moran, K.: The early Miocene onset of a ventilated circulation regime in the Arctic Ocean, Nature, 447, 986–990, https://doi.org/10.1038/nature05924, 2007.

Japsen, P., Green, P. F., Bonow, J. M., Nielsen, T. F. D., and Chalmers, J. A.: From volcanic plains to glaciated peaks: Burial, uplift and exhumation history of southern East Greenland after opening of the NE Atlantic, Global and Planetary Change, 116, 91–114, https://doi.org/10.1016/j.gloplacha.2014.01.012, 2014.

Jaramillo, C., Romero, I., D'Apolito, C., Bayona, G., Duarte, E., Louwye, S., Escobar, J., Luque, J., Carrillo-Briceño, J. D., Zapata, V., Mora, A., Schouten, S., Zavada, M., Harrington, G., Ortiz, J., and Wesselingh, F. P.: Miocene flooding events of western Amazonia, Science Advances, 3, e1601693, https://doi.org/10.1126/sciadv.1601693, 2017.

Jaramillo, C., Hoorn, K., Perrigo, A., and Antonelli, A.: Evolution of the Isthmus of Panama: biological, paleoceanographic and paleoclimatological implications, Mountains, climate and biodiversity, 4, 323–338, 2018.

Jeffery, M. L., Poulsen, C. J., and Ehlers, T. A.: Impacts of Cenozoic global cooling, surface uplift, and an inland seaway on South American paleoclimate and precipitation δ18O, GSA Bulletin, 124, 335–351, https://doi.org/10.1130/B30480.1, 2012.

Ji, S., Nie, J., Lechler, A., Huntington, K. W., Heitmann, E. O., and Breecker, D. O.: A symmetrical CO2 peak and asymmetrical climate change during the middle Miocene, Earth and Planetary Science Letters, 499, 134–144, https://doi.org/10.1016/j.epsl.2018.07.011, 2018.

Johnson, S. J., Levine, R. C., Turner, A. G., Martin, G. M., Woolnough, S. J., Schiemann, R., Mizielinski, M. S., Roberts, M. J., Vidale, P. L., Demory, M.-E., and Strachan, J.: The resolution sensitivity of the South Asian monsoon and Indo-Pacific in a global 0.35° AGCM, Clim Dyn, 46, 807–831, https://doi.org/10.1007/s00382-015-2614-1, 2016.

Kaplan, J. O.: Geophysical applications of vegetation modeling, Lund University, 2001.

Karp, A. T., Holman, A. I., Hopper, P., Grice, K., and Freeman, K. H.: Fire distinguishers: Refined interpretations of polycyclic aromatic hydrocarbons for paleo-applications, Geochimica et Cosmochimica Acta, 289, 93–113, https://doi.org/10.1016/j.gca.2020.08.024, 2020.

Keeling, C. D., Bacastow, R. B., Bainbridge, A. E., Ekdahl, C. A., Guenther, P. R., Waterman, L. S., and Chin, J. F. S.: Atmospheric carbon dioxide variations at Mauna Loa Observatory, Hawaii, Tellus, 28, https://doi.org/10.3402/tellusa.v28i6.11322, 1976.

Kirillova, V., Osborne, A. H., Störling, T., and Frank, M.: Miocene restriction of the Pacific-North Atlantic throughflow strengthened Atlantic overturning circulation, Nat Commun, 10, 4025, https://doi.org/10.1038/s41467-019-12034-7, 2019.

Kissling, E. and Schlunegger, F.: Rollback Orogeny Model for the Evolution of the Swiss Alps, Tectonics, 37, 1097–1115, https://doi.org/10.1002/2017TC004762, 2018.

Knorr, G. and Lohmann, G.: Climate warming during Antarctic ice sheet expansion at the Middle Miocene transition, Nature Geoscience, 7, 376–381, https://doi.org/10.1038/ngeo2119, 2014.

https://doi.org/10.5194/egusphere-2026-3595
Preprint. Discussion started: 3 August 2026

Konrad, W., Katul, G., Roth-Nebelsick, A., and Grein, M.: A reduced order model to analytically infer atmospheric CO2 concentration from stomatal and climate data, Advances in Water Resources, 104, 145–157, https://doi.org/10.1016/j.advwatres.2017.03.018, 2017.

Krapp, M. and Jungclaus, J. H.: The Middle Miocene climate as modelled in an atmosphere-ocean-biosphere model, Climate of the Past, 7, 1169–1188, https://doi.org/10.5194/cp-7-1169-2011, 2011.

Krsnik, E., Methner, K., Campani, M., Botsyun, S., Mutz, S. G., Ehlers, T. A., Kempf, O., Fiebig, J., Schlunegger, F., and Mulch, A.: Miocene high elevation in the Central Alps, Solid Earth, 12, 2615–2631, https://doi.org/10.5194/se-12-2615-2021, 2021.

Kuhnt, W., Holbourn, A., Hall, R., Zuvela, M., and Käse, R.: Neogene history of the Indonesian throughflow. In Continent-Ocean Interactions Within East Asian Marginal Seas (eds P. Clift, W. Kuhnt, P. Wang and D. Hayes), https://doi.org/10.1029/149GM16, 2004.

Kürschner, W. M., Kvaček, Z., and Dilcher, D. L.: The impact of Miocene atmospheric carbon dioxide fluctuations on climate and the evolution of terrestrial ecosystems, Proceedings of the National Academy of Sciences, 105, 449–453, https://doi.org/10.1073/pnas.0708588105, 2008.

Kurum, S., Onal, A., Boztug, D., Spell, T., and Arslan, M.: 40Ar/39Ar age and geochemistry of the post-collisional Miocene Yamadag volcanics in the Arapkir area (Malatya Province), eastern Anatolia, Turkey, Journal of Asian Earth Sciences, 33, 229–251, 2008.

Kutzbach, J. E.: Modeling of Paleoclimates, in: Advances in Geophysics, vol. 28, edited by: Saltzman, B., Elsevier, 159–196, https://doi.org/10.1016/S0065-2687(08)60223-X, 1985.

Ladant, J.-B., Millot-Weil, J., de Lavergne, C., Green, J. A. M., Nguyen, S., and Donnadieu, Y.: The Role of Tidal Mixing in Shaping Early Eocene Deep Ocean Circulation and Oxygenation, Paleoceanography and Paleoclimatology, 39, e2023PA004822, https://doi.org/10.1029/2023PA004822, 2024.

Lanari, R., Faccenna, C., Natali, C., Şengül Uluocak, E., Fellin, M. G., Becker, T. W., Göğüş, O. H., Youbi, N., Clementucci, R., and Conticelli, S.: The Atlas of Morocco: A Plume-Assisted Orogeny, Geochemistry, Geophysics, Geosystems, 24, e2022GC010843, https://doi.org/10.1029/2022GC010843, 2023.

Laskar, J., Fienga, A., Gastineau, M., and Manche, H.: La2010: a new orbital solution for the long-term motion of the Earth, Astronomy & Astrophysics, 532, A89, https://doi.org/10.1051/0004-6361/201116836, 2011.

Lear, C. H., Coxall, H. K., Foster, G. L., Lunt, D. J., Mawbey, E. M., Rosenthal, Y., Sosdian, S. M., Thomas, E., and Wilson, P. A.: Neogene ice volume and ocean temperatures: Insights from infaunal foraminiferal Mg/Ca paleothermometry, Paleoceanography, 30, 1437–1454, https://doi.org/10.1002/2015PA002833, 2015.

Lemarchand, D., Gaillardet, J., Lewin, É., and Allègre, C. J.: The influence of rivers on marine boron isotopes and implications for reconstructing past ocean pH, Nature, 408, 951–954, https://doi.org/10.1038/35050058, 2000.

LeMasurier, W. E.: Tectono-magmatic domes: the stationary plate equivalent of a linear volcanic chain, Bull Volcanol, 84, 48, https://doi.org/10.1007/s00445-022-01558-4, 2022.

Lenton, T.M., Milkoreit, M., Willcock, S., Abrams, J.F., Mc Kay, D.L.A., Buxton, J.E., Donges, J., Loriani, S., Wunderling, N., Alkemade, F., and Barrett, M.: Global tipping points report 2025, University of Exeter, Exeter, 2025.

Levy, R., Harwood, D., Florindo, F., Sangiorgi, F., Tripati, R., Eynatten, H. von, Gasson, E., Kuhn, G., Tripati, A., DeConto, R., Fielding, C., Field, B., Golledge, N., McKay, R., Naish, T., Olney, M., Pollard, D., Schouten, S., Talarico, F., Warny, S., Willmott, V., Acton, G., Panter, K., Paulsen, T., Taviani, M., and Team, S. S.: Antarctic ice sheet sensitivity to atmospheric CO2 variations in the early to mid-Miocene, Proceedings of the National Academy of Sciences, 113, 3453–3458, https://doi.org/10.1073/pnas.1516030113, 2016.

Lewis, A. R. and Ashworth, A. C.: An early to middle Miocene record of ice-sheet and landscape evolution from the Friis Hills, Antarctica, GSA Bulletin, 128, 719–738, https://doi.org/10.1130/B31319.1, 2016.

Lhomme, N., Clarke, G. K. C., and Ritz, C.: Global budget of water isotopes inferred from polar ice sheets, Geophysical Research Letters, 32, https://doi.org/10.1029/2005GL023774, 2005.

Li, S.-F., Valdes, P. J., Farnsworth, A., Davies-Barnard, T., Su, T., Lunt, D. J., Spicer, R. A., Liu, J., Deng, W.-Y.-D., Huang, J., Tang, H., Ridgwell, A., Chen, L.-L., and Zhou, Z.-K.: Orographic evolution of northern Tibet shaped vegetation and plant diversity in eastern Asia, Science Advances, 7, eabc7741, https://doi.org/10.1126/sciadv.abc7741, 2021.

Licht, A., Quade, J., Kowler, A., Santos, M. de los, Hudson, A., Schauer, A., Huntington, K., Copeland, P., and Lawton, T.: Impact of the North American monsoon on isotope paleoaltimeters: Implications for the paleoaltimetry of the American southwest, American Journal of Science, 317, 1–33, https://doi.org/10.2475/01.2017.01, 2017.

Liu, L.: The ups and downs of North America: Evaluating the role of mantle dynamic topography since the Mesozoic, Reviews of Geophysics, 53, 1022–1049, https://doi.org/10.1002/2015RG000489, 2015.

https://doi.org/10.5194/egusphere-2026-3595
Preprint. Discussion started: 3 August 2026

Liu, X., Herold, N., and Huber, M.: Atlantic Meridional Overturning Circulation Influence on the Annual Mean Intertropical Convergence Zone Location in the Miocene, Geophysical Research Letters, 51, e2024GL109159, https://doi.org/10.1029/2024GL109159, 2024.

Londoño, L., Royer, D. L., Jaramillo, C., Escobar, J., Foster, D. A., Cárdenas-Rozo, A. L., and Wood, A.: Early Miocene CO2 estimates from a Neotropical fossil leaf assemblage exceed 400 ppm, American Journal of Botany, 105, 1929–1937, https://doi.org/10.1002/ajb2.1187, 2018.

Lunt, D. J., Valdes, P. J., Haywood, A., and Rutt, I. C.: Closure of the Panama Seaway during the Pliocene: implications for climate and Northern Hemisphere glaciation, Climate Dynamics, 30, 1–18, https://doi.org/10.1007/s00382-007-0265-6, 2008.

Lunt, D. J., Jones, T. D., Heinemann, M., Huber, M., LeGrande, A., Winguth, A., Loptson, C., Marotzke, J., Roberts, C. D., Tindall, J., Valdes, P., and Winguth, C.: A model–data comparison for a multi-model ensemble of early Eocene atmosphere–ocean simulations: EoMIP, Climate of the Past, 8, 1717–1736, https://doi.org/10.5194/cp-8-1717-2012, 2012.

Lunt, D. J., Huber, M., Anagnostou, E., Baatsen, M. L. J., Caballero, R., DeConto, R., Dijkstra, H. A., Donnadieu, Y., Evans, D., Feng, R., Foster, G. L., Gasson, E., Heydt, A. S. von der, Hollis, C. J., Inglis, G. N., Jones, S. M., Kiehl, J., Turner, S. K., Korty, R. L., Kozdon, R., Krishnan, S., Ladant, J.-B., Langebroek, P., Lear, C. H., LeGrande, A. N., Littler, K., Markwick, P., Otto-Bliesner, B., Pearson, P., Poulsen, C. J., Salzmann, U., Shields, C., Snell, K., Stärz, M., Super, J., Tabor, C., Tierney, J. E., Tourte, G. J. L., Tripati, A., Upchurch, G. R., Wade, B. S., Wing, S. L., Winguth, A. M. E., Wright, N. M., Zachos, J. C., and Zeebe, R. E.: The DeepMIP contribution to PMIP4: experimental design for model simulations of the EECO, PETM, and pre-PETM (version 1.0), Geoscientific Model Development, 10, 889–901, https://doi.org/10.5194/gmd-10-889-2017, 2017.

Lunt, D. J., Bragg, F., Chan, W.-L., Hutchinson, D. K., Ladant, J.-B., Morozova, P., Niezgodzki, I., Steinig, S., Zhang, Z., Zhu, J., Abe-Ouchi, A., Anagnostou, E., Boer, A. M. de, Coxall, H. K., Donnadieu, Y., Foster, G., Inglis, G. N., Knorr, G., Langebroek, P. M., Lear, C. H., Lohmann, G., Poulsen, C. J., Sepulchre, P., Tierney, J. E., Valdes, P. J., Volodin, E. M., Jones, T. D., Hollis, C. J., Huber, M., and Otto-Bliesner, B. L.: DeepMIP: model intercomparison of early Eocene climatic optimum (EECO) large-scale climate features and comparison with proxy data, Climate of the Past, 17, 203–227, https://doi.org/10.5194/cp-17-203-2021, 2020.

Lunt, D. J., Wright, N. M., Vaes, B., Salzmann, U., Rae, J. W. B., Hickler, T., Hutchinson, D. K., Brugger, J., Zhu, J., Steinig, S., Meckler, A. N., Inglis, G. N., Evans, D., de Boer, A. M., Otto-Bliesner, B. L., Burls, N., Zhang, Y., Sluijs, A., Reichgelt, T., Niezgodzki, I., Meissner, K., Ladant, J.-B., Kelemen, F. D., Huber, M., Greenwood, D., Green, M., Boscolo-Galazzo, F., Blau, M. T., and Baatsen, M.: DeepMIP-Eocene-p2: Experimental design for Phase 2 of the early Eocene component of the the CMIP7/PMIP7 Deep-time Model Intercomparison Project (DeepMIP-Eocene), EGUsphere, 1–30, https://doi.org/10.5194/egusphere-2025-6135, 2026.

https://doi.org/10.5194/egusphere-2026-3595
Preprint. Discussion started: 3 August 2026

MacFarling Meure, C., Etheridge, D., Trudinger, C., Steele, P., Langenfelds, R., van Ommen, T., Smith, A., and Elkins, J.: Law Dome CO_2, CH_4 and N_2O ice core records extended to 2000 years BP, Geophysical Research Letters, 33, https://doi.org/10.1029/2006GL026152, 2006.

Markwick, P. J.: The palaeogeographic and palaeoclimatic significance of climate proxies for data-model comparisons, in: Deep-Time Perspectives on Climate Change: Marrying the Signal from Computer Models and Biological Proxies, vol. 2, edited by: Williams, M., Haywood, A. M., Gregory, F. J., and Schmidt, D. N., Geological Society of London, 0, https://doi.org/10.1144/TMS002.13, 2007.

Marschalek, J. W., Zurli, L., Talarico, F., van de Flierdt, T., Vermeesch, P., Carter, A., Beny, F., Bout-Roumazeilles, V., Sangiorgi, F., Hemming, S. R., Pérez, L. F., Colleoni, F., Prebble, J. G., van Peer, T. E., Perotti, M., Shevenell, A. E., Browne, I., Kulhanek, D. K., Levy, R., Harwood, D., Sullivan, N. B., Meyers, S. R., Griffith, E. M., Hillenbrand, C.-D., Gasson, E., Siegert, M. J., Keisling, B., Licht, K. J., Kuhn, G., Dodd, J. P., Boshuis, C., De Santis, L., and McKay, R. M.: A large West Antarctic Ice Sheet explains early Neogene sea-level amplitude, Nature, 600, 450–455, https://doi.org/10.1038/s41586-021-04148-0, 2021.

Martínez, C., Jaramillo, C., Correa-Metrío, A., Crepet, W., Moreno, J. E., Aliaga, A., Moreno, F., Ibañez-Mejia, M., and Bush, M. B.: Neogene precipitation, vegetation, and elevation history of the Central Andean Plateau, Science Advances, 6, eaaz4724, https://doi.org/10.1126/sciadv.aaz4724, 2020.

Mather, B. R., Müller, R. D., Zahirovic, S., Cannon, J., Chin, M., Ilano, L., Wright, N. M., Alfonso, C., Williams, S., Tetley, M., and Merdith, A.: Deep time spatio-temporal data analysis using pyGPlates with PlateTectonicTools and GPlately, Geoscience Data Journal, 11, 3–10, https://doi.org/10.1002/gdj3.185, 2024.

McGregor, S., Timmermann, A., Jin, F.-F., and Kessler, W. S.: Charging El Niño with off-equatorial westerly wind events, Climate Dynamics, 47, 1111–1125, https://doi.org/10.1007/s00382-015-2891-8, 2015.

McKay, R., Cockrell, J., Shevenell, A. E., Laberg, J. S., Burns, J., Patterson, M., Kim, S., Naish, T., Harwood, D., Levy, R., Marschalek, J., van de Flierdt, T., Saki, I., Keisling, B., de Sousa, I. M. C., Cortese, G., Sangiorgi, F., Leckie, R. M., Dodd, J., Duncan, B., Pérez, L. F., Romans, B. W., Kim, S., Bombard, S., Browne, I., van Peer, T., Seki, O., Colleoni, F., Kulhanek, D., De Santis, L., and the IODP Expedition 374 Science Team: Miocene ice sheet dynamics and sediment deposition in the central Ross Sea, Antarctica, GSA Bulletin, 137, 1267–1291, https://doi.org/10.1130/B37613.1, 2025.

McKay, R. M., De Santis, L., Kulhanek, D. K., Ash, J., Beny, F., Browne, I., Cortese, G., Cordeiro de Sousa, I., Dodd, J., Esper, O., and others: Expedition 374 summary, Proceedings of the International Ocean Discovery Program, 2019.

https://doi.org/10.5194/egusphere-2026-3595
Preprint. Discussion started: 3 August 2026

Medvedev, S., Hartz, E. H., and Faleide, J. I.: Erosion-driven vertical motions of the circum Arctic: Comparative analysis of modern topography, Journal of Geodynamics, 119, 62–81, https://doi.org/10.1016/j.jog.2018.04.003, 2018.

Meehl, G. A., Boer, G. J., Covey, C., Latif, M., and Stouffer, R. J.: Intercomparison makes for a better climate model, Eos, Transactions American Geophysical Union, 78, 445–451, https://doi.org/10.1029/97EO00276, 1997.

Meissner, K. J., Bralower, T. J., Alexander, K., Jones, T. D., Sijp, W., and Ward, M.: The Paleocene-Eocene Thermal Maximum: How much carbon is enough?, Paleoceanography, 29, 946–963, https://doi.org/10.1002/2014PA002650, 2014.

Mejía, L. M., Méndez-Vicente, A., Abrevaya, L., Lawrence, K. T., Ladlow, C., Bolton, C., Cacho, I., and Stoll, H.: A diatom record of CO2 decline since the late Miocene, Earth and Planetary Science Letters, 479, 18–33, https://doi.org/10.1016/j.epsl.2017.08.034, 2017.

Merdith, A. S., Williams, S. E., Collins, A. S., Tetley, M. G., Mulder, J. A., Blades, M. L., Young, A., Armistead, S. E., Cannon, J., Zahirovic, S., and Müller, R. D.: Extending full-plate tectonic models into deep time: Linking the Neoproterozoic and the Phanerozoic, Earth-Science Reviews, 214, 103477, https://doi.org/10.1016/j.earscirev.2020.103477, 2021.

Miao, Y., Fang, X., Sun, J., Xiao, W., Yang, Y., Wang, X., Farnsworth, A., Huang, K., Ren, Y., Wu, F., Qiao, Q., Zhang, W., Meng, Q., Yan, X., Zheng, Z., Song, C., and Utescher, T.: A new biologic paleoaltimetry indicating Late Miocene rapid uplift of northern Tibet Plateau, Science, 378, 1074–1079, https://doi.org/10.1126/science.abo2475, 2022.

Michon, L., Famin, V., and Quidelleur, X.: Evolution of the East African Rift System from trap-scale to plate-scale rifting, Earth-Science Reviews, 231, 104089, https://doi.org/10.1016/j.earscirev.2022.104089, 2022.

Miller, K. G., Browning, J. V., Schmelz, W. J., Kopp, R. E., Mountain, G. S., and Wright, J. D.: Cenozoic sea-level and cryospheric evolution from deep-sea geochemical and continental margin records, Science Advances, 6, eaaz1346, https://doi.org/10.1126/sciadv.aaz1346, 2020.

Miller, K. G., Schmelz, W. J., Browning, J. V., Rosenthal, Y., Hess, A. V., Kopp, R. E., and Wright, J. D.: Global Mean and Relative Sea-Level Changes Over the Past 66 Myr: Implications for Early Eocene Ice Sheets, Earth Science, Systems and Society, 4, 10091, https://doi.org/10.3389/esss.2023.10091, 2024.

Missenard, Y., Taki, Z., Frizon de Lamotte, D., Benammi, M., Hafid, M., Leturmy, P., and Sébrier, M.: Tectonic styles in the Marrakesh High Atlas (Morocco): The role of heritage and mechanical stratigraphy, Journal of African Earth Sciences, 48, 247–266, https://doi.org/10.1016/j.jafrearsci.2007.03.007, 2007.

https://doi.org/10.5194/egusphere-2026-3595
Preprint. Discussion started: 3 August 2026

Modak, A., Bala, G., Cao, L., and Caldeira, K.: Why must a solar forcing be larger than a CO2 forcing to cause the same global mean surface temperature change?, Environ. Res. Lett., 11, 044013, https://doi.org/10.1088/1748-9326/11/4/044013, 2016.

Molnar, P.: Comment (2) on “Formation of the Isthmus of Panama” by O’Dea et al., Science Advances, 3, e1602320, https://doi.org/10.1126/sciadv.1602320, 2017.

Molnar, P., Boos, W. R., and Battisti, D. S.: Orographic Controls on Climate and Paleoclimate of Asia: Thermal and Mechanical Roles for the Tibetan Plateau, Annual Review of Earth and Planetary Sciences, 38, 77–102, https://doi.org/10.1146/annurev-earth-040809-152456, 2010.

Montelli, A., Gulick, S. P. S., Fernandez, R., Frederick, B. C., Shevenell, A. E., Leventer, A., and Blankenship, D. D.: Seismic stratigraphy of the Sabrina Coast shelf, East Antarctica: Early history of dynamic meltwater-rich glaciations, GSA Bulletin, 132, 545–561, https://doi.org/10.1130/B35100.1, 2020.

Montes, C., Cardona, A., McFadden, R., Moron, S. E., Silva, C. A., Restrepo-Moreno, S., Ramirez, D. A., Hoyos, N., Wilson, J., Farris, D., Bayona, G. A., Jaramillo, C. A., Valencia, V., Bryan, J., and Flores, J. A.: Evidence for middle Eocene and younger land emergence in central Panama: Implications for Isthmus closure, Geological Society of America Bulletin, 124, 780–799, https://doi.org/10.1130/b30528.1, 2012.

Montes, C., Cardona, A., Jaramillo, C., Pardo, A., Silva, J. C., Valencia, V., Ayala, C., Perez-Angel, L. C., Rodriguez-Parra, L. A., Ramirez, V., and Nino, H.: Middle Miocene closure of the Central American Seaway, Science, 348, 226–229, https://doi.org/10.1126/science.aaa2815, 2015.

Morice, C. P., Kennedy, J. J., Rayner, N. A., Winn, J. P., Hogan, E., Killick, R. E., Dunn, R. J. H., Osborn, T. J., Jones, P. D., and Simpson, I. R.: An Updated Assessment of Near-Surface Temperature Change From 1850: The HadCRUT5 Data Set, Journal of Geophysical Research: Atmospheres, 126, e2019JD032361, https://doi.org/10.1029/2019JD032361, 2021.

Morley, C.: Early syn-rift igneous dike patterns, northern Kenya Rift (Turkana, Kenya): Implications for local and regional stresses, tectonics, and magma-structure interactions, Geosphere, 16, 890–918, 2020.

Mouthereau, F.: Timing of uplift in the Zagros belt/Iranian plateau and accommodation of late Cenozoic Arabia–Eurasia convergence, Geological Magazine, 148, 726–738, https://doi.org/10.1017/S0016756811000306, 2011.

Müller, R. D., Sdrolias, M., Gaina, C., and Roest, W. R.: Age, spreading rates, and spreading asymmetry of the world’s ocean crust, Geochemistry, Geophysics, Geosystems, 9, https://doi.org/10.1029/2007GC001743, 2008a.

https://doi.org/10.5194/egusphere-2026-3595
Preprint. Discussion started: 3 August 2026

Müller, R. D., Sdrolias, M., Gaina, C., Steinberger, B., and Heine, C.: Long-Term Sea-Level Fluctuations Driven by Ocean Basin Dynamics, Science, 319, 1357–1362, https://doi.org/10.1126/science.1151540, 2008b.

Müller, R. D., Cannon, J., Williams, S., and Dutkiewicz, A.: PyBacktrack 1.0: A Tool for Reconstructing Paleobathymetry on Oceanic and Continental Crust, Geochemistry, Geophysics, Geosystems, 19, 1898–1909, https://doi.org/10.1029/2017GC007313, 2018.

Munk, W. H.: Abyssal recipes, Deep Sea Research and Oceanographic Abstracts, 13, 707–730, https://doi.org/10.1016/0011-7471(66)90602-4, 1966.

Naik, T. J., de Boer, A. M., Coxall, H. K., Burls, N. J., Bradshaw, C. D., Donnadieu, Y., Farnsworth, A., Frigola, A., Herold, N., Huber, M., Karami, M. P., Knorr, G., LeGrande, A. N., Li, Y., Lohmann, G., Lunt, D. J., Prange, M., and Zhang, Y.: Ocean Meridional Overturning Circulation During the Early and Middle Miocene, Paleoceanography and Paleoclimatology, 40, e2024PA005055, https://doi.org/10.1029/2024PA005055, 2025.

Nicholls, Z., Lewis, J., Makin, M., Nattala, U., Zhang, G. Z., Mutch, S. J., Tescari, E., and Meinshausen, M.: Regionally aggregated, stitched and de-drifted CMIP-climate data, processed with netCDF-SCM v2.0.0, Geoscience Data Journal, 8, 154–198, https://doi.org/10.1002/gdj3.113, 2021.

O'Dea, A., Lessios, H. A., Coates, A. G., Eytan, R. I., Restrepo-Moreno, S. A., Cione, A. L., Collins, L. S., de Queiroz, A., Farris, D. W., Norris, R. D., Stallard, R. F., Woodburne, M. O., Aguilera, O., Aubry, M.-P., Berggren, W. A., Budd, A. F., Cozzuol, M. A., Coppard, S. E., Duque-Caro, H., Finnegan, S., Gasparini, G. M., Grossman, E. L., Johnson, K. G., Keigwin, L. D., Knowlton, N., Leigh, E. G., Leonard-Pingel, J. S., Marko, P. B., Pyenson, N. D., Rachello-Dolmen, P. G., Soibelzon, E., Soibelzon, L., Todd, J. A., Vermeij, G. J., and Jackson, J. B. C.: Formation of the Isthmus of Panama, Science Advances, 2, e1600883, https://doi.org/10.1126/sciadv.1600883, 2016.

Okay, A. I., Zattin, M., and Cavazza, W.: Apatite fission-track data for the Miocene Arabia-Eurasia collision, Geology, 38, 35–38, https://doi.org/10.1130/G30234.1, 2010.

O'Neill, C., Müller, D., and Steinberger, B.: On the uncertainties in hot spot reconstructions and the significance of moving hot spot reference frames, Geochemistry, Geophysics, Geosystems, 6, https://doi.org/10.1029/2004GC000784, 2005.

Osborne, A. H., Newkirk, D. R., Groeneveld, J., Martin, E. E., Tiedemann, R., and Frank, M.: The seawater neodymium and lead isotope record of the final stages of Central American Seaway closure, Paleoceanography, 29, 715–729, https://doi.org/10.1002/2014PA002676, 2014.

Osman, M. B., Tierney, J. E., Zhu, J., Tardif, R., Hakim, G. J., King, J., and Poulsen, C. J.: Globally resolved surface temperatures since the Last Glacial Maximum, Nature, 599, 239–244, https://doi.org/10.1038/s41586-021-03984-4, 2021.

Özkul, C., Temizel, İ., Özburan, M., Arslan, M., and Kibici, Y.: Geochronology and geochemistry of the Miocene volcanics from the Kütahya area: Constraints for post-collisional magmatism in western Anatolia, Turkey, Journal of African Earth Sciences, 195, 104679, https://doi.org/10.1016/j.jafrearsci.2022.104679, 2022.

Pagani, M., Freeman, K. H., and Arthur, M. A.: Late Miocene Atmospheric CO2 Concentrations and the Expansion of C4 Grasses, Science, 285, 876–879, https://doi.org/10.1126/science.285.5429.876, 1999.

Passchier, S., Browne, G., Field, B., Fielding, C. R., Krissek, L. A., Panter, K., Pekar, S. F., and and ANDRILL-SMS Science Team: Early and middle Miocene Antarctic glacial history from the sedimentary facies distribution in the AND-2A drill hole, Ross Sea, Antarctica, GSA Bulletin, 123, 2352–2365, https://doi.org/10.1130/B30334.1, 2011.

Paxman, G. J. G., Jamieson, S. S. R., Hochmuth, K., Gohl, K., Bentley, M. J., Leitchenkov, G., and Ferraccioli, F.: Reconstructions of Antarctic topography since the Eocene–Oligocene boundary, Palaeogeography, Palaeoclimatology, Palaeoecology, 535, 109346, https://doi.org/10.1016/j.palaeo.2019.109346, 2019.

Paxman, G. J. G., Gasson, E. G. W., Jamieson, S. S. R., Bentley, M. J., and Ferraccioli, F.: Long-Term Increase in Antarctic Ice Sheet Vulnerability Driven by Bed Topography Evolution, Geophysical Research Letters, 47, e2020GL090003, https://doi.org/10.1029/2020GL090003, 2020.

Pearson, P. N. and Palmer, M. R.: Atmospheric carbon dioxide concentrations over the past 60 million years, Nature, 406, 695–699, https://doi.org/10.1038/35021000, 2000.

Pérez, L. F., Santis, L. D., McKay, R. M., Larter, R. D., Ash, J., Bart, P. J., Böhm, G., Brancatelli, G., Browne, I., Colleoni, F., Dodd, J. P., Geletti, R., Harwood, D. M., Kuhn, G., Laberg, J. S., Leckie, R. M., Levy, R. H., Marschalek, J., Mateo, Z., Naish, T. R., Sangiorgi, F., Shevenell, A. E., Sorlien, C. C., van de Flierdt, T., and International Ocean Discovery Program Expedition 374 Scientists: Early and middle Miocene ice sheet dynamics in the Ross Sea: Results from integrated core-log-seismic interpretation, GSA Bulletin, 134, 348–370, https://doi.org/10.1130/B35814.1, 2021.

Pérez-Angel, L. C., Da, J., Flynn, A. G., Havranek, R. E. E., Novak, J., Romero, I. C., Saslaw, M., and Zhu, F.: A new compilation of terrestrial temperatures during the Miocene, in: AGU Fall Meeting Abstracts, PP41C-0313, 2024.

Pik, R., Marty, B., Carignan, J., Yirgu, G., and Ayalew, T.: Timing of East African Rift development in southern Ethiopia: Implication for mantle plume activity and evolution of topography, Geology, 36, 167–170, https://doi.org/10.1130/G24233A.1, 2008.

Pillot, Q., Donnadieu, Y., Sarr, A.-C., Ladant, J.-B., and Suchéras-Marx, B.: Evolution of Ocean Circulation in the North Atlantic Ocean During the Miocene: Impact of the Greenland Ice Sheet and the

https://doi.org/10.5194/egusphere-2026-3595
Preprint. Discussion started: 3 August 2026

Eastern Tethys Seaway, Paleoceanography and Paleoclimatology, 37, e2022PA004415, https://doi.org/10.1029/2022PA004415, 2022.

Poblete, F., Dupont-Nivet, G., Licht, A., van Hinsbergen, D. J. J., Roperch, P., Mihalynuk, M. G., Johnston, S. T., Guillocheau, F., Baby, G., Fluteau, F., Robin, C., van der Linden, T. J. M., Ruiz, D., and Baatsen, M. L. J.: Towards interactive global paleogeographic maps, new reconstructions at 60, 40 and 20 Ma, Earth-Science Reviews, 214, 103508, https://doi.org/10.1016/j.earscirev.2021.103508, 2021.

Poorter, H., Pons, T. L., Reichgelt, T., Poorter, H., Pons, T. L., and Reichgelt, T.: Stomatal Density and Index Are More Responsive to Light Intensity than to [CO2]: A Meta-Analysis and Implications for Paleo-CO2 Reconstruction, PlantEcophys, 1, 1, https://doi.org/10.53941/plantecophys.2025.100001, 2025.

Pound, M. J., Haywood, A. M., Salzmann, U., and Riding, J. B.: Global vegetation dynamics and latitudinal temperature gradients during the Mid to Late Miocene (15.97–5.33Ma), Earth-Science Reviews, 112, 1–22, 2012.

Rae, J. W. B., Zhang, Y. G., Liu, X., Foster, G. L., Stoll, H. M., and Whiteford, R. D. M.: Atmospheric CO2 over the Past 66 Million Years from Marine Archives, Annual Review of Earth and Planetary Sciences, 49, 1–33, https://doi.org/10.1146/annurev-earth-082420-063026, 2021a.

Rae, J. W. B., Zhang, Y. G., Liu, X., Foster, G. L., Stoll, H. M., and Whiteford, R. D. M.: Atmospheric CO2 over the Past 66 Million Years from Marine Archives, Annual Review of Earth and Planetary Sciences, 49, 609–641, https://doi.org/10.1146/annurev-earth-082420-063026, 2021b.

Reichgelt, T. and D'Andrea, W. J.: Plant carbon assimilation rates in atmospheric CO2 reconstructions, New Phytologist, 223, 1844–1855, https://doi.org/10.1111/nph.15914, 2019.

Reichgelt, T. and West, C. K.: Insights into greener Miocene biomes and globally enhanced terrestrial productivity from fossil leaves, Evolving Earth, 3, 100058, https://doi.org/10.1016/j.eve.2025.100058, 2025.

Renoult, M., de Boer, A., and Berntell, E.: Shaping the mid-Miocene warmth: a sensitivity study on paleogeography, CO_2 and model physics, EGUsphere, 1–27, https://doi.org/10.5194/egusphere-2025-5078, 2025.

Retallack, G. J.: Soil Carbon Dioxide Planetary Thermostat, Astrobiology, 22, 116–123, https://doi.org/10.1089/ast.2020.2415, 2022.

Riahi, K., van Vuuren, D. P., Kriegler, E., Edmonds, J., O'Neill, B. C., Fujimori, S., Bauer, N., Calvin, K., Dellink, R., Fricko, O., Lutz, W., Popp, A., Cuaresma, J. C., Kc, S., Leimbach, M., Jiang, L., Kram, T., Rao, S., Emmerling, J., Ebi, K., Hasegawa, T., Havlik, P., Humpenöder, F., Da Silva, L. A., Smith,

https://doi.org/10.5194/egusphere-2026-3595
Preprint. Discussion started: 3 August 2026

S., Stehfest, E., Bosetti, V., Eom, J., Gernaat, D., Masui, T., Rogelj, J., Strefler, J., Drouet, L., Krey, V., Luderer, G., Harmsen, M., Takahashi, K., Baumstark, L., Doelman, J. C., Kainuma, M., Klimont, Z., Marangoni, G., Lotze-Campen, H., Obersteiner, M., Tabeau, A., and Tavoni, M.: The Shared Socioeconomic Pathways and their energy, land use, and greenhouse gas emissions implications: An overview, Global Environmental Change, 42, 153–168, https://doi.org/10.1016/j.gloenvcha.2016.05.009, 2017.

Richards, F. D., Hoggard, M. J., Cowton, L. R., and White, N. J.: Reassessing the Thermal Structure of Oceanic Lithosphere With Revised Global Inventories of Basement Depths and Heat Flow Measurements, Journal of Geophysical Research: Solid Earth, 123, 9136–9161, https://doi.org/10.1029/2018JB015998, 2018.

Roberts, C. D., LeGrande, A. N., and Tripati, A. K.: Climate sensitivity to Arctic seaway restriction during the early Paleogene, Earth and Planetary Science Letters, 286, 576–585, https://doi.org/10.1016/j.epsl.2009.07.026, 2009.

Rohling, E. J., Rohling, E. J., Sluijs, A., Dijkstra, H. A., Köhler, P., van de Wal, R. S. W., von der Heydt, A. S., Beerling, D. J., Berger, A., Bijl, P. K., Crucifix, M., DeConto, R., Drijfhout, S. S., Fedorov, A., Foster, G. L., Ganopolski, A., Hansen, J., Hönisch, B., Hooghiemstra, H., Huber, M., Huybers, P., Knutti, R., Lea, D. W., Lourens, L. J., Lunt, D., Masson-Delmotte, V., Medina-Elizalde, M., Otto-Bliesner, B., Pagani, M., Pälike, H., Renssen, H., Royer, D. L., Siddall, M., Valdes, P., Zachos, J. C., Zeebe, R. E., and PALAEOSENS Project Members: Making sense of palaeoclimate sensitivity, Nature, 491, 683–691, https://doi.org/10.1038/nature11574, 2012.

Rohling, E. J., Foster, G. L., Gernon, T. M., Grant, K. M., Heslop, D., Hibbert, F. D., Roberts, A. P., and Yu, J.: Comparison and Synthesis of Sea-Level and Deep-Sea Temperature Variations Over the Past 40 Million Years, Reviews of Geophysics, 60, e2022RG000775, https://doi.org/10.1029/2022RG000775, 2022.

Royer, D. L., Wing, S. L., Beerling, D. J., Jolley, D. W., Koch, P. L., Hickey, L. J., and Berner, R. A.: Paleobotanical Evidence for Near Present-Day Levels of Atmospheric CO2 During Part of the Tertiary, Science, 292, 2310–2313, https://doi.org/10.1126/science.292.5525.2310, 2001.

Rugenstein, J. K. C., Methner, K., Kukla, T., Mulch, A., Lüdecke, T., Fiebig, J., Meltzer, A., Wegmann, K. W., Zeitler, P., and Chamberlain, C. P.: Clumped isotope constraints on warming and precipitation seasonality in Mongolia following Altai uplift, American Journal of Science, 322, 28–54, https://doi.org/10.2475/01.2022.02, 2022.

Sangiorgi, F., Bijl, P. K., Passchier, S., Salzmann, U., Schouten, S., McKay, R., Cody, R. D., Pross, J., Flierdt, T. van de, Bohaty, S. M., Levy, R., Williams, T., Escutia, C., and Brinkhuis, H.: Southern Ocean warming and Wilkes Land ice sheet retreat during the mid-Miocene, Nature Communications, 9, 1–11, https://doi.org/10.1038/s41467-017-02609-7, 2018.

https://doi.org/10.5194/egusphere-2026-3595
Preprint. Discussion started: 3 August 2026

Sarr, A.-C., Donnadieu, Y., Bolton, C. T., Ladant, J.-B., Licht, A., Fluteau, F., Laugié, M., Tardif, D., and Dupont-Nivet, G.: Neogene South Asian monsoon rainfall and wind histories diverged due to topographic effects, Nat. Geosci., 15, 314–319, https://doi.org/10.1038/s41561-022-00919-0, 2022.

Schmittner, A. and Egbert, G. D.: An improved parameterization of tidal mixing for ocean models, Geoscientific Model Development, 7, 211–224, https://doi.org/10.5194/gmd-7-211-2014, 2014.

Segev, A., Avni, Y., Shahar, J., and Wald, R.: Late Oligocene and Miocene different seaways to the Red Sea–Gulf of Suez rift and the Gulf of Aqaba–Dead Sea basins, Earth-Science Reviews, 171, 196–219, https://doi.org/10.1016/j.earscirev.2017.05.004, 2017.

Sembroni, A., Faccenna, C., Becker, T. W., Molin, P., and Abebe, B.: Long-term, deep-mantle support of the Ethiopia-Yemen Plateau, Tectonics, 35, 469–488, https://doi.org/10.1002/2015TC004000, 2016.

Sepulchre, P., Arsouze, T., Donnadieu, Y., Dutay, J. C., Jaramillo, C., Bras, J. L., Martin, E., Montes, C., and Waite, A. J.: Consequences of shoaling of the Central American Seaway determined from modeling Nd isotopes, Paleoceanography, 29, 176–189, https://doi.org/10.1002/2013pa002501, 2014.

Sherwood, S. C., Webb, M. J., Annan, J. D., Armour, K. C., Forster, P. M., Hargreaves, J. C., Hegerl, G., Klein, S. A., Marvel, K. D., Rohling, E. J., Watanabe, M., Andrews, T., Braconnot, P., Bretherton, C. S., Foster, G. L., Hausfather, Z., Heydt, A. S., Knutti, R., Mauritsen, T., Norris, J. R., Proistosescu, C., Rugenstein, M., Schmidt, G. A., Tokarska, K. B., and Zelinka, M. D.: An Assessment of Earth's Climate Sensitivity Using Multiple Lines of Evidence, Reviews of Geophysics, 58, e2019RG000678, https://doi.org/10.1029/2019rg000678, 2020.

Shevenell, A. E., Kennett, J. P., and Lea, D. W.: Middle Miocene Southern Ocean Cooling and Antarctic Cryosphere Expansion, Science, 305, 1766–1770, https://doi.org/10.1126/science.1100061, 2004.

Shevenell, A. E., Kennett, J. P., and Lea, D. W.: Middle Miocene ice sheet dynamics, deep-sea temperatures, and carbon cycling: A Southern Ocean perspective, Geochem. Geophys. Geosyst., 9, Q02006, https://doi.org/10.1029/2007GC001736, 2008.

Simmons, H. L., Jayne, S. R., Laurent, L. C. St., and Weaver, A. J.: Tidally driven mixing in a numerical model of the ocean general circulation, Ocean Modelling, 6, 245–263, https://doi.org/10.1016/S1463-5003(03)00011-8, 2004.

Sosdian, S. M., Greenop, R., Hain, M. P., Foster, G. L., Pearson, P. N., and Lear, C. H.: Constraining the evolution of Neogene ocean carbonate chemistry using the boron isotope pH proxy, Earth and Planetary Science Letters, 498, 362–376, https://doi.org/10.1016/j.epsl.2018.06.017, 2018.

Spaur, S., Koning, D. J., Heizler, M., Aby, S., Williamson, G., Knott, J. R., Acosta, R. P., and Rugenstein, J. K. C.: The Hydroclimate and Environmental Response to Middle Miocene Warming in

https://doi.org/10.5194/egusphere-2026-3595
Preprint. Discussion started: 3 August 2026

the Southwestern USA: Stable Isotope Evidence, Paleoceanography and Paleoclimatology, 40, e2024PA005056, https://doi.org/10.1029/2024PA005056, 2025.

Spicer, R. A., Su, T., Valdes, P. J., Farnsworth, A., Wu, F.-X., Shi, G., Spicer, T. E. V., and Zhou, Z.: The topographic evolution of the Tibetan Region as revealed by palaeontology, Palaeobio Palaeoenv, 101, 213–243, https://doi.org/10.1007/s12549-020-00452-1, 2021a.

Spicer, R. A., Su, T., Valdes, P. J., Farnsworth, A., Wu, F.-X., Shi, G., Spicer, T. E. V., and Zhou, Z.: Why ‘the uplift of the Tibetan Plateau’ is a myth, Natl Sci Rev, 8, nwaa091, https://doi.org/10.1093/nsr/nwaa091, 2021b.

Stap, L. B., Köhler, P., and Lohmann, G.: Including the efficacy of land ice changes in deriving climate sensitivity from paleodata, Earth System Dynamics, 10, 333–345, https://doi.org/10.5194/esd-10-333-2019, 2019.

Stap, L. B., Berends, C. J., Scherrenberg, M. D. W., van de Wal, R. S. W., and Gasson, E. G. W.: Net effect of ice-sheet–atmosphere interactions reduces simulated transient Miocene Antarctic ice-sheet variability, The Cryosphere, 16, 1315–1332, https://doi.org/10.5194/tc-16-1315-2022, 2022.

Stärz, M., Jokat, W., Knorr, G., and Lohmann, G.: Threshold in North Atlantic-Arctic Ocean circulation controlled by the subsidence of the Greenland-Scotland Ridge, Nat Commun, 8, 15681, https://doi.org/10.1038/ncomms15681, 2017a.

Stärz, M., Jokat, W., Knorr, G., and Lohmann, G.: Threshold in North Atlantic-Arctic Ocean circulation controlled by the subsidence of the Greenland-Scotland Ridge, Nat Commun, 8, 15681, https://doi.org/10.1038/ncomms15681, 2017b.

Staver, A. C., Archibald, S., and Levin, S. A.: The Global Extent and Determinants of Savanna and Forest as Alternative Biome States, Science, 334, 230–232, https://doi.org/10.1126/science.1210465, 2011.

Stein, C. A. and Stein, S.: A model for the global variation in oceanic depth and heat flow with lithospheric age, Nature, 359, 123–129, https://doi.org/10.1038/359123a0, 1992.

Steinig, S., Abe-Ouchi, A., de Boer, A. M., Chan, W.-L., Donnadieu, Y., Hutchinson, D. K., Knorr, G., Ladant, J.-B., Morozova, P., Niezgodzki, I., Poulsen, C. J., Volodin, E. M., Zhang, Z., Zhu, J., Evans, D., Inglis, G. N., Meckler, A. N., and Lunt, D. J.: DeepMIP-Eocene-p1: multi-model dataset and interactive web application for Eocene climate research, Sci Data, 11, 970, https://doi.org/10.1038/s41597-024-03773-4, 2024.

Steinig, S., Williams, C., Burls, N. J., Cramwinckel, M. J., Farnsworth, A., Foster, G., Hopcroft, P., Inglis, G., Lear, C., Osprey, A., Pancost, R., Roberts, W., Selar, A., Stone, E., Wood, R., Zhu, J., and

Lunt, D.: Super warm early Eocene simulations with HadGEM3-GC31-LL, Journal of Geophysical Researc: Atmospheres, In Prep, 2026.

Steinthorsdottir, M., Jardine, P. E., and Rember, W. C.: Near-Future pCO2 During the Hot Miocene Climatic Optimum, Paleoceanography and Paleoclimatology, 36, e2020PA003900, https://doi.org/10.1029/2020PA003900, 2021a.

Steinthorsdottir, M., Coxall, H. K., Boer, A. M. de, Huber, M., Barbolini, N., Bradshaw, C. D., Burls, N. J., Feakins, S. J., Gasson, E., Henderiks, J., Holbourn, A. E., Kiel, S., Kohn, M. J., Knorr, G., Kürschner, W. M., Lear, C. H., Liebrand, D., Lunt, D. J., Mörs, T., Pearson, P. N., Pound, M. J., Stoll, H., and Strömberg, C. A. E.: The Miocene: The Future of the Past, Paleoceanography and Paleoclimatology, 36, https://doi.org/10.1029/2020pa004037, 2021b.

Steinthorsdottir, M., Coxall, H. K., de Boer, A. M., Huber, M., Barbolini, N., Bradshaw, C. D., Burls, N. J., Feakins, S. J., Gasson, E., Henderiks, J., Holbourn, A. E., Kiel, S., Kohn, M. J., Knorr, G., Kürschner, W. M., Lear, C. H., Liebrand, D., Lunt, D. J., Mörs, T., Pearson, P. N., Pound, M. J., Stoll, H., and Strömberg, C. a. E.: The Miocene: The Future of the Past, Paleoceanography and Paleoclimatology, 36, e2020PA004037, https://doi.org/10.1029/2020PA004037, 2021c.

Stiles, E., Novak, J., Mitsunaga, B., Hare, V., Saslaw, M., Rugenstein, J., Beck, C. C., Jukar, A., George, S., Lee, D., Strömberg, C., Uno, K. T., Vetter, L., and Zhu, F.: Global Terrestrial Hydrologic Change Since the Mid-Miocene Climatic Optimum: A New Compilation of Hydroclimate Proxy Records and Implications for Future Change, in: AGU Fall Meeting Abstracts, PP41C-0314, 2024.

Stoll, H. M., Guitian, J., Hernandez-Almeida, I., Mejía, L. M., Phelps, S., Polissar, P., Rosenthal, Y., Zhang, H., and ZIVERI, P.: Upregulation of phytoplankton carbon concentrating mechanisms during low CO2 glacial periods and implications for the phytoplankton pCO2 proxy, Quaternary Science Reviews, 208, 1–20, https://doi.org/10.1016/j.quascirev.2019.01.012, 2019.

Straume, E. O., Gaina, C., Medvedev, S., and Nisancioglu, K. H.: Global Cenozoic Paleobathymetry with a focus on the Northern Hemisphere Oceanic Gateways, Gondwana Research, 86, 126–143, https://doi.org/10.1016/j.gr.2020.05.011, 2020.

Straume, E. O., Nummelin, A., Gaina, C., and Nisancioglu, K. H.: Climate transition at the Eocene–Oligocene influenced by bathymetric changes to the Atlantic–Arctic oceanic gateways, Proceedings of the National Academy of Sciences, 119, e2115346119, https://doi.org/10.1073/pnas.2115346119, 2022.

Straume, E. O., Steinberger, B., Becker, T. W., and Faccenna, C.: Impact of mantle convection and dynamic topography on the Cenozoic paleogeography of Central Eurasia and the West Siberian Seaway, Earth and Planetary Science Letters, 630, 118615, https://doi.org/10.1016/j.epsl.2024.118615, 2024.

Straume, E. O., Faccenna, C., Becker, T. W., Steinberger, B., Licht, A., Sembroni, A., Gvirtzman, Z., and Ballato, P.: Collision, mantle convection and Tethyan closure in the Eastern Mediterranean, Nat Rev Earth Environ, 6, 299–317, https://doi.org/10.1038/s43017-025-00653-2, 2025.

Strömberg, C. A. E., Dunn, R. E., Crifò, C., and Harris, E. B.: Phytoliths in Paleoecology: Analytical Considerations, Current Use, and Future Directions, in: Methods in Paleoecology: Reconstructing Cenozoic Terrestrial Environments and Ecological Communities, edited by: Croft, D. A., Su, D. F., and Simpson, S. W., Springer International Publishing, Cham, 235–287, https://doi.org/10.1007/978-3-319-94265-0_12, 2018.

Sugden, D. E.: The East Antarctic Ice Sheet: Unstable Ice or Unstable Ideas?, Transactions of the Institute of British Geographers, 21, 443–454, https://doi.org/10.2307/622590, 1996.

Sundell, K. E., Eden, R., Styron, R. H., Villarreal, D. P., Usnayo, P., Saylor, J. E., Göğüş, O. H., Lapen, T. J., Finney, B., Cardenas, J., and Carlotto, V.: Tectonic and climatic controls on late Cenozoic intra-arc basin development in the central Andes of southern Peru, Earth and Planetary Science Letters, 666, 119487, https://doi.org/10.1016/j.epsl.2025.119487, 2025.

Super, J. R., Thomas, E., Pagani, M., Huber, M., O'Brien, C., and Hull, P. M.: North Atlantic temperature and pCO2 coupling in the early-middle Miocene, 46, 519–522, https://doi.org/10.1130/g40228.1, 2018.

Swezey, C. S.: Cenozoic stratigraphy of the Sahara, Northern Africa, Journal of African Earth Sciences, 53, 89–121, 2009.

Sykes, T. J. S.: A correction for sediment load upon the ocean floor: Uniform versus varying sediment density estimations—implications for isostatic correction, Marine Geology, 133, 35–49, https://doi.org/10.1016/0025-3227(96)00016-3, 1996.

Takahashi, K. and Battisti, D. S.: Processes Controlling the Mean Tropical Pacific Precipitation Pattern. Part I: The Andes and the Eastern Pacific ITCZ, https://doi.org/10.1175/JCLI4198.1, 2007.

Tanner, T., Rae, J., Hernández-Almeida, I., Zhang, H., Jaggi, M., Dumont, M., Jurikova, H., Bernasconi, S. M., and Stoll, H.: Multi-Proxy Estimates of Sea Surface Temperature and CO2 in the Western Atlantic During the Late Miocene, Paleoceanography and Paleoclimatology, 40, e2025PA005142, https://doi.org/10.1029/2025PA005142, 2025.

THE CENOZOIC CO2 PROXY INTEGRATION PROJECT (CENCO2PIP) CONSORTIUM: Toward a Cenozoic history of atmospheric CO2, Science, 382, eadi5177, https://doi.org/10.1126/science.adi5177, 2023.

https://doi.org/10.5194/egusphere-2026-3595
Preprint. Discussion started: 3 August 2026

Thiede, J., Jessen, C., Knutz, P., Kuijpers, A., Mikkelsen, N., Nørgaard-Pedersen, N., and Spielhagen, R. F.: Millions of years of Greenland Ice Sheet history recorded in ocean sediments, Polarforschung, 80, 141–159, 2011.

Tian, D., Leong, W. J., Fröhlich, Y., Grund, M., Schlitzer, W., Jones, M., Toney, L., Yao, J., Tong, J.-H., Magen, Y., Materna, K., Belem, A., Newton, T., Anant, A., Ziebarth, M., Quinn, J., Uieda, L., and Wessel, P.: PyGMT: A Python interface for the Generic Mapping Tools, , https://doi.org/10.5281/zenodo.17156962, 2025.

Tierney, J. E., Poulsen, C. J., Montañez, I. P., Bhattacharya, T., Feng, R., Ford, H. L., Hönisch, B., Inglis, G. N., Petersen, S. V., Sagoo, N., Tabor, C. R., Thirumalai, K., Zhu, J., Burls, N. J., Foster, G. L., Goddéris, Y., Huber, B. T., Ivany, L. C., Turner, S. K., Lunt, D. J., McElwain, J. C., Mills, B. J. W., Otto-Bliesner, B. L., Ridgwell, A., and Zhang, Y. G.: Past climates inform our future., Science (New York, N.Y.), 370, https://doi.org/10.1126/science.aay3701, 2020.

Traverse, A.: Production, dispersal, sedimentation and taphonomy of spores/pollen in relation to the interpretation of palynofloras, in: Paleopalynology, Springer, 497–542, 2007.

Tuerena, R. E., Williams, R. G., Mahaffey, C., Vic, C., Green, J. A. M., Naveira-Garabato, A., Forryan, A., and Sharples, J.: Internal Tides Drive Nutrient Fluxes Into the Deep Chlorophyll Maximum Over Mid-ocean Ridges, Global Biogeochemical Cycles, 33, 995–1009, https://doi.org/10.1029/2019GB006214, 2019.

Tweedy, R. R., Strömberg, C. A. E., Reichgelt, T., Kinyanjui, R. N., Kimeu, M., Munyaka, V., and Uno, K. T.: African C3 grass *n*-alkane distributions & plant chemotaxonomy, Organic Geochemistry, 208, 104994, https://doi.org/10.1016/j.orggeochem.2025.104994, 2025.

Vachula, R. S., Sae-Lim, J., and Li, R.: A critical appraisal of charcoal morphometry as a paleofire fuel type proxy, Quaternary Science Reviews, 262, 106979, https://doi.org/10.1016/j.quascirev.2021.106979, 2021.

Vallejo-Hincapié, F., Pardo-Trujillo, A., Barbosa-Espitia, Á., Aguirre, D., Celis, S. A., Giraldo-Villegas, C. A., Plata-Torres, Á., Trejos-Tamayo, R., Salazar-Ríos, A., Flores, J.-A., Aubry, M.-P., Gallego, F., Delgado, E., and Foster, D.: Miocene vanishing of the Central American Seaway between the Panamá Arc and the South American Plate, GSA Bulletin, 136, 4798–4814, https://doi.org/10.1130/B37499.1, 2024.

Vetel, W. and Le Gall, B.: Dynamics of prolonged continental extension in magmatic rifts: the Turkana Rift case study (North Kenya), Geological Society, London, Special Publications, https://doi.org/https://doi.org/10.1144/gsl.sp.2006.259.01.17, 2006.

Wang, C., Ding, L., Xiong, Z., Allen, M. B., Laskowski, A. K., Garzanti, E., Zhang, Q., Cai, F., Wang, H., Song, P., Li, Y., Ping, F., Farnsworth, A., Lunt, D. J., Valdes, P. J., Li, Z., Wu, C., and Qasim, M.:

https://doi.org/10.5194/egusphere-2026-3595
Preprint. Discussion started: 3 August 2026

Timing of initial collision and suturing processes in the Himalaya and Zagros, Nat Rev Earth Environ, 6, 357–376, https://doi.org/10.1038/s43017-025-00669-8, 2025.

Wang, Y., Momohara, A., Wang, L., Lebreton-Anberrée, J., and Zhou, Z.: Evolutionary History of Atmospheric CO2 during the Late Cenozoic from Fossilized Metasequoia Needles, PLOS ONE, 10, e0130941, https://doi.org/10.1371/journal.pone.0130941, 2015.

Wessel, P., Luis, J. F., Uieda, L., Scharroo, R., Wobbe, F., Smith, W. H. F., and Tian, D.: The Generic Mapping Tools Version 6, Geochemistry, Geophysics, Geosystems, 20, 5556–5564, https://doi.org/10.1029/2019GC008515, 2019a.

Wessel, P., Luis, J. F., Uieda, L., Scharroo, R., Wobbe, F., Smith, W. H. F., and Tian, D.: The Generic Mapping Tools Version 6, Geochemistry, Geophysics, Geosystems, 20, 5556–5564, https://doi.org/10.1029/2019GC008515, 2019b.

Wheeler, L. B., Galewsky, J., Herold, N., and Huber, M.: Late Cenozoic surface uplift of the southern Sierra Nevada (California, USA): A paleoclimate perspective on lee-side stable isotope paleoaltimetry, Geology, 44, 451–454, https://doi.org/10.1130/G37718.1, 2016.

White, R. H., Battisti, D. S., and Roe, G. H.: Mongolian Mountains Matter Most: Impacts of the Latitude and Height of Asian Orography on Pacific Wintertime Atmospheric Circulation, https://doi.org/10.1175/JCLI-D-16-0401.1, 2017.

Whiteford, R., Heaton, T. J., Henehan, M. J., Anagnostou, E., Jurikova, H., Foster, G. L., and Rae, J. W. B.: Reconstruction of Cenozoic δ11Bsw Using a Gaussian Process, Paleoceanography and Paleoclimatology, 39, e2023PA004769, https://doi.org/10.1029/2023PA004769, 2024.

Wichura, H., Bousquet, R., Oberhänsli, R., Strecker, M. R., and Trauth, M. H.: Evidence for middle Miocene uplift of the East African Plateau, Geology, 38, 543–546, https://doi.org/10.1130/G31022.1, 2010.

Wichura, H., Jacobs, L. L., Lin, A., Polcyn, M. J., Manthi, F. K., Winkler, D. A., Strecker, M. R., and Clemens, M.: A 17-My-old whale constrains onset of uplift and climate change in east Africa, Proceedings of the National Academy of Sciences, 112, 3910–3915, https://doi.org/10.1073/pnas.1421502112, 2015.

Wilmes, S.-B., Green, J. A. M., and Schmittner, A.: Enhanced vertical mixing in the glacial ocean inferred from sedimentary carbon isotopes, Commun Earth Environ, 2, 166, https://doi.org/10.1038/s43247-021-00239-y, 2021.

Witkowski, C. R., von der Heydt, A. S., Valdes, P. J., van der Meer, M. T. J., Schouten, S., and Sinninghe Damsté, J. S.: Continuous sterane and phytane δ13C record reveals a substantial pCO2

https://doi.org/10.5194/egusphere-2026-3595
Preprint. Discussion started: 3 August 2026

decline since the mid-Miocene, Nat Commun, 15, 5192, https://doi.org/10.1038/s41467-024-47676-9, 2024.

Wright, N. M., Seton, M., Williams, S. E., Whittaker, J. M., and Müller, R. D.: Sea-level fluctuations driven by changes in global ocean basin volume following supercontinent break-up, Earth-Science Reviews, 208, 103293, https://doi.org/10.1016/j.earscirev.2020.103293, 2020.

Wunsch, C. and Ferrari, R.: VERTICAL MIXING, ENERGY, AND THE GENERAL CIRCULATION OF THE OCEANS, Annual Review of Fluid Mechanics, 36, 281–314, https://doi.org/10.1146/annurev.fluid.36.050802.122121, 2004.

Xing, Y., Gandolfo, M. A., Onstein, R. E., Cantrill, D. J., Jacobs, B. F., Jordan, G. J., Lee, D. E., Popova, S., Srivastava, R., Su, T., Vikulin, S. V., Yabe, A., and Linder, H. P.: Testing the Biases in the Rich Cenozoic Angiosperm Macrofossil Record, International Journal of Plant Sciences, 177, 371–388, https://doi.org/10.1086/685388, 2016.

Zahirovic, S., Eleish, A., Doss, S., Pall, J., Cannon, J., Pistone, M., Tetley, M. G., Young, A., and Fox, P.: Subduction and carbonate platform interactions, Geoscience Data Journal, 9, 371–383, https://doi.org/10.1002/gdj3.146, 2022.

Zhang, Y., Wei, J., Li, Z., Dai, N., Zheng, W., Yin, Q., de Boer, A., Shi, Z., and Zhang, L.: Weakened and Irregular Miocene Climate Response to Orbital Forcing compared to the modern day, EGUsphere, 1–15, https://doi.org/10.5194/egusphere-2025-4485, 2025.

Zhang, Y. G., Pagani, M., Liu, Z., Bohaty, S. M., and DeConto, R.: A 40-million-year history of atmospheric CO2, Philosophical Transactions of the Royal Society A: Mathematical, Physical and Engineering Sciences, 371, 20130096, https://doi.org/10.1098/rsta.2013.0096, 2013.

Zhang, Y. G., Henderiks, J., and Liu, X.: Refining the alkenone-*p*CO2 method II: Towards resolving the physiological parameter '*b*,' Geochimica et Cosmochimica Acta, 281, 118–134, https://doi.org/10.1016/j.gca.2020.05.002, 2020.

Zhang, Z., Nisancioglu, K. H., Flatøy, F., Bentsen, M., Bethke, I., and Wang, H.: Tropical seaways played a more important role than high latitude seaways in Cenozoic cooling, Climate of the Past, 7, 801–813, https://doi.org/10.5194/cp-7-801-2011, 2011.

Zhu, F., Zhu, J., Si, W., Nirenberg, J., Herbert, T., Tierney, J., Acosta, R. P., Burls, N., and Evans, D.: Model-data synthesis of benthic isotopes suggests a warmer Miocene Climatic Optimum, https://doi.org/10.21203/rs.3.rs-7124543/v1, 2025.

Zhu, J., Poulsen, C. J., and Tierney, J. E.: Simulation of Eocene extreme warmth and high climate sensitivity through cloud feedbacks, Science Advances, 5, eaax1874, https://doi.org/10.1126/sciadv.aax1874, 2019.

https://doi.org/10.5194/egusphere-2026-3595
Preprint. Discussion started: 3 August 2026

Zhu, J., Poulsen, C. J., and Otto-Bliesner, B. L.: Modeling Past Hothouse Climates as a Means for Assessing Earth System Models and Improving the Understanding of Warm Climates, Annual Review of Earth and Planetary Sciences, 52, 351–78, https://doi.org/10.1146/annurev-earth-032320-100333, 2024.

Zuo, M., Sun, Y., Zhao, Y., Ramstein, G., Ding, L., and Zhou, T.: South Asian summer monsoon enhanced by the uplift of the Iranian Plateau in Middle Miocene, Climate of the Past, 20, 1817–1836, https://doi.org/10.5194/cp-20-1817-2024, 2024.